

https://dspace.org/

Analysis and design of dissipative frequency selective two-layer conductive structures

Leeburn, Dominic Andrew

2014-02-12
http://hdl.handle.net10539/13737

Downloaded from a DSpace repository. https://dspace.org/

Analysis and design of dissipative frequency selective two-layer conductive structures

Dominic Andrew Leeburn

A dissertation submitted to the Faculty of Engineering and the Built Environment, University of the Witwatersrand, Johannesburg, in fulfilment of the requirements for the degree of Master of Science in Engineering.

February 2013

Declaration

I declare that this dissertation is my own, unaided work, other than where specifically acknowledged. It is being submitted for the degree of Master of Science in Engineering at University of the Witwatersrand, Johannesburg. It has not been submitted before for any degree or examination at any other university.

Signed at _____ on _____ , 2013.

_____
Dominic Leeburn

Abstract

In the drive towards power electronic integration, planar structures are widely used. Applications for the use of these structures are varied. These have been shown to have potential advantages with regard to reduction in size and cost. Much work has been done with regard to integration, but generally from an intuitive perspective, and without a general approach.

An important part of power electronic integration is EMI filtering. One way in which this is achieved is through dissipative filtering. It is demonstrated that this can be done for planar structures through the use of multi-layered conductors. Planar conductors have a particularly distinct advantage in that they are low profile and can be miniaturised. The resulting focus of this dissertation is an investigation into the characterisation of two-layer conductors in terms of how the properties of the two layers contribute to the frequency dependent resistance of the conductor. This is done with a direct view towards dissipative filtering.

This investigation begins with a description of the method of characterisation of two-layered conductors, and the construction of a parametric study around this. A contribution of this dissertation is the demonstration that the parametric space can be reduced without loss of generality of the characterisation. The results of this characterisation are used to demonstrate the importance of the total conductivity and total permeability as concepts. This concept provides flexibility in the design of two-layer dissipative filters.

The concept of a single-layer approximation is presented and investigated. It is shown to even further simplify the model used for multi-layered conductors, and presents a good first level understanding of what the frequency dependent resistance of the structure will be. This concept is shown to be useful in the design of two-layered conductors, and may be generalisable to multiple layers. A second contribution of this work is the presentation of design equations based upon this approximation for five different scenarios. This contribution includes the limits to the dimensions of the two-layer structure, with the conclusion that some specifications do not have physically realisable forms.

The final, major contribution that this work presents is as follows. In terms of dissipative filtering, it is shown under differential-mode excitation that the desired properties of the inner layer of the conductor should be: less conductive than the outer layer, and more permeable than the outer layer. These conditions are shown to provide a steeper gradient of resistance increase with respect to frequency. This conclusion is verified experimentally, which provides confidence in the modelling technique this dissertation is based upon.

Acknowledgement

First and foremost I would like to thank my family. The support that you all have shown me over the last two years has been phenomenal. I am not sure I could have done it with out you. To my father, Kieron, for your technical insight and the many late nights we spent discussing my masters, and righting the problems of the world while doing so. And especially for not letting me give up, and convincing me to stick through it all. To my mother, Alex, for just being there when I was feeling like things were not going my way. The coffees, the lunches the fun, interesting conversations. For your acceptance if I was have having a bad day and letting me know that it was all ok, that I could take time, relax, recover. To my sister, Sarah, you are awesome. Just plain thank you for being there, for keeping me sane as the months went by. Stay like that. I love you all.

To all my friends who were there for me during this time. Your support for me was exceptional. For the good times we had, for keeping me nicely distracted from the stress of this degree, for making me realise the stress was unnecessary. I appreciate everything you have done, everything we have said, every occasion we have shared.

Finally to my supervisor, Prof. Hofsajer. I most certainly could not have accomplished this work without your knowledge and insight, especially with regards to electromagnetics, and the physics behind it. Your help was indispensable in the times I did not know what direction to take. I appreciate the efforts you have put in for me especially in the last few weeks. Lastly, thank you for teaching me about technical communication, teaching me to always say precisely what I mean, and when to say it.

Table of Contents

Chapter One - Introduction

1.1. Introduction 2
1.2. Historical Perspective on Power electronic Integration 3
1.3. Integrated Dissipative filters 4
1.4. Multi-layered Conductors 5
1.5. Dissertation Breakdown 7
1.6. References 9

Chapter Two - Problem Background and Parametric Space

2.1. Introduction 12
2.2. Process of Describing a Multi-layered Conductor 12
2.2.1. Basic derivation and explanation of electromagnetic equations 12
2.2.2. Example of a two-layer structure 15
2.2.3. Parametric study 16
2.2.4. Limitations 19
2.3. Potential for Single Layer Approximations 19
2.4. Reduction of the parameter space 22
2.4.1. Equivalence between Common- and Differential-Mode Structures 23
2.4.2. Conductor Rescaling 27
2.4.2.1. Proof that conductors can be rescaled 27
2.4.2.2. Demonstration of conductor rescaling 29
2.5. Conclusion 30
2.6. References 31

Chapter Three- Parametric Study of Two-Layer Structures

3.1. Introduction 33
3.2. Variations in σ_1 34
3.3. Variations in σ_2 37
3.4. Variations in μ_1 39

3.5. Variations in μ_2 41
3.6. Analysis of parametric study conclusions 43
3.7. Conclusion 46
3.8. References 47

Chapter Four - Single Layer Approximation

4.1. Introduction 49
4.2. Divergence of the single layer approximation 49
4.3. Observations on the single layer approximation 51
4.4. Design of two layer structures 53
4.4.1. Design with arbitrary materials 53
4.4.1.1. Example of arbitrary material design 54
4.4.2. Design with existing materials 56
4.4.2.1. Specifying both knee-resistances 57
4.4.2.2. Specifying both knee-frequencies 58
4.4.2.3. Specifying f_{high} and R_{DC} 59
4.4.2.4. Specifying R_H and f_{low} 60
4.4.2.5. Specifying R_{DC} and f_{low} 60
4.5. Conclusion 61
4.6. References 62

Chapter Five - Experimental Verification

5.1. Introduction 64
5.2. Experiment Design 64
5.3. Justification of Experiment 67
5.4. Experimental Results 68
5.4.1. Determination of material properties 68
5.4.2. Results 69
5.4.2.1. Single Layer Aluminium 69
5.4.2.2. Aluminium and Brass 70
5.4.2.3. Aluminium and Nickel 71
5.4.3. Consolidation of results 72

5.5. Conclusion 73
5.6. References 73

Chapter Six - Conclusion and Recommendations

6.1. Introduction 75
6.2. Characterisation of two-layer conductors 75
6.3. Single Layer Approximation 76
6.4. Dissipative filters 77
6.5. Consolidated conclusions 77
6.6. Recommendations for future work 78

Appendix A - Background Theory

Acknowledgement 80
A.1. Introduction 80
A.2. Single Layer Solution 80
A.3. Multi-Layer Generalisation 85
A.4. Resistance calculations 86
A.5. References 86

Chapter One – Introduction

Table of Contents

1.1. Introduction 2
1.2. Historical Perspective on Power electronic Integration 3
1.3. Integrated Dissipative filters 4
1.4. Multi-layered Conductors 5
1.5. Dissertation Breakdown 7
1.6. References 9

1.1. Introduction

There is a continual push towards decreasing the costs of electronic products, but with an increase in functionality. Further to this, effort is being directed to efficient energy processing due to resource availability and environmental effects [1]. As such, there is a drive to power electronic integration in an effort to reduce the size of components, and reduce costs. Due to the pervasiveness of electronic devices in all areas of human life, the electromagnetic compatibility (EMC) of these devices is an important part of power electronic design. This is in order to avoid electromagnetic interference (EMI) between devices. Figure 1.1 [2] shows a flow chart of areas related to power electronic integration. The highlighted path indicates the focus of this dissertation. In any power electronic design, there are three factors to be considered: Electrical characteristics, Mechanical characteristics and Thermal characteristics [2]. These three are intrinsically linked, especially with regard to power electronic integration. For example, the volume of the structure (a mechanical characteristic) is linked to the energy that the structure can store and process (an electrical characteristic). Focus is restricted here to electrical considerations.

A use of lumped elements is in ac/ac and dc/dc converters. These passive components within a power electronic device often comprise more than 50% of the volume of the device [3]. Reducing the size of these energy storage components requires a higher switching frequency. Because of this, (conducted) EMI becomes a significant issue, and as such, must be dealt with within the design of power electronic devices [4]. In order to achieve compliance for conducted emissions, passive lumped LC filters are often used. With typical switched converters, both an input and output filter are required which contribute to a large portion of the cost [5]. These lumped elements can only be reduced in size to a certain extent, and as such, integration of these elements into a single structure is desired. It would be beneficial if the structure itself could be used to filter EMI. This has been attempted, but a general approach has not yet been formulated.

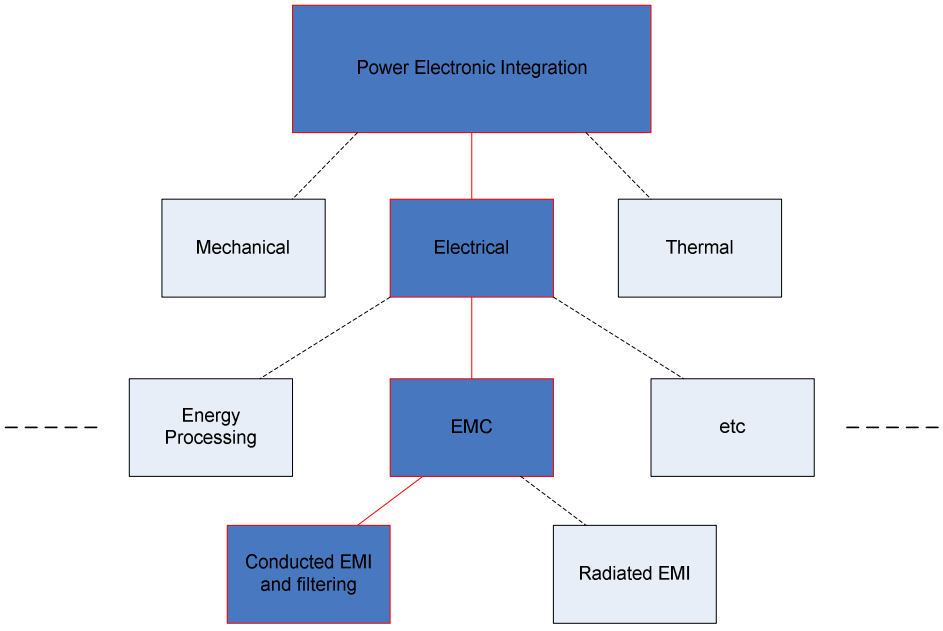


Figure 1.1. Diagram of areas related to Power Electronic Integration

1.2. Historical Perspective on Power electronic Integration

In much of the literature, integrated passive structures typically have the same form, with differences between structures depending on the application for which it is used. The typical form of an integrated structure is shown in Figure 1.2. Planar materials are stacked one upon the other. These materials may be conductive, magnetic, insulating, or dielectric, and may have an encapsulating ferrite material in order to increase the integrated inductance of the structure. There may be fewer or more layers than those represented in the figure. The use of this form is pervasive [5] – [16].

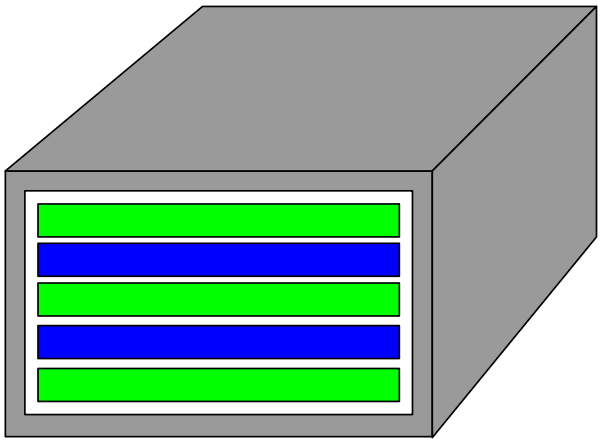


Figure 1.2. Typical integrated passive planar structure

Many different circuits have been integrated. A conceptual example of an integrated LC filter is given in [5] where a metallised dielectric material is placed within a ferrite core. This metallised dielectric is essentially a three-layered structure, two conductive layers with a dielectric layer between the two. This takes the typical form shown above. The author makes mention that more layers are possible depending on applications. An application that does require more than three layers of materials is that of an integrated resonant transformer (LLCT), and has been designed in [9] [13] [17]. The major advantages of these planar integrated structures are that they naturally create low profile structures, and allow for better thermal management due to the greater surface area to volume ratio [12]. Further to this, it may potentially lead to an easier, and therefore cheaper, manufacturing process.

As said previously, planar integration is a pervasive concept currently. In order to achieve high levels of integration, a modular approach is necessary [18] where Boroyevich suggests that it is possible to break a power converter into four Power Electronic Building Blocks (PEBBs). These four are Active PEBBs for switching functions, Passive PEBBs for energy storage, Filter PEBBs specifically for EMC, and Control PEBBs for the controlling functions of the device. As such, it is important to focus on the potential integration of each of these separately. Here, it is chosen to focus on the technology for the possible integration of EMI filters for the use in power electronics, especially seeing as they account for a large portion of the volume of a power electronic device [3].

1.3. Integrated Dissipative filters

The objective of a dissipative filter is to conduct low frequency current, but dissipate high frequency current. This can be done through the use of the skin- and proximity-effects [6]. Dissipative filtering for high frequencies is not a new concept and has existed for a long time; the first appearance of which was 1957 [19] with low pass co-axial cables being widely used in the automotive industry for ignition cables [20]. A large portion of the early work by Mayer focussed on ferrites and composites that are lossy at high frequencies [6] with respect to co-axial conductors. There has thus far been little work in this respect with regard to planar integrated structures. Given the pervasiveness of their use in the current drive towards power electronic integration, it is worth pursuing this course of research.

A conductor under differential mode excitation is depicted in Figure 1.3, with the current density distribution at 10MHz shown in Figure 1.4. The structure simulated (in Maxwell Student Version) has a conductor thickness of 200µm, and a separation distance of 200µm. It is clear that the skin- and proximity-effects are present. There is a go and return conductor, where the current in each interacts with the current in the other, and causing a change in the distribution of the current density from the uniform distribution expected at DC. Because it is in differential mode, the current migrates towards the inner surface of the conductor. In the common-mode configuration, where current is in the same direction in both conductors, the current is expected to migrate towards the outer boundary of the conductors.

The resistance of a general single conductor under differential mode is shown in Figure 1.5 on a log-log scale. The skin- and proximity-effects are unavoidable. They will always be present, and cause an increase in resistance from a given frequency – depending upon the properties of the conductor. The only notable difference between various conductors is that the knee-point and DC-resistance may change; the shape of the curve, however, will not change.

Superimposed on this figure is the ideal response for an ideal low pass dissipative filter. It is vastly different from the resistance of the single conductor. Because the shape of the resistance curve cannot be changed, it is not possible to get the high frequency resistance to be closer to that of the ideal low pass filter. The question that arises now is whether the filtering effects can be improved. It is quite clear that this cannot be done for a single homogenous conductor because the shape of its response cannot be changed. While there may be many solutions to this, it will be shown in this dissertation that a better filtering effect is in fact possible for a multi-layered planar conductor. This will have the distinct advantage of lending itself easily to integration.

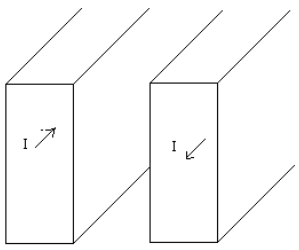


Figure 1.3. Example of conductor under differential mode excitation

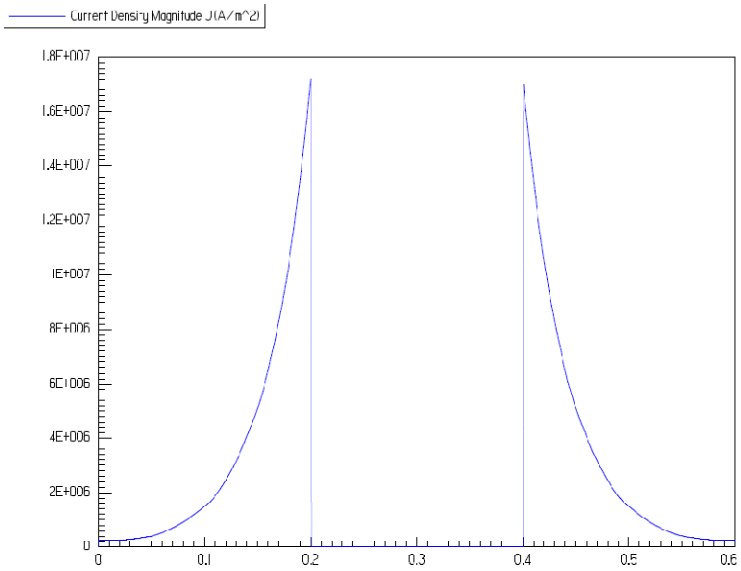


Figure 1.4. Current Density distribution of differential mode conductor at 10MHz

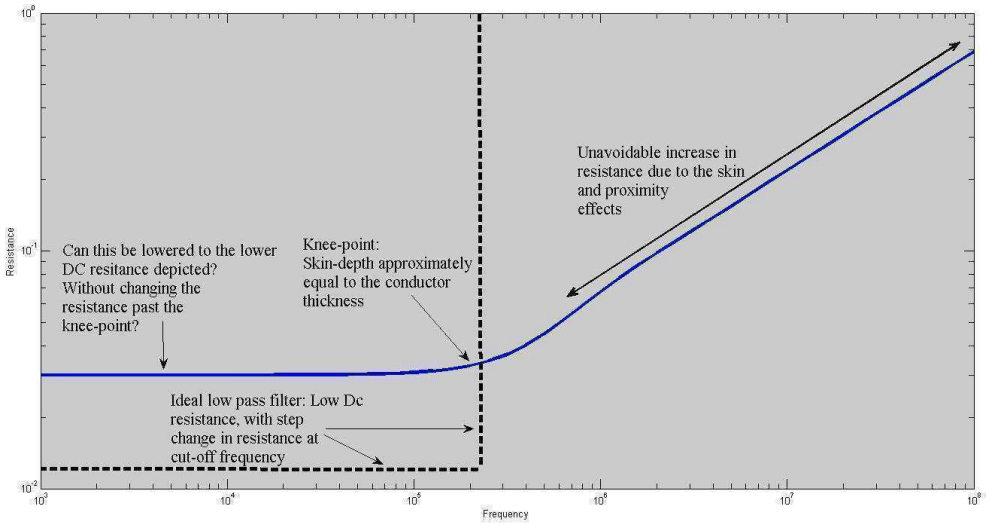


Figure 1.5. Low pass filter and skin effect resistance

1.4. Multi-layered Conductors

A multi-layered conductor is any conductor which consists of more than one conductive material. The boundaries of these material layers are parallel to each other with the most common configurations being either planar or co-axial [21]. Focus will be placed on planar conductors for this dissertation because of their relevance to power electronic integration as shown above.

A representation of a planar multi-layered conductor is shown in Figure 1.6. Each layer in the conductor may have its own permeability and its own conductivity – which may be low enough to be considered an insulator. A current which flows within a conductor will distribute itself according to the conductive and magnetic properties of the materials. As the frequency of the excitation increases, the skin- and proximity-effects begin to affect the

current distribution. In the differential mode, the current will still migrate towards the boundary between the two conductors. However, it is expected that the way in which he current migrates as a function of frequency is very much dependent on the properties of the multi-layered conductor, and will almost certainly not be as simple as that for a single layer conductor.

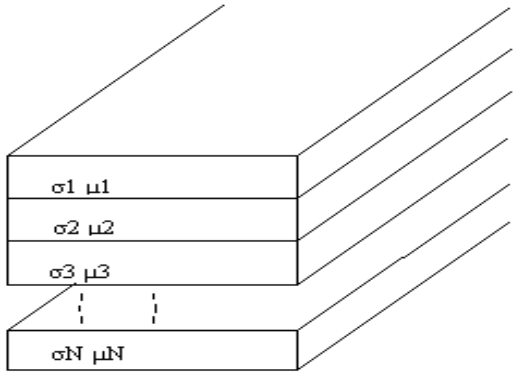


Figure 1.6. Generic multi-layered planar conductor

The particular reason to investigate multi-layered conductors is that, generally in previous work related to integration, the conductive layers are all used as homogenous materials. A multi-layered conductor is just a set of homogenous material. The concept behind a dissipative filter of this type is to use the skin- and proximity-effects in order to create better attenuation at higher frequencies. Referring to Figure 1.4, it can be seen that replacing the portion of the conductor where the high-frequency current flows with a material of a certain lower conductivity will cause more dissipation of power at this frequency through conversion into heat.

This idea was explored in some detail in [6]. The hypothesis in this case is that the skin- and proximity-effects could be used to increase high frequency resistance and therefore increasing the extent to which high frequency noise is attenuated through power-electronic interconnects. It was found that this concept is very much realisable, but this work did not formulate a general approach to creating these structures.

As an application specific example of multi-layered conductors, reference is made to the work by Luo et al [10]. In this case, the focus was to produce a better design for a busbar filter for a motor drive system. The main issue addressed in this work was that a busbar filter, while good for EMI containment, in general, is not well suited to motor drives because the motor has a much lower switching frequency (typically tens of kHz), whereas the traditional busbar filter will begin attenuation at frequencies closer to the hundreds of kHz. In this case, the proposed solution was to plate the conductors in nickel, giving an effective multi-layered conductor. The key concept in this work was again the use of the skin- and proximity-effects to force the current into low-conductive (nickel) paths. A further example of this use of multi-layered conductors is [8].

Both bodies of work, [6] and [10], required extensive use of 2D-FEM simulations in order to help with the design of these filters. These are very computationally intensive and can generally only be solved at one frequency at a time. Obtaining a frequency response would require many simulations of the same structure at various frequencies, thus adding to the time required to obtain the results. The reason 2D-FEM is required in the work above the difficulty of obtaining an analytical solution for such multi-layered structures. An analytical solution to these structures would drastically reduce the computational time required for simulation. The work by Brink [21] presents a body of work which derives analytical equations and solutions of field distributions to a subset of planar and cylindrical structures, namely those structures in which the equations can be reduced to a one-dimensional problem to a very good approximation. It presents a generalisation to an n-layered conductor as given in Figure 1.6.

A further observation on [6], [8] and [10] is that the work was concerned with complete integration, resulting in multiple simultaneous complex effects arising from this. That is, the integrated structures included inductors, capacitors and resistors, with separation of these components from testing being difficult. The advantage to [21] is that it presents an analytical solution to the resistance and inductance of the multi-layered conductor itself, in isolation. The true advantage to this capability is that it allows for better understanding of how multi-layered conductors behave, and from there can inform decisions in terms of future design of integrated power electronic components.

1.5. Dissertation Breakdown

To place this dissertation in context, Brink's work was geared towards a general approach to the solution of field distributions in a multi-layered conductor and the derivation of frequency dependent impedance equations. The work went as far as to experimentally verify the analytical one-dimensional equations derived, but did not use this theory to characterise multi-layered conductors.

The purpose of this dissertation is to characterise two-layered structures and introduce concepts that can be used as design tools for these conductors. The analytical theory of [21] is used in order to conduct a fairly exhaustive parametric study of two-layer conductors, in terms of the permeability, conductivity, and relative thicknesses of each layer. The study will specifically look at the frequency dependent resistance of the structure, and from this perspective, attempt to obtain an indication of how the physical properties and geometry of the structure contribute to the frequency dependent resistance. This will aid in the understanding of how multi-layered conductors can contribute to power electronic integration; in this case with particular regard to dissipative filters.

Due to the dependence upon [21], it will be discussed in depth in Chapter 2 first and demonstrated how the theory is used in order to conduct the parametric study. Included in this chapter is the proposition of a "successive single-layer approximation" first suggested in [22] and [23]. Further to this, it is shown how the parameter space of the exhaustive parametric study can be reduced; the parameter space in this case being variations in the conductivity, permeability and thickness of each layer. As such, Chapter 2 essentially represents a more in

depth and rigorous discussion of the purpose of this dissertation, with some key insight into the relevance of certain aspects of the problem.

Chapter 3 is dedicated to the parametric study. Throughout this study, the results of each set of parametric variations are presented and discussed thoroughly. To a large extent this chapter represents the characterisation of two-layer structures.

An in depth look into the concept of "successive single-layer approximations" is given in Chapter 4. The purpose here is to show that a set of single layer approximations can be used to isolate approximate frequency/resistance knee-points. An advantage to this is that a rough "sketch" of the frequency response of a structure can be obtained. This particular work will show some interesting results, insights and perspectives on the concept of multi-layered conductors. It will also demonstrate the use of this approximation as a design tool.

An experiment is conducted and the results are presented in Chapter 5. The results will demonstrate some of the conclusions reached in the parametric study of Chapter 3, and will serve to illustrate that the analysis technique used in this dissertation is valid and useful.

Chapter 6 presents the conclusions and gives recommendations of future work. A summarised and graphical outline is given in Figure 1.7.

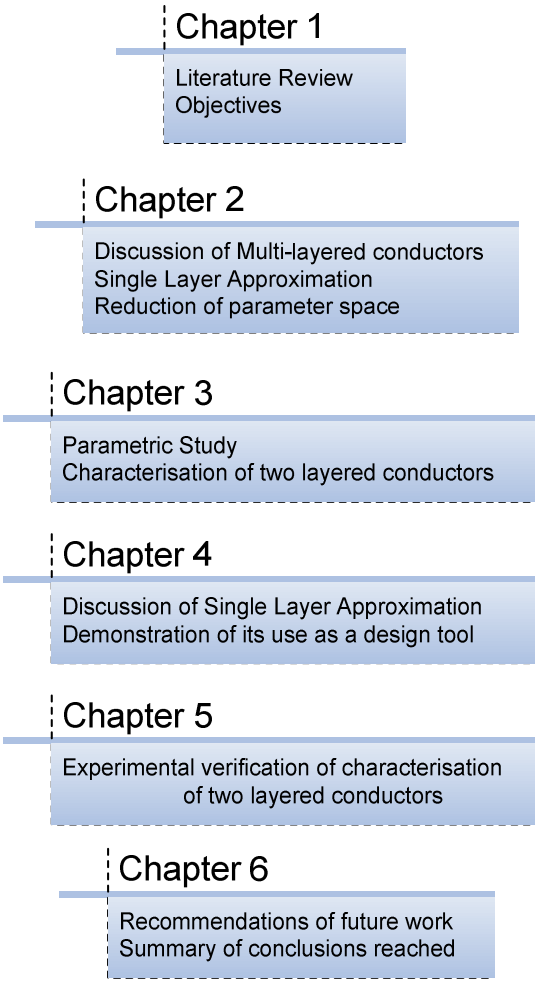


Figure 1.7. Dissertation breakdown

1.6. References

[1] FC Lee and JD van Wyk, "Power Electronics at the dawn of the new millenium - Status and Future," in *IEEE PESC Conference*, Charlseton, NC, 1999, pp. 3-12.

[2] M Gerber and J Ferreira, "A System Integration Philosophy forDemanding Requirements in Power Electronics," in *Inductry Applicaitons Conference*, 2007, pp. 1389-1396.

[3] D Boroyevich et al., "High Density System Integration for Medium Power Applicaitions," in *CPIS*, Nuremburg, 2010.

[4] J Biela et al., "Passive and Active Hybrid Integrated EMI Filters," *IEEE Transactions in Power Electronics*, vol. 24, no. 5, pp. 1340-1349, May 2009.

[5] SJ Marais, JA Ferreira, and JD van Wyk, "Integrated Filters for Switch-Mode Power Supplies," in *30th Inductry Applicaitons Conference*, 1995, pp. 809-816.

[6] Van Wyk et al, "Power Electronic Interconnects: Skin- and Proximity Effect-based Frequency Selective Multi-path Propagation," *IEEE Transactions on Power Electronics*, vol. 20, no. 3, pp. 600-610, May 2005.

[7] R Chen, F Canales, Yang B, and JD van Wyk, "Volumatric Optimal Design of Passive Integrated Power Electronics Module (IPEM) for Distrubuted Power System (DPS) Front -End DC/DC Converter," *IEEE transactions on Inductry Applications*, vol. 41, no. 1, pp. 9-17, January/February 2005.

[8] Munteanu C, Racasan A, Antonescu O Hebedean C, "Technologies to Increase HF Losses in Planer Structures and their limitiations," in *13th International Conference on Optimization of Electrical and Electronic Equipment*, 2012, pp. 48-53.

[9] JT Strydom, JD van Wyk, and JA Ferreira, Electromagnetic Limits of Planar Integrated Resonant/Transformer Structures for Power Electronic Applications, 2000, International Workshop on Integrated Power Packaging.

[10] F Luo et al., "An improved Design for Transmission Line Busbar EMI filter," in *Energy Conversion Congress and Exposition*, 2010, pp. 1232-1238.

[11] A Portolan and IW Hofsajer, "The Analysis and Design of an Inter-Winding Shielding Structure of a High Frequency Transformer," in *IEEE PES Power Africa 2007 Conference and Exposition*, Johannesburg, 2007.

[12] A Racasan, C Munteanu, V Topa, C Pacurar, and C Hebedean, "Minimization of the Equivalent Parallel Capacitance in Planar Magnetic Integrated Structures," in *Optimization of Electrical and Electronic Equipment*, 2012, pp. 219-224.

[13] MB Gerber, IW Hofsajer, and WA Cronje, "Construction and Modelling of a planar multi-layer electromagnetically integrated LCCT component," in *Industry Applicaitons Conference*, 2000, pp. 3044-3050.

[14] PJ Wolmarans, JD van Wyk, CK Campbell, and JD van Wyk jnr, "Technology for Integrated RF-EMI Transmision Line Filters for Integrateed Power Electronic Modules," in *Industry Applications Conference*, 2002, pp. 1774-1780.

[15] JA Ferreira, IW Hofsajer, and JD van Wyk, "Exploiting the Third Dimension in Power Electronics Packaging," in *Applied Power Electronics Conference and Exposition*, 1997, pp. 419-423.

[16] E Waffenscmidt, B Ackerman, and JA Ferreira, "Design Method and Material Technologies for Passives in Printed Circuit Board Embedded Circuits," *IEEE Transactions on Power Electronics*, vol. 20, no. 3, pp. 576-584, May 2005.

[17] R Chen, JD van Wyk, S Wang, and WG Odendaal, "Planar Electromagnetic Integration Technologies for Integrated EMI filters," in *IEEE Industry Applications Conference*, 2003, pp. 1582-1588.

[18] D Boroyevich, "Building Block Integration in Power Electronics," in *International Symposium on Inductrial Electronics*, 2010, pp. 3673-3678.

[19] F Mayer, "Absorptive Low-Pass Cables: State of the Art and an Outlook to the Future," *IEEE Transactions on Electromagnetic Compatibility*, vol. 28, no. 1, pp. 7-17, February 1986.

[20] F Mayer, "Electromagnetic Compatibility: Anti-interference Wires, Cables, and Filters," *IEEE Transactions on Electromagnetic Compatibility*, vol. 8, no. 3, pp. 153-160, September 1966.

[21] E Brink, *Aspects of Electromagnetic Field Distributions in Multipath Conductive Structures*. Ph.D Thesis: University of the Witwatersrand, 2011.

[22] NJ Botes, "Aspects of Computational Electromagnetics for the Treatment of Multi-layer Composite Conductive Structures," University of the Witwatersrand, Lab Project 2011.

[23] FJ Lange, "Aspects of Computational Electromagnetics for the treatment of Multi-layer Composite Conductive structures - Impedance Profile Prediction," University of the Witwatersrand, Lab Project 2011.

Chapter Two-
Problem Structure and Parameter Space

Table of Contents

2.1. Introduction 12
2.2. Process of Describing a Multi-layered Conductor 12
2.2.1. Basic derivation and explanation of electromagnetic equations 12
2.2.2. Example of a two-layer structure 15
2.2.3. Parametric study 16
2.2.4. Limitations 19
2.3. Potential for Single Layer Approximations 19
2.4. Reduction of the parameter space 22
2.4.1. Equivalence between Common- and Differential-Mode Structures 23
2.4.2. Conductor Rescaling 27
2.4.2.1. Proof that conductors can be rescaled 27
2.4.2.2. Demonstration of conductor rescaling 29
2.5. Conclusion 30
2.6. References 31

2.1. Introduction

This chapter deals mainly with the background for modelling and simulating multi-layer conductors. First, details on how a multi-layer conductor is described electromagnetically and how the frequency dependent resistance is calculated are given. This is followed by an example two-layer structure in order to demonstrate how this process is followed. This background theory provides a good basis from which to investigate the effect that each of the parameters has upon the resistance of the structure.

Further to this, this chapter proposes that there is an approximation for these multi-layered conductors in terms of Single-Layer equivalent materials. The reasoning behind this proposal is presented and as such gives reason to why this concept is pursued through the ensuing research. Having pursued this, it will be shown later that this concept presents a tool for the design of multi-layered structures.

Due to the dual direction of investigation, namely the effects of material properties, and the validity of the proposed single-layer approximation, this chapter also addresses the issue of reduction of the parametric space. This will decrease the volume of results that need to be obtained in pursuing these goals. It will be shown that the parametric study can be reduced to consider only differential mode conductors where the thickness of each layer is the same.

2.2. Process of Describing a Multi-layered Conductor

2.2.1. Basic derivation and explanation of electromagnetic equations

A multi-layered conductor is any conductive structure that comprises more than one conductive material. For the purposes of this dissertation, these conductive materials are taken to be layered in a planar form. A further restriction is that all materials are assumed to be linear. This allows for easier modelling of the conductor, and therefore easier derivation of the equations that govern the electromagnetics of multi-layered conductors.

An example of a two layer structure is given in Figure 2.1. Layer 1 is labelled as $\boldsymbol{l_1}$, and layer 2 is labelled as $\boldsymbol{l_2}$. If there were more layers, they would be labelled similarly. Each layer may have its own conductivity, permeability, and thickness. For layer i, in a generalised multi-layered conductor, these material properties are labelled σ_i, μ_i and b_i respectively.

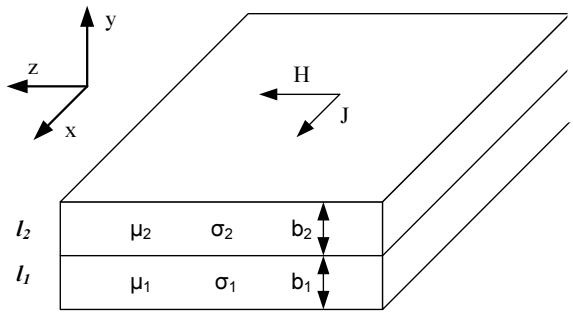


Figure 2.1. Two Layer Structure

Depending upon the current within the conductor and the currents within any conductor nearby, the multi-layered conductor will be subject to the skin- and proximity-effect. These effects affect the distribution of the current within the conductor, as well as the field intensities.

For a planar multi-layer conductor, the Cartesian co-ordinate system is the most convenient choice. For a sufficiently well dimensioned structure, the equations governing the electromagnetic properties of the structure can be approximated fairly accurately to the one-dimensional case [1] [2] [3]. This means that the magnetic field (*H*), electric field (*E*) and current density (*J*) at any point in the structure will only have components in one of the three directions as can be seen in Figure 2.1. The current density and electric field are in the same direction. The typical dimensions necessary for the one-dimensional approximation to be valid is that the width of the conductor be significantly larger than the overall thickness of the conductor. This ratio should be greater than 25:1 [1]. The total length of the conductor should also be very long relative to the other dimensions. Both of these conditions are necessary in order to ignore edge effects, thus allowing a one-dimensional approximation. A further advantage to a long conductor is that the resistance is higher, and therefore easier to measure.

Given that these conditions are met, the structure can be considered to be a semi-infinite strip for the purposes of modelling and shown in Figure 2.2. In other words, the single conductor can be considered to be infinitely wide, infinitely long, but of finite thickness. From this approximation, the equations defining the electromagnetics of the structure are given as (1) to (3) where ω is the angular frequency of excitation. These equations are derived from Maxwell's Equations, and the appropriate application of Faraday's Law and Ampere's Law. The constants *A* and *B* are found through consideration of the boundary conditions of the structure. It should be noticed that each of the fields only has a component in one of the three directions, as denoted by the subscripts in the equations. This simplification comes as a result of the one-dimensional approximation. A more in-depth derivation of these equations is given in Appendix A. The derivation is to a very large extent taken from [1]. The constant *D* is given in (4), where δ is the classical skin-depth. An important observation is that these equations are in the frequency domain.

$$E_x(y) = Acosh(Dy) + Bsinh(Dy) \qquad (1)$$

$$H_z(y) = \frac{D}{j\omega\mu} E_x(y) \qquad (2)$$

$$J_x(y) = \sigma E_x(y) \qquad (3)$$

$$D = (1+j)\sqrt{\frac{\omega\mu\sigma}{2}} = \frac{1+j}{\delta} \qquad (4)$$

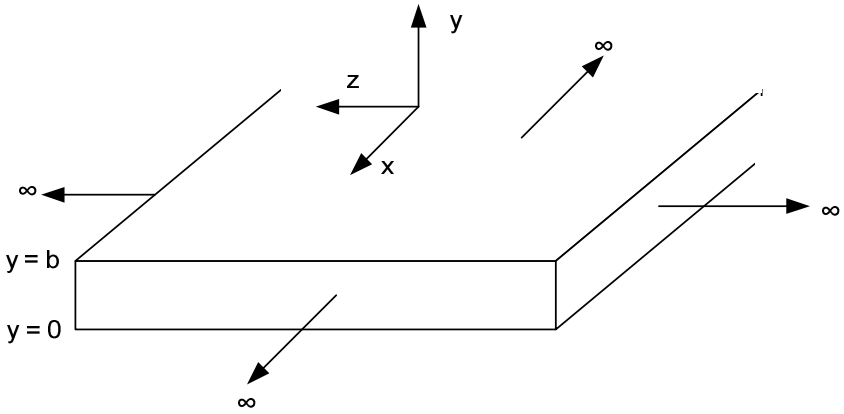


Figure 2.2. Semi-infinite strip

A multi-layered conductor is just a set of single layered conductors. As such, these equations above apply to each layer in any multi-layered conductor since they are analytical derivations based upon a general conductivity, permeability and layer thickness. This is provided that the conductor satisfies the geometrical constraints outlined above. The difference between single-layer and multi-layer conductors is that in the case of the multi-layered conductor, the field at the boundary between successive layers is not known. These can be calculated by enforcing the continuity of the electric and magnetic fields across the boundaries between successive pairs of conductive layers. This enforcement of continuity comes from consideration of Faraday's and Ampere's Laws. Through this enforcement and consideration of the outer boundary conditions, the constants A and B can be solved for each layer. Thus, for any multi-layered conductor, the fields and current density distribution at any given frequency are known. This will be shown in the example given in section 2.2.2.

Two assumptions are necessary in order to compute the fields. The first is that the total current within the conductor is known, as well as the total current within any nearby conductors. The second, but more important assumption is that the nearby conductor is geometrically parallel to the conductor in question and is subject to the same restrictions as the multi-layered conductor in question shown in Figure 2.3. The purpose of the nearby conductor is to be the source of the proximity effect for the conductor in question. For the model and equations to work, it is vitally important that the incident magnetic field sourced from this second conductor be parallel to the conductor in question. Making this assumption is necessary to enforce the restrictions needed on the incident magnetic field. These assumptions apply equally to both the single layer case, and the multi-layer case.

Since this field is dependent only upon the total current within the nearby conductor, the structure of the nearby conductor is unimportant. It may or may not be a multi-layered conductor; the only important restriction on this conductor is that it must satisfy the criteria for a 1D approximation – which requires that this conductor be equal in width to the conductor in question. In terms of experimentation for this dissertation, the nearby conductor will be the same as the conductor in question for the sake of convenience.

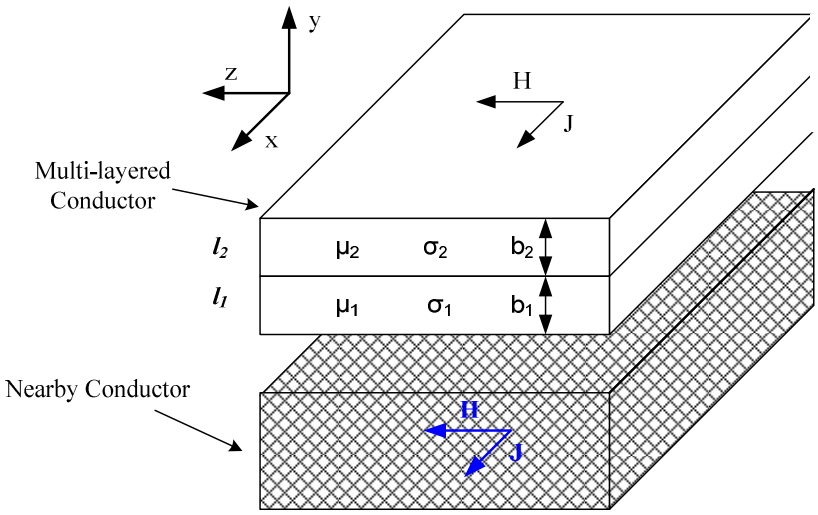


Figure 2.3. Restrictions to be placed on the nearby conductor

The magnetic field intensity at the two outer boundaries is not a function of the material properties. They depend entirely upon the total current within the conductor, as well as the total current in a nearby conductor. Calculation of the boundary conditions is necessary in order to allow computation of the fields. Once these fields are known, it is possible to calculate the frequency dependent resistance. This is done by considering the total power dissipated per unit length by the structure. This is described in (5). The integral is taken across the total thickness of the conductor. Since there are multiple layers, the integral will take the form of a sum of the integrals of the current density in each layer. It is this equation which forms the central basis of the parametric study conducted.

$$R = \frac{width \int_0^{b_1+b_2} |J_x(y)|^2 dy}{I_{Total}{}^2} \qquad (5)$$

2.2.2. Example of a two-layer structure

A two-layer structure of width 25mm is presented to illustrate the procedure discussed above. The properties of the two layers are given in Table 2.1. The current in the conductor is given as I_A= 5A at each frequency. Since the structure is considered under the differential mode, the current in the nearby conductor is I_B = -I_A.

Table 2.1. Example Structure Properties

	Conductivity	Permeability	Thickness
Layer 1 (l_1)	10^5	$20\mu_0$	100μm
Layer 2 (l_2)	10^6	μ_0	100μm

The field distributions are calculated at 1kHz, and at 100MHz in order to demonstrate how the fields change with respect to frequency and are shown on the same set of axes in Figure 2.4 where the layers are labelled according to Figure 2.3. One thing to note is that the electric

field and magnetic field intensity are continuous at 100µm, the boundary between the two layers, at both frequencies. This is necessary because of Faraday's Law and Ampere's Law, and helps verify that the equations have been implemented correctly.

It can quite clearly be seen that the fields "migrate" to one side of the conductor. This is especially relevant in terms of the current density, since it is necessary for the power dissipation equation used in order to calculate resistance. It is quite clear from this figure that the resistance will be higher at 100MHz than at 1kHz since the current is now concentrated in a smaller area of the conductor. Not only that, but the majority of the current is also in layer 1, which has a lower conductivity. This is under differential mode excitation, under common mode the current in both conductors is in the same direction. Because of this, the fields migrate to the other side of the conductor as shown in Figure 2.5. Comparing the 100MHz plot in Figure 2.4 and Figure 2.5, it can be seen that the distributions are not symmetrical. This is because the fields are interacting with different materials in different ways as it migrates across the conductor. It can however be shown that this common mode scenario is equivalent to a differential mode conductor. This will be shown in the following section.

Now that the fields have been computed, the next step is to calculate the resistance of the structure as a function of frequency. This is done by solving for the current density at every given frequency, and then computing the resistance using (5) for each frequency. Figure 2.6 shows the resistance of the structure as a function of frequency. The range is from 100kHz to 100MHz with 10 samples per decade in order to give a reasonably continuous plot. The resistance below 100kHz is effectively DC in this example and is therefore not included.

2.2.3. Parametric study

Calculating this resistance is fairly easy to do since the process uses analytical equations in order to compute the fields. This, as has been described earlier, presents a much easier process than that required by numerical methods and 2D-FEM simulations. The distinct advantage to this is that the process allows for a large number of results to be obtained quickly, and as such lends itself for use in a parametric study. Looking at Figure 2.6 it is quite clear that there are features to the frequency dependent resistance that require explanation, in particular, as annotated, the fact that there are different gradients in the resistance curve as frequency increases.

It will be shown that these features are results of the properties of the materials themselves, and it is the contributions of these materials for which the parametric study, first and foremost, will be used.

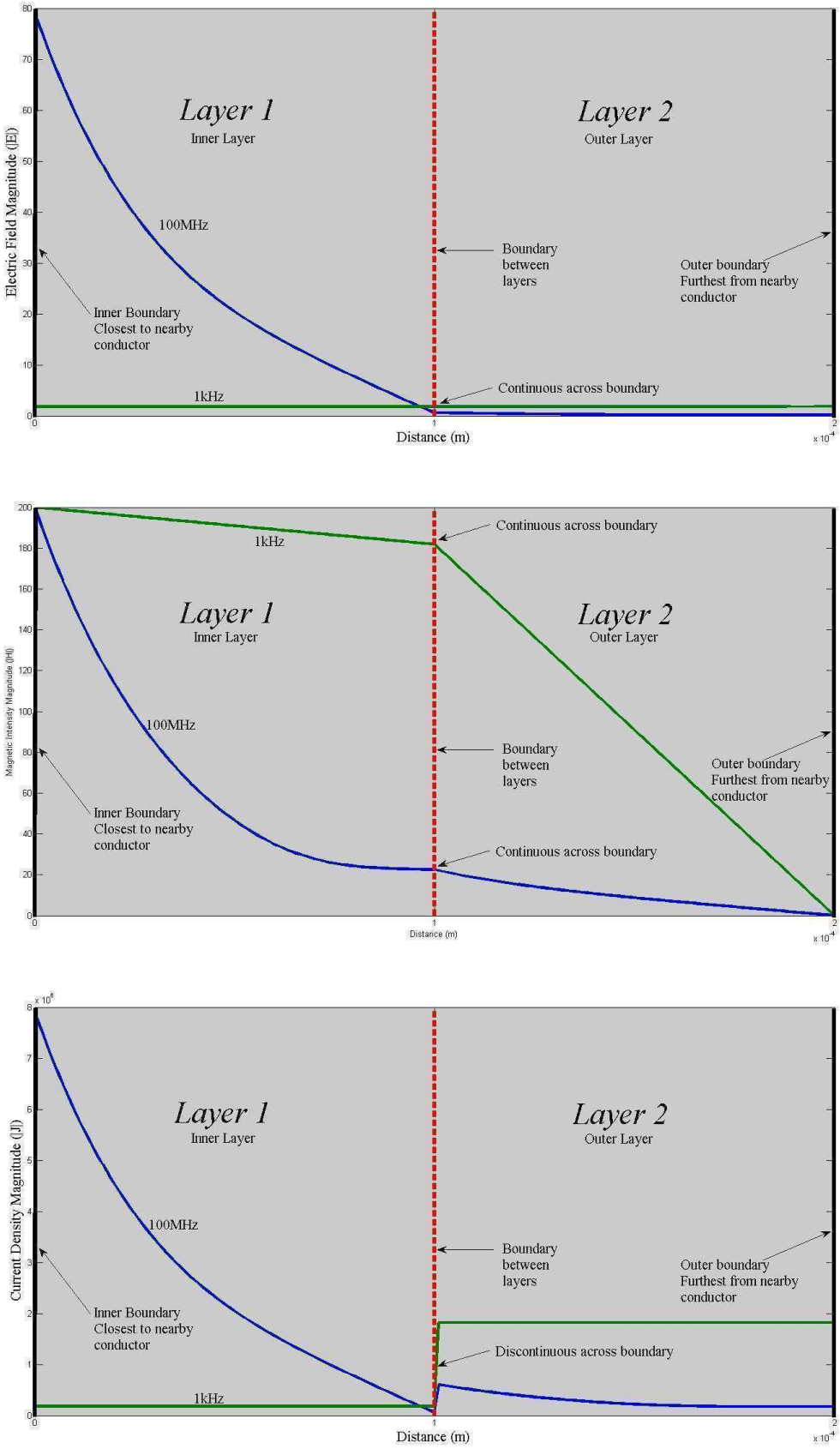


Figure 2.4. Field distributions at 1kHz and 100MHz

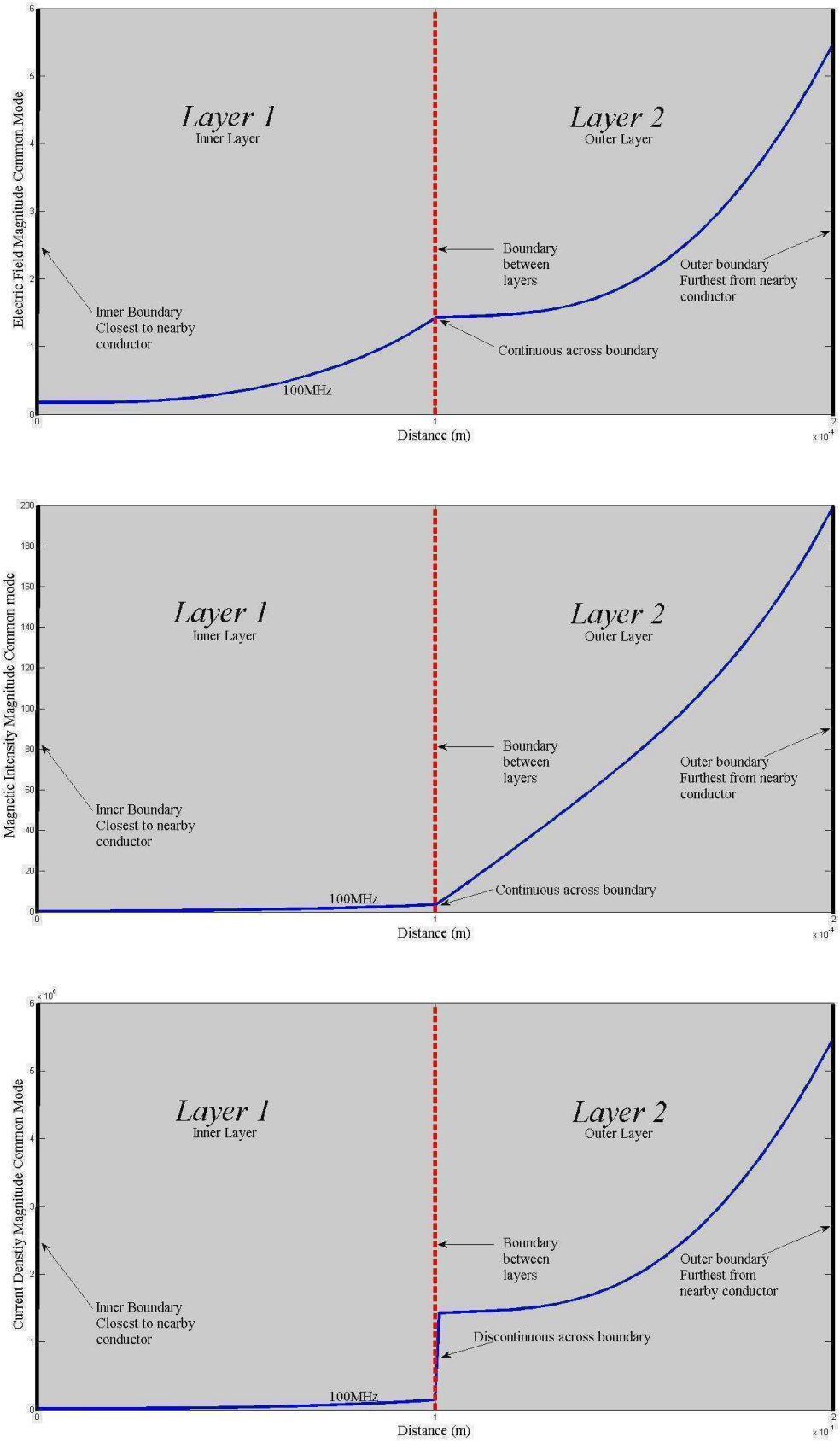


Figure 2.5. Field distributions at 100MHz under Common Mode excitation

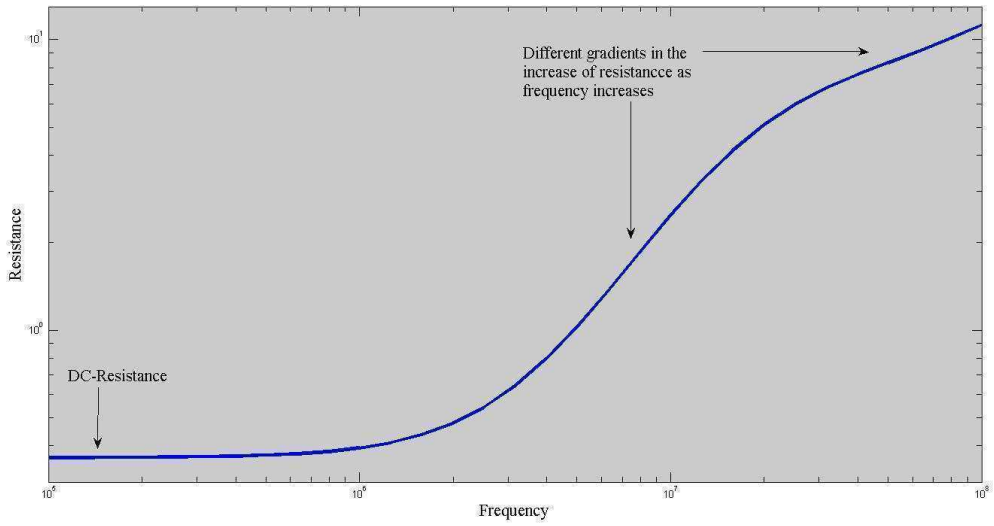


Figure 2.6. Frequency dependent resistance of the example structure [$\Omega.m^{-1}$]

2.2.4. Limitations

It is however important to understand that this particular approximation has limitations, in that it can only model structures that can conceivably be reduced to a one-dimensional scenario. As an example, the experimental work done in [4], cannot be reduced since the two conductors are of different cross-section, and are therefore not the parallel conductors required. However, the conditions do seem to be met by the work of [5], in that the conductors are very long, and the two conductors are of the same dimension and parallel to each other.

2.3. Potential for Single Layer Approximations

For a single layer conductor, the frequency response is well understood. The concept of the skin-depth is particularly useful in this respect. This is given in (6). The frequency, at which the conductor is as thick as the skin depth, can be called the "knee-point" of the resistance curve. The frequency dependent resistance for a single layer conductor of thickness 100µm, conductivity $133x10^5$, and relative permeability 10, is given in Figure 2.7. The frequency at which the skin-depth is equal to 100µm is approximately 190kHz. It can be seen quite clearly in Figure 2.7 that this is roughly where the resistance starts increasing exponentially.

$$\delta = \sqrt{\frac{2}{\omega\sigma\mu}} \qquad (6)$$

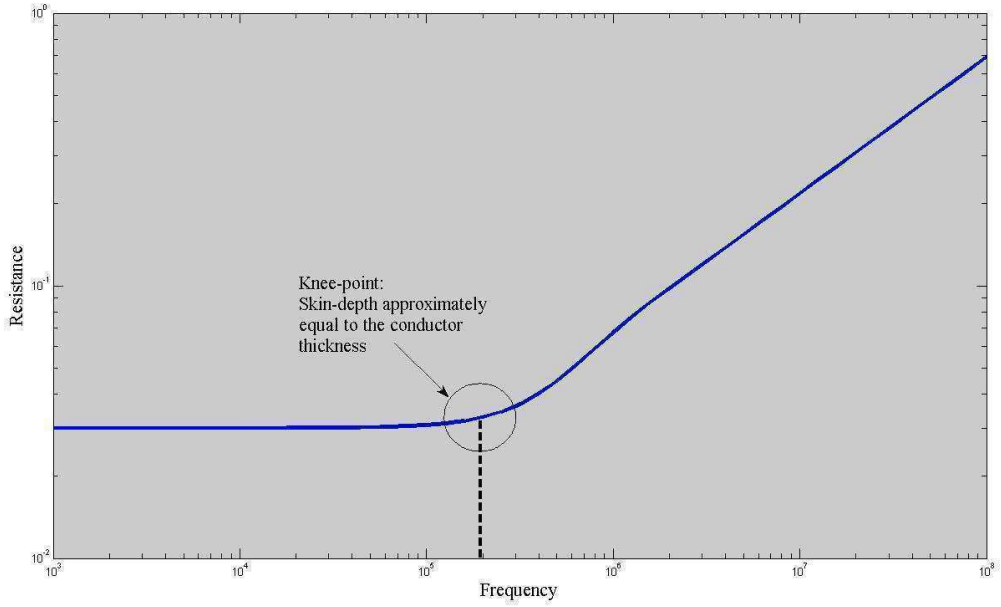


Figure 2.7. Single Layer Frequency dependent Resistance

For a structure with two conductive layers, the skin depth does not have meaning, especially at frequencies at which the current is distributed throughout both layers. This is because of the different material properties. Due to the skin- and proximity-effects, however, the current will, at sufficiently high frequencies, be confined to just one of the layers. This is very similar to the concept presented in [4] in terms of the use of the effect for the sake of dissipative filters. In this case, the skin depth does have meaning simply because the current is only in one layer, which means that effectively there is only a single layer conductor at this point. This asks the question as to whether the concept of skin depth can be generalised to multi-layer conductors. This was addressed in [6] and [7]. A brief discussion of this work is given in the next few paragraphs.

The first observation to make is that at sufficiently low frequencies, the resistance of a two layer structure is essentially constant and is given by (7). In a concept similar to that used to calculate the RMS of a signal, it is possible to calculate what the effective conductivity of a *single layer* conductor of the same thickness should be in order to produce the *same* DC resistance. The effective conductivity for a general two-layered conductor is given in (8). It can be seen that the denominator of (7) is the numerator of (8). The question that requires answering now is whether this can also be applied to the permeabilities, and if so, what form this approximation should take.

The proposed form for the permeability transformation is analogous to that for the conductivities and is given in (9). The average (8) gives a material which has the same effective DC resistance as the composite material, while the average (9) in conjunction with (8) helps define the skin-depth and knee frequency of this new approximated conductor.

It is expected that this equivalent material will show a similar increase in resistance at approximately the same frequency as that of the composite. It should be emphasised that

what has effectively been done here is to define an imaginary homogenous conductor whereas a multi-layered conductor is specifically a real non-homogenous structure composed of a stack of homogenous layers. This idea will be followed throughout the parametric study, and explored in more detail later. This will serve to justify whether it is in fact possible to model a multi-layered conductor as a set of single-layer approximations and, if so, to what extent. As such, it will be possible to evaluate this technique's value as a design tool.

$$R_{DC} = \frac{width}{\sigma_1 b_1 + \sigma_2 b_2} \quad (7)$$

$$\sigma_{eq} = \frac{\sigma_1 b_1 + \sigma_2 b_2}{b_1 + b_2} \quad (8)$$

$$\mu_{eq} = \frac{\mu_1 b_1 + \mu_2 b_2}{b_1 + b_2} \quad (9)$$

Since the current density migrates in one direction – i.e. towards the boundary of the conductor – as a function of frequency, there are two single-layer approximations for a two layer structure. The logic behind this is that the current successively leaves the outermost layers due to the proximity effect. This can be seen in Figure 2.8 where the current density from Figure 2.4 has been reproduced for convenience. At low frequencies, the current is in both layers, and so they both contribute to an approximation. At sufficiently high frequencies, the current is mostly in the inner layer, resulting in the second approximation with only a contribution from the inner layer itself. Each of these equivalent materials will have its own knee-frequency, and it is hypothesised that they serve as an approximation of the resistance of the composite conductor. The knee frequency of each successive approximation will be higher than that of the previous layer. This is clear because the effective thickness of the conductor decreases, which naturally causes a higher knee-frequency to be expected.

Figure 2.9 demonstrates the resistance of a two layer structure and on the same set of axes is given the resistance of the two equivalent single layer conductors. These equivalent conductors were calculated using the approximation directly. It can be seen that at low frequencies, the resistance of the composite converges upon the resistance of the first approximation; while at high frequencies, the composite converges on the second approximation. This suggests that the approximation technique is in fact possible, and as such warrants exploration in the parametric study.

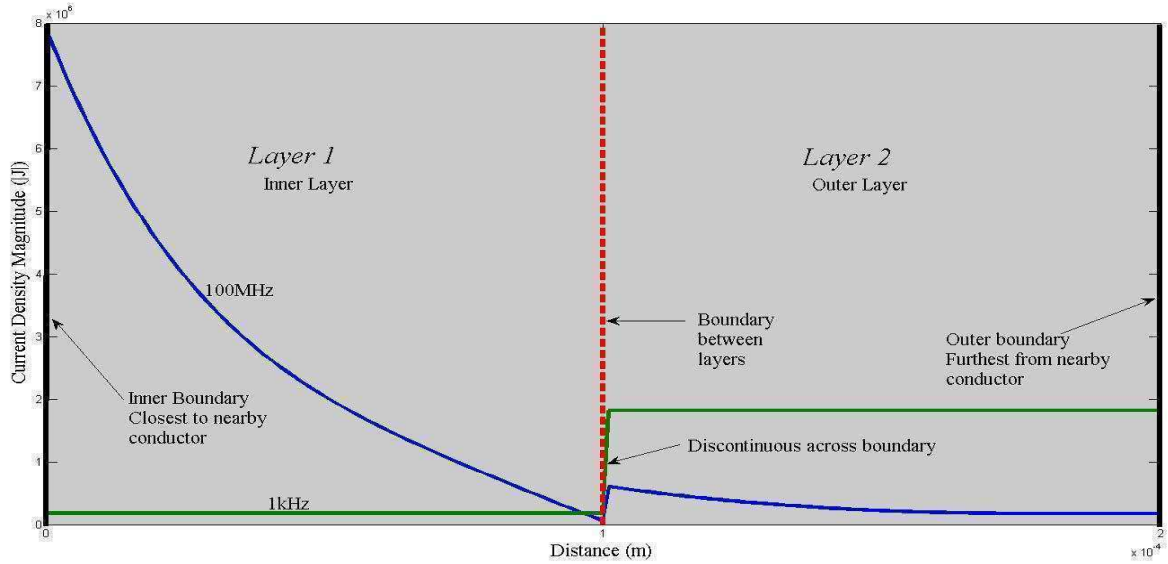


Figure 2.8. Current density distributions at 1kHz and 100MHz

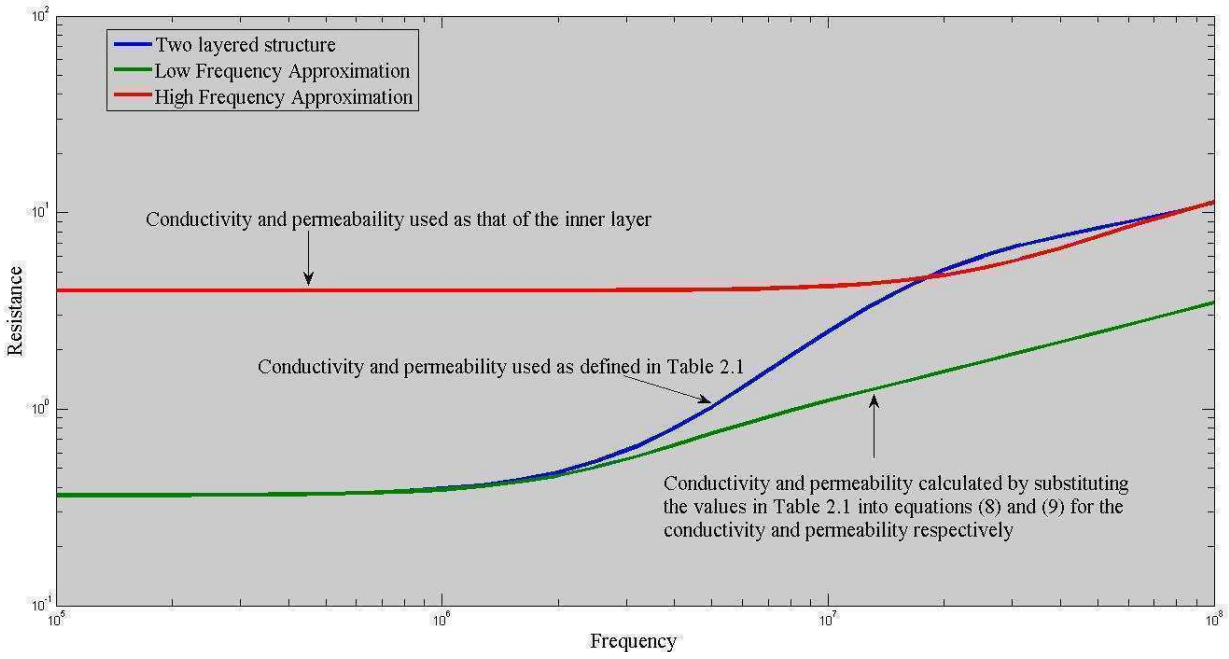


Figure 2.9. Demonstration of the single layer approximation

2.4. Reduction of the parameter space

As laid out above, the objectives of the parametric study are twofold. Firstly, it seeks to characterise the effects that each material property has upon the frequency dependent resistance. Secondly, it needs to verify the validity of the single layer approximation. For every two layered structure, there are six material properties (conductivity, permeability and thickness for each layer), each of which can be varied continuously. Further to this, the structure can be placed under both common-mode and differential-mode scenarios.

Because of the two objectives, it is possible that simulation across the entire parameter space will become intractable. It would be ideal if the parameter space could be reduced, but importantly, in such a way that key features are not lost. This section shows two ways in which this can be done. The first is to demonstrate that common-mode and differential-mode excitation is equivalent, resulting in restriction to just the differential mode. The second is to demonstrate that conductors can be rescaled but provide the same response, which results in restricting the study to structures which have layers of the same thickness.

2.4.1. Equivalence between Common- and Differential-Mode Structures

The purpose of the ensuing discussion is to demonstrate that there is an equivalence between the responses of multi-layered structures under common and differential mode excitation. This equivalence is through an effective geometric transformation. As this equivalence is shown to be true, it is possible to restrict attention in the parametric study to just structures under differential mode excitation. This gives the advantage of reducing the problem size, since every parametric curve produced, is representative of two possible structures under different excitation. In other words, every differential mode structure is exactly representative of *a* common mode structure. Furthermore, the geometry of this common-mode structure is defined through the geometry of the differential-mode structure.

The key difference between these two configurations lies in the boundary conditions. As said previously, the value of the boundary condition depends only upon the total current within the conductor, and in any nearby conductor. It does not depend upon the material properties. For the purpose of this discussion, as in every discussion in this dissertation, attention is restricted to the condition that there is only the conductor in question and one other nearby conductor. It is best to consider the boundary conditions as a sum of the boundary magnetic fields set up by each conductor individually.

In the first conductor – the conductor in question – the boundary field along the two planar edges will be equal in magnitude but opposite in direction. This is due to Ampere's Law, where we also ignore the magnetic field along the smaller edges of the conductor since they do not form a part of the one-dimensional approximation. In the nearby conductor, the boundary field along the two planar edges of the conductor in question will be the same in both magnitude and direction; this is due to the semi-infinite flat approximation (the field cannot attenuate with distance since the conductor is approximated as an infinite plate). Figure 2.10 demonstrates the directions of the boundary fields given by both conductors under the common mode condition. Here, H_1 is defined as the outer boundary magnetic field intensity, and H_0 is defined as the inner boundary magnetic field intensity. The a and b subscripts represent the contribution to the magnetic field intensity from I_a and I_b respectively. It is clear that the fields at the inner boundary will subtract, while the fields at the outer boundary will add. In the case of the differential mode case, illustrated in Figure 2.11, it is clear that the opposite is true. The fields will cancel at the outer boundary, while they will add at the inner boundary.

Equations to describe the value of the boundary conditions are given as (10) and (11), the derivation for which can be found in Appendix A as well. An important observation here is

that for the sake of consistency in these equations, the currents I_a and I_b are defined as positive in the same direction. It is clear that the difference between the common mode and differential mode manifests itself as an effective swapping of the two boundary conditions. It is worth re-iterating that these boundaries are independent of the properties of the multi-layer conductor.

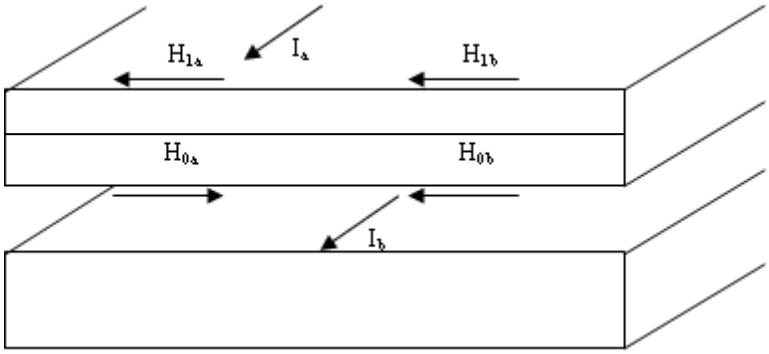


Figure 2.10. Boundary conditions as given by the two conductors in common mode

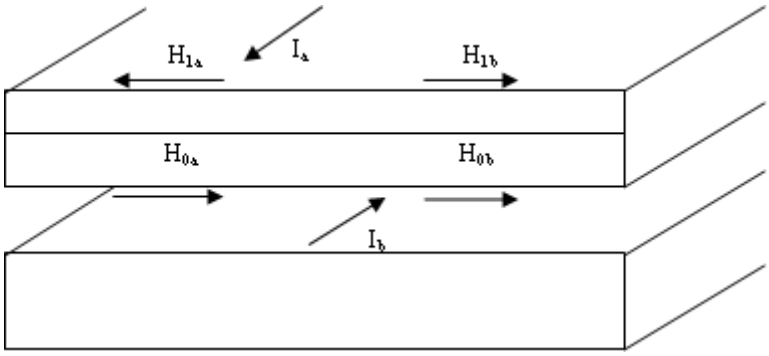


Figure 2.11. Boundary conditions as given by the two conductors in differential mode

$$H_1 = \frac{1}{2w}(I_b + I_a) \qquad (10)$$

$$H_0 = \frac{1}{2w}(I_b - I_a) \qquad (11)$$

The way in which the resistance changes with frequency does however depend upon the material properties, as well as the boundary conditions. So, for a given structure, it will have a different response under common mode and differential mode excitation. This is because each boundary condition interacts with a different material and its respective properties, naturally causing a different response. The conductor in question does not, however, "know" how these boundary conditions are created. It has a given response based on *what* the boundary conditions are, and not on *how* the boundary conditions are created. In order to demonstrate this point, compare Figure 2.10 with Figure 2.12. It is clear that the boundary conditions of the conductor in question are the same in both figures. However, Figure 2.10 shows a common mode configuration while Figure 2.12 shows a differential mode configuration. Since the conductor in question is subjected to the same boundary conditions in both cases, it is the *same* multi-layered conductor in both cases, and as such, it will have the same response.

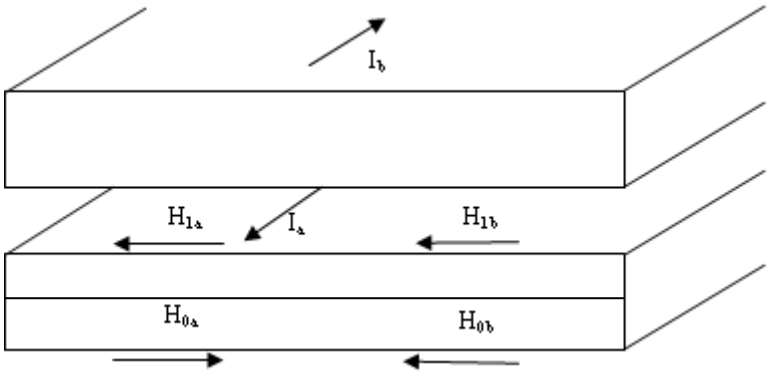


Figure 2.12. Comparison of differential and common mode structure

For the sake of consistency, it is desirable to either always have the conductor in question above, or below the nearby conductor. For the sake of this research, the conductor in question will always be assumed to be above the nearby conductor as in Figure 2.11. In order to bring the structure in Figure 2.12 in line with this convention, the entire figure must be reflected. As such, it becomes clear that a differential mode structure is equivalent to a common mode structure where the layers have been reversed in order. This may become clearer in a notational description.

The response of a multi-layered conductor shall be defined as (12), physically representing the multi-layered portion of Figure 2.3, reproduced for convenience in Figure 2.13 and including the current within the two conductors, where $\boldsymbol{l_1}$ and $\boldsymbol{l_2}$ are placeholders representing the conductivity, permeability and thickness of layers 1 and 2 respectively. Successive layers are successively further away from the inner boundary where the nearby conductor is situated. The equivalence between common-mode and differential mode structures can be succinctly described (13). This can be further reduced with the addition of some notation (14) which perhaps makes the equivalence between the common mode and differential mode clearer. I_a and I_b represent the currents in the conductor in question, and the nearby conductor respectively. A generalisation is given as (15). In conclusion, it is not necessary to simulate a structure under both common and differential excitation since the response is exactly that of a transposed structure. The parametric study thus is reduced to half the number of possible structures and excitation modes.

It is interesting to note that (13) applies even when there is a mixture of common- and differential-mode currents present in the system. Substituting the currents as indicated on each side of (13) into (10) and (11) results in boundary values that have effectively been switched. Again, it is this switching, in conjunction with the switching of layers that produces the equivalence between common- and differential-mode structures.

$$\boldsymbol{M}(\boldsymbol{l_1}, \boldsymbol{l_2}, I_a, I_b) \qquad (12)$$

$$\boldsymbol{M}(\boldsymbol{l_1}, \boldsymbol{l_2}, I_a, I_b) = \boldsymbol{M}(\boldsymbol{l_2}, \boldsymbol{l_1}, I_a, -I_b) \qquad (13)$$

$$\boldsymbol{M_{DM}}(\boldsymbol{l_1}, \boldsymbol{l_2}) = \boldsymbol{M_{CM}}(\boldsymbol{l_2}, \boldsymbol{l_1}) \qquad (14)$$

$$\boldsymbol{M_{DM}}(\boldsymbol{l_1}, \boldsymbol{l_2}, \dots, \boldsymbol{l_n}) = \boldsymbol{M_{CM}}(\boldsymbol{l_n}, \boldsymbol{l_{n-1}}, \dots, \boldsymbol{l_1}) \qquad (15)$$

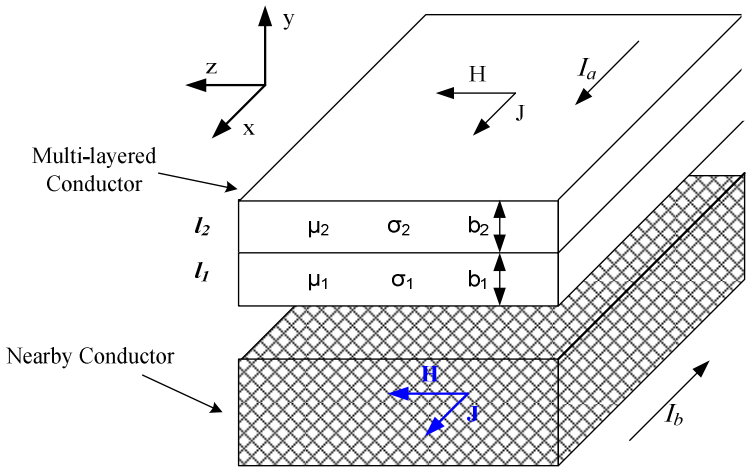


Figure 2.13. Two Layer Structure

Implicit within this discussion is that in order to create a structure that has the same response under both common and differential mode, it needs to be symmetrical. In other words, the reversal of the layers must give the exact same structure as before the reversal. This is only possible for structures with an odd number of layers. The reason is that a symmetrical even-layered structure must, by definition, have its centre two layers as the same material. This is equivalent to a single layer of that material, just twice the thickness and thus reduces to an *n-1* layered structure – which is odd. Figure 2.14 shows a structure which will have the same common and differential mode responses, which is again, as always subject to the same restrictions as before. From (14)

$$\boldsymbol{M_{DM}(l_1, l_2, l_3) = M_{CM}(l_3, l_2, l_1)}$$

But l_1 is identical to l_3 and so

$$\boldsymbol{M_{DM}(l_1, l_2, l_1) = M_{CM}(l_1, l_2, l_1)}$$

And because the arguments are the same here, it is clear that the common- and differential-mode responses will be the same.

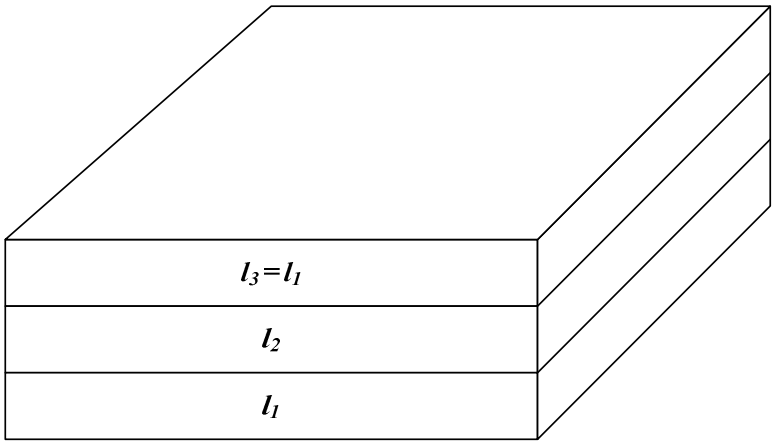


Figure 2.14. Structure with the same common and differential mode response

2.4.2. Conductor Rescaling

2.4.2.1. Proof that conductors can be rescaled

In this section, it is proved that for a given conductor with its material properties, a thicker (or thinner) conductor with its conductivity and permeability suitably scaled will produce the exact same frequency dependent resistance. This dissertation contribution will be used in subsequent chapters for the sake of reducing the number of simulations that need to be done.

Consider two conductors *A* and *B* of the same width *w*, but with their own respective properties (shown in cross-section in Figure 2.15):

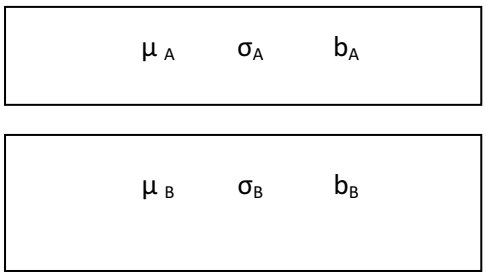


Figure 2.15. Two different conductors

Assume, however, that the total current within the conductor is known (I_T) and that the conductors conform to the following restrictions:

$$\mu_B = \alpha\mu_A\,; \qquad \sigma_B = \alpha\sigma_A \qquad and \qquad \alpha = \frac{b_A}{b_B}$$

Where α may be any positive value. When there is no externally applied field (in other words, the pure skin effect), the current density in each of these conductors is given by:

$$J_A(y) = \frac{I_T}{2w}\frac{D_A}{sinh(D_A y)}[\cosh(D_A y) + \cosh\,(D_A(y - b_A))]$$

$$J_B(y) = \frac{I_T}{2w}\frac{D_B}{sinh(D_B y)}[\cosh(D_B y) + \cosh\,(D_B(y - b_B))]$$

Where

$$D_i = \frac{1+j}{\delta_i} \text{ and } \delta_i = \sqrt{\frac{2}{\omega\mu_i\sigma_i}}$$

Since $\frac{I_T}{2w}$ is a constant and is a scaling factor in both current densities it will be ignored.

Applying the above assumptions, it can be shown that

$$\delta_A = \alpha\delta_B$$

And that therefore

$$D_B = \alpha D_A$$

The power dissipated in the first conductor is given as

$$P_A = \frac{1}{\sigma_A}\int_0^{b_A} |J_A(y)|^2 dy$$

And the power dissipated in the second conductors is given as

$$P_B = \frac{1}{\sigma_B}\int_0^{b_B} |J_B(y)|^2 dy$$

$$P_B = \frac{1}{\sigma_B}\int_0^{b_B} \left|\frac{D_B}{sinh(D_B y)}[\cosh(D_B y) + \cosh\left(D_B(y - b_B)\right)]\right|^2 dy$$

$$P_B = \frac{1}{\alpha\sigma_A}\int_0^{b_B} \left|\frac{\alpha D_A}{sinh(\alpha D_A y)}\left[\cosh(\alpha D_A y) + \cosh\left(\alpha D_A(y - b_A)\right)\right]\right|^2 dy$$

$$P_B = \frac{1}{\alpha\sigma_A}\int_0^{b_B} \left|\frac{\alpha D_A}{sinh(\alpha D_A y)}[\cosh(\alpha D_A y) + \cosh(\alpha D_A y - D_A b_A)]\right|^2 dy$$

Applying the substitution

$$Y = \alpha y$$

The following is obtained

$$P_B = \frac{1}{\alpha\sigma_A}\int_0^{\alpha b_B} \left|\frac{\alpha D_A}{sinh(D_A Y)}[\cosh(D_A Y) + \cosh(D_A Y - D_A b_A)]\right|^2 \frac{dY}{\alpha}$$

Since α is a constant it can be taken out of the integral completely, resulting in

$$P_B = \frac{1}{\sigma_A}\int_0^{b_A} \left|\frac{D_A}{sinh(D_A Y)}\left[\cosh(D_A Y) + \cosh\left(D_A(Y - b_A)\right)\right]\right|^2 dY$$

$$P_B = \frac{1}{\sigma_A}\int_0^{b_A} |J_A(Y)|^2\, dY$$

With the final result being that

$$P_A = P_B$$

Since they have the same power dissipation, they have the same resistance at every frequency, thus showing that the two conductors are equivalent under the assumptions laid out above.

The same argument applies when the conductors are placed under external excitation only (pure proximity effect in this case), as well as to the combination of the two effects.

This means that it is in fact possible to eliminate one of the properties of the conductors from affecting the simulations. The result above shows that this can be done. For a given two layer structure, it is possible to transform one of the layers such that one of its properties becomes equal to the corresponding property of the second layer. This would be done by solving for α.

A relationship between these conductors is as follows

$$\mu_B b_B = \mu_A b_A \qquad \sigma_B b_B = \sigma_A b_A$$

Each of these four terms will be called the "total permeability" and "total conductivity" of their respective layers. Because of this proof, any conductor with the same total permeability and total conductivity as a different conductor, will have the exact same effect on the response of the structure.

2.4.2.2. Demonstration of conductor rescaling

Taking the same structure given in the example given in section 2.2.2 to demonstrate how solving for the resistance would be carried out, the properties of which are given here again in Table 2.2. If, for arguments sake, there was a desire to simulate the structure such that the conductivities were the same but not change the response of the structure, solving for the value of α as defined in the proof above is required.

Table 2.2. Material properties of a specified two layer structure

	Conductivity	Permeability	Thickness
Layer 1	10^5	$20\mu_0$	100μm
Layer 2	10^6	μ_0	100μm

What is wanted can be shown graphically in Figure 2.16 (not to scale), such that $\sigma'_2 = \sigma_1$ but without changing the overall response of the structure. As such in this case, the value for α that is needed is given by $\sigma'_2 = \alpha\ \sigma_2$ which gives α = 0.1. By applying this to the other properties, the following values are derived: $\mu'_2 = \mu_0/10$ and $b'_2 = 1\text{mm}$. It should be emphasised here that it is not an issue for now that the derived permeability is less than μ_0. All that is being shown here is that it is possible to mathematically change the properties of a conductor but achieve the same response. The response of the initial structure and that of the transformed structure are given in Figure 2.17. The two responses are exactly the same, and so it is not possible to distinguish between them in the figure.

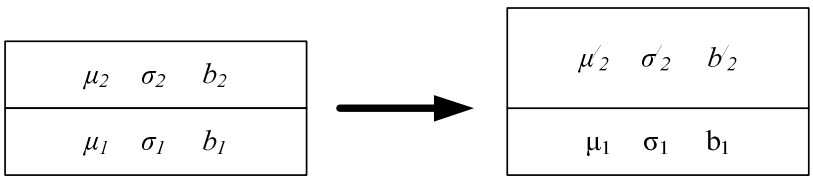


Figure 2.16. Graphical representation of the transformation

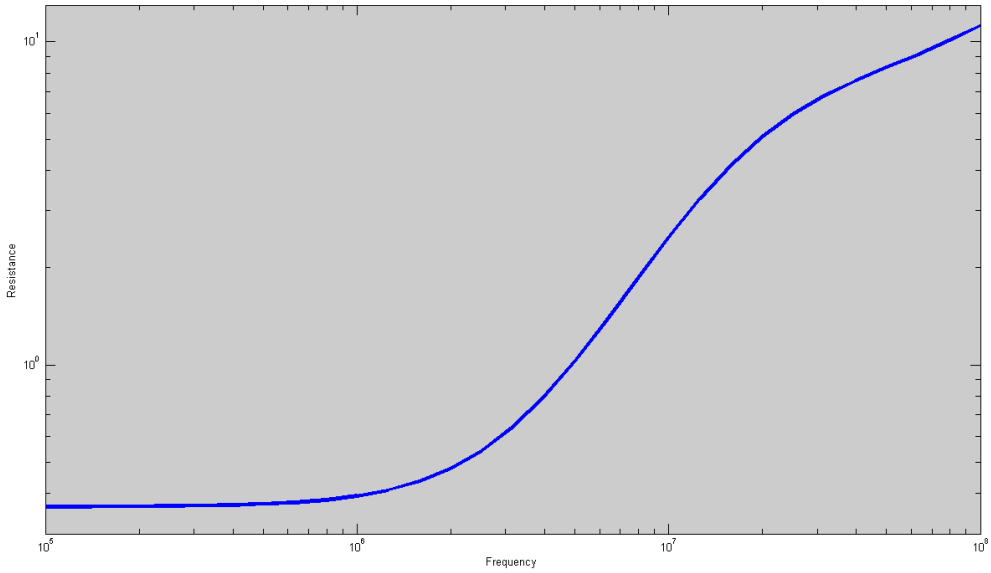


Figure 2.17. Demonstration of conductor transformation

Now that it is clear that conductors can be rescaled, the parametric study does not need to include simulations which vary the thickness of the layers. The reason for this is that a layer can always be rescaled in order to give an exactly equivalent conductor with the same thickness as the second layer.

2.5. Conclusion

This chapter has presented the concept of how the field distributions within a multi-layered conductor are mathematically modelled. It has also been demonstrated how to use this model to simulate a two-layered structure in order to obtain a frequency dependent resistance. This has been done analytically and as such reduces calculation time. Having demonstrated this process, it is now possible to conduct a parametric study in order to gain insight into the behaviour of the resistance of two-layer conductors as a function of the material properties. In conjunction with this, it has been proposed that it is possible to use an equivalent single layer approximation of the two layer conductor to model the low frequency, and high frequency resistance of the composite, with approximations of the knee-frequencies.

With regard to the parametric study, the equivalence between common and differential mode conductors has been presented and as such, halves the parameter space. In addition to this, the rescaling of conductors demonstrated above means that the parameter space is again effectively halved because there is now no need to simulate changes in thickness. This equivalence may present itself as a useful design tool. This is explored in Chapter 4.

2.6. References

[1] E Brink, *Aspects of Electromagnetic Field Distributions in Multipath Conductive Structures*. Ph.D Thesis: University of the Witwatersrand, 2011.

[2] PL Dowell, "Effects of Eddy Currents in Transformer Windings," *Proceedings of the IEEE*, vol. 113, no. 8, August 1966.

[3] R L Stoll, *The Analysis of Eddy Currents*.: Oxford University Press, 1974.

[4] Van Wyk et al, "Power Electronic Interconnects: Skin- and Proximity Effect-based Frequency Selective Multi-path Propagation," *IEEE Transactions on Power Electronics*, vol. 20, no. 3, pp. 600-610, May 2005.

[5] F Luo et al., "An improved Design for Transmission Line Busbar EMI filter," in *Energy Conversion Congress and Exposition*, 2010, pp. 1232-1238.

[6] NJ Botes, "Aspects of Computational Electromagnetics for the Treatment of Multi-layer Composite Conductive Structures," University of the Witwatersrand, Lab Project 2011.

[7] FJ Lange, "Aspects of Computational Electromagnetics for the treatment of Multi-layer Composite Conductive structures - Impedance Profile Prediction," University of the Witwatersrand, Lab Project 2011.

Chapter Three – Parametric Studies of Two-Layer Structures

Table of Contents

3.1. Introduction....33
3.2. Variations in σ_1....34
3.3. Variations in σ_2....37
3.4. Variations in μ_1....39
3.5. Variations in μ_2....41
3.6. Analysis of parametric study conclusions....43
3.7. Conclusion....46
3.8. References....47

3.1. Introduction

In this chapter the results of a parametric study of two layer structures is presented. For a two layer structure there are six parameters that can be varied in total. These are the permeability, conductivity and thickness of each of the layers. As previously discussed, it was decided to keep the thicknesses of each of the layers equal and constant throughout the study.

The reason the layers are kept constant is because a multi-layered conductor is scalable, the layers are kept equal in thickness because of conductor rescaling discussed in Chapter Two. It is important to emphasise here that there is a difference between the scalability of a two layered conductor, and the concept of "conductor rescaling". Scalability in this case refers specifically to increasing the size of the conductor as a whole. In other words, if the structure is made bigger but with the same materials, the response will look the same but will be shifted in frequency and DC resistance. This effectively means that the structure can be normalised to a chosen structure dimension, and as such the layers can be kept constant. Conductor rescaling, on the other hand, refers to modifying the dimensions and properties of a *single* layer such that the overall response remains exactly the same. This means that a conductor's properties can always be rescaled to have the same thickness as the other layer.

By keeping the layer thicknesses restricted, it is easier to obtain information about how each of the other 4 material properties affects the resistance of the structure. Each set of parametric studies is based off an initial set of parameters as laid out in Table 3.1.

In each set of simulations, three of the four parameters are kept constant while the fourth is varied. Each set of calculations is presented in the same way as shown in the annotated example of Figure 3.1. From the previous chapter, a single layer approximation was proposed and that for a two layer structure there are two approximations possible. Each different scenario within a calculation set is presented on the same set of axes as its two proposed single-layer approximations. Each proposed approximation has its own knee-point (related to the skin-depth) which is shown in the figure. This set of calculations is then followed by a figure with the frequency responses of each real structure in order to extract a trend that demonstrates the effect that the specific parameter has upon the frequency response. In every set, there is a plot which seems to only have two lines. This corresponds to the point at which both layers have the exact same three properties' values. What this means is that the low-frequency approximation returns unmodified equivalent parameters, and as such, will track the real structure's response exactly.

All simulations were conducted in Wolfram Mathematica 9, while all figures were created using MATLAB R2008b.

Table 3.1. Initial values of parameters for the parametric study

Parameter	Value
μ_1 and μ_2	$10\mu_0$
σ_1 and σ_2	13.3×10^6
b_1 and b_2	$50\mu m$

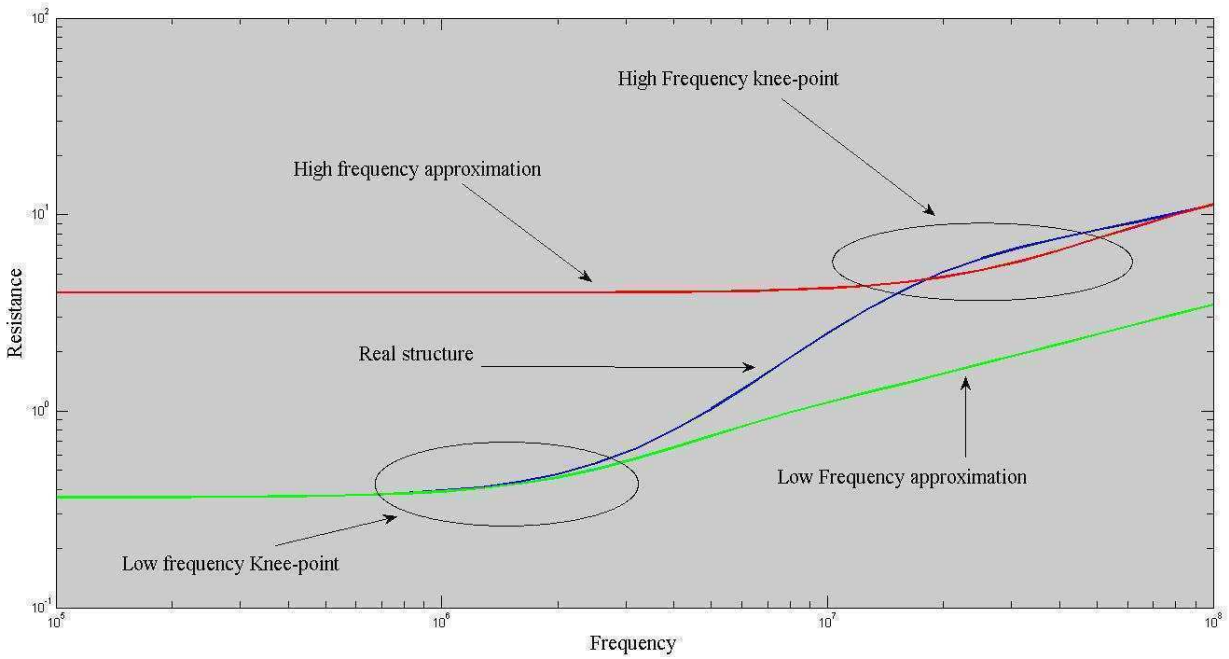


Figure 3.1. Annotated resistance plot of parametric study

3.2. Variations in σ_1

In this case, the parameters are as set out in Table 3.1, with variations in σ_1.

$$\sigma_1 \in \{\sigma_2/20;\ \sigma_2/10;\ \sigma_2/5;\ \sigma_2/2;\ \sigma_2;\ 2\sigma_2;\ 5\sigma_2;10\ \sigma_2;\ 20\sigma_2\}$$

Figure 3.2 shows each case in the form of Figure 3.1. The two single layer approximations converge well upon the multi-layered conductor. The high frequency approximation converges upon the two-layered conductor at high frequency, while the low frequency approximation converges upon the DC resistance. The knee-points in this case are in reasonable agreement. Figure 3.3 shows the resistance of each of the structures on the same set of axes. With lower layer 1 conductivities, the DC resistance increases, as expected.

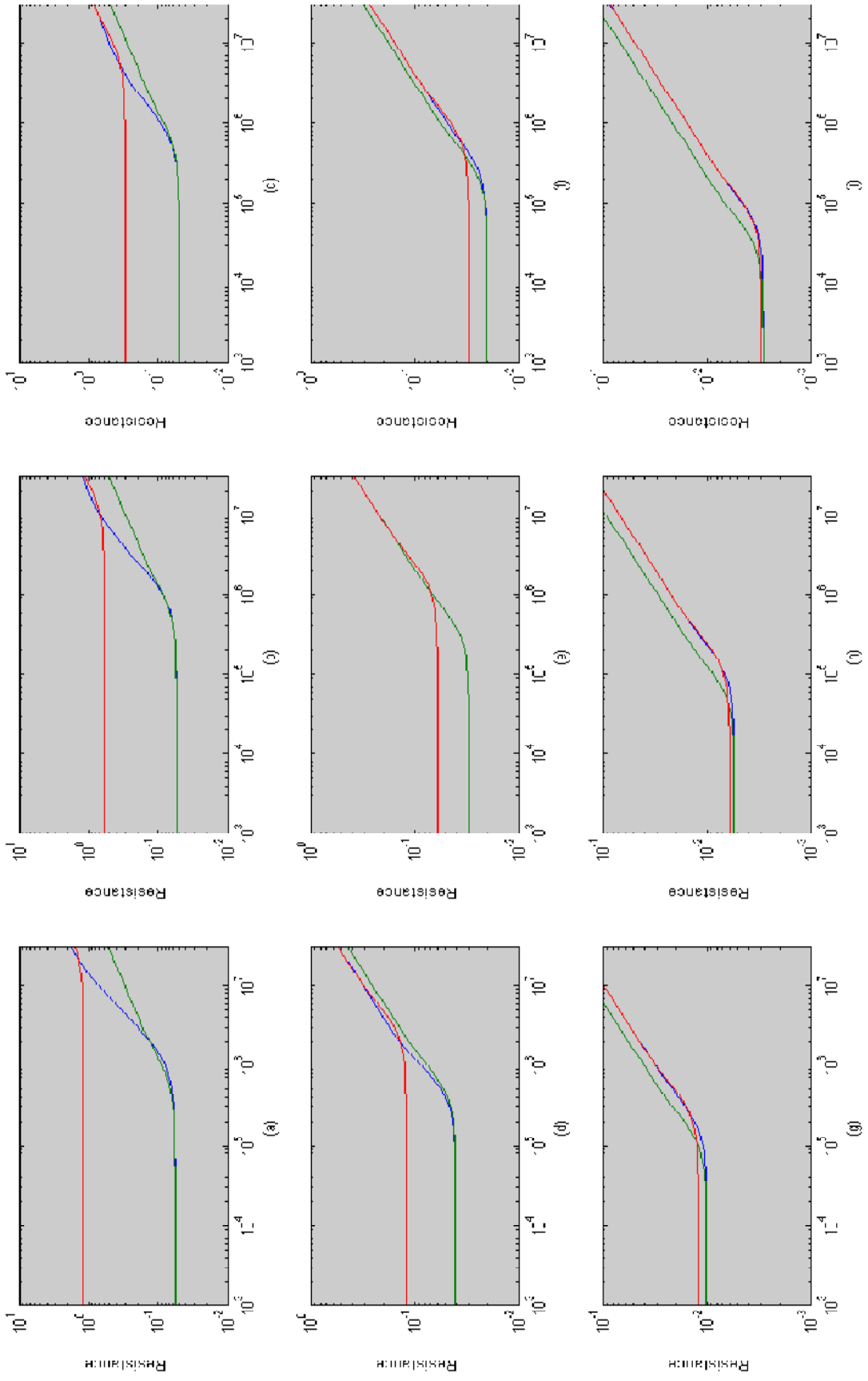


Figure 3.2. Parametric variation of σ_1, with single layer equivalent

Attention is drawn to the fact that some of the frequency responses intersect each other as indicated in the figure. Between the two frequencies indicated the curve with the higher conductivity actually has a resistance higher than that of a structure with a "worse" conductor in it. It was suggested in [1] that there is a maximum resistance achievable with respect to σ_1, analytically verified here. This is a justified conclusion because from the figure, the resistance at 600kHz increases as conductivity decreases until curve *(a)*. By the time the conductivity has reached that of *(b)* it is back to this same resistance. Therefore there must be a maximum resistance at a conductivity between those of *(a)* and *(b)*. This can be rationalised as follows. The conductivity of *(b)* is so low that the current is forced to stay in the second layer for higher frequencies and as such, the increase in resistance happens later (with respect to frequency). Figure 3.4 shows how the resistance of the structure changes with respect to σ_1, where σ_1 has been normalised by σ_2. As suggested, the maximum resistance does in fact occur between the two conductivities identified in Figure 3.3.

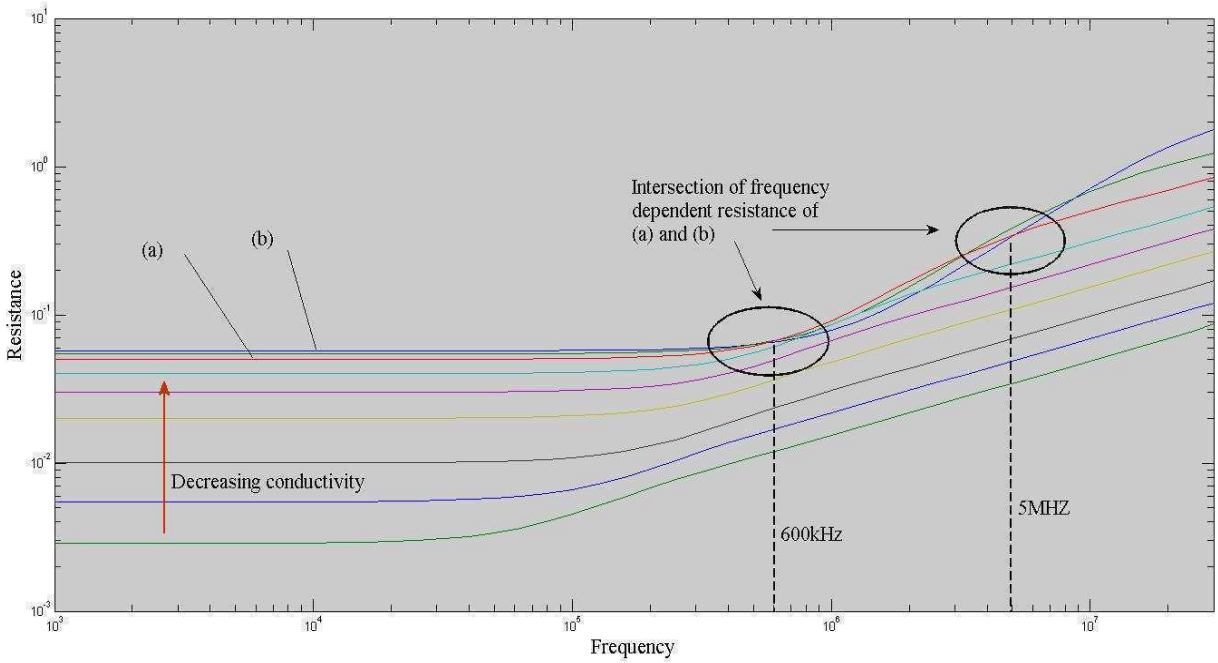


Figure 3.3. Frequency response of all structures for variations in σ_1

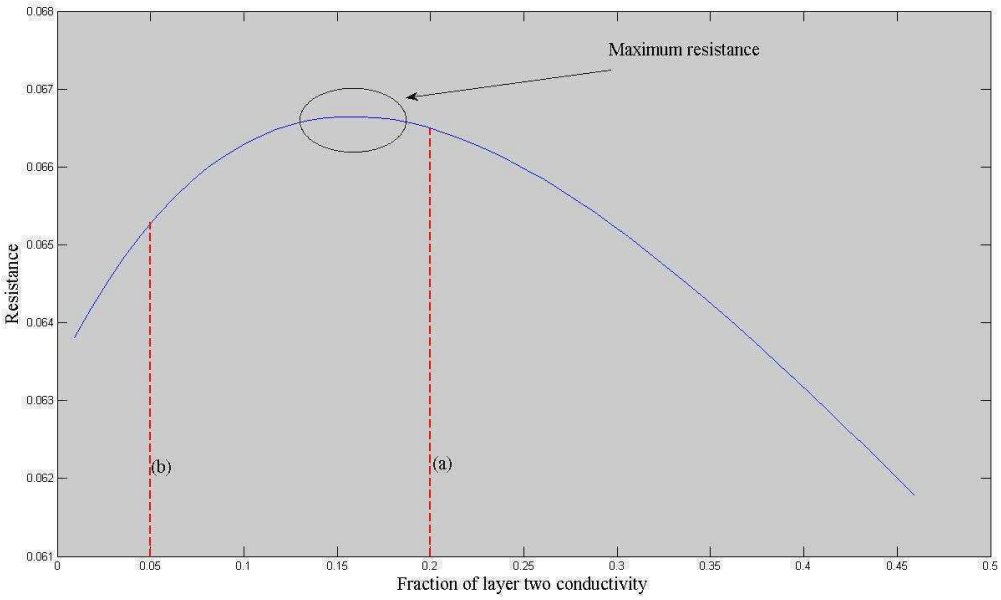


Figure 3.4. Demonstration of maximum resistance as a function of inner conductivity at 600kHz

3.3. Variations in σ_2

In this case, the parameters are as set out in Table 3.1, with variations in σ_2.

$$\sigma_2 \in \{\sigma_1/20;\ \sigma_1/10;\ \sigma_1/5;\ \sigma_1/2;\ \sigma_1;\ 2\sigma_1;\ 5\sigma_1;10\ \sigma_1;\ 20\ \sigma_1\}$$

Figure 3.5 shows each case in the form of Figure 3.1. The multi-layered conductor has resistance which converges to the low frequency approximation at DC, and to the high frequency approximation at high frequencies. Again, the knee points in these cases are in reasonably good agreement. Figure 3.6 shows the resistance of each structure indicated on the same set of axes. Each resistance curve converges to the same high frequency resistance. This is expected because it is entirely defined by the parameters of the first layer which are not changed at all in this case. It does however show that the DC resistance can drastically change. This implies that the DC resistance can be reduced significantly, while the high frequency resistance is kept at the same values.

The converse, and perhaps more important, perspective is that this at first glance represents a good dissipative low-pass filter. A better low-pass filter, in fact, than would be possible with a single layer equivalent. Especially at the higher values of σ_2 in Figure 3.5, it can be seen that the resistance is much higher beyond the first knee point than the equivalent single layer structure. It seems that relative values of σ_1 and σ_2 are of importance to the frequency responses. The greater the ratio between the two, the larger the difference will be between the DC resistance and high frequency resistance. The fact that σ_1 is not varied in this case, makes this evident. A conclusion that can be made here is that the greater the ratio between the two conductors, the more attenuation is possible. This again goes back to the concepts laid out in [1] where in order to increase the performance/attenuation at high frequencies, the areas of the conductor are replaced with a material of lower conductivity.

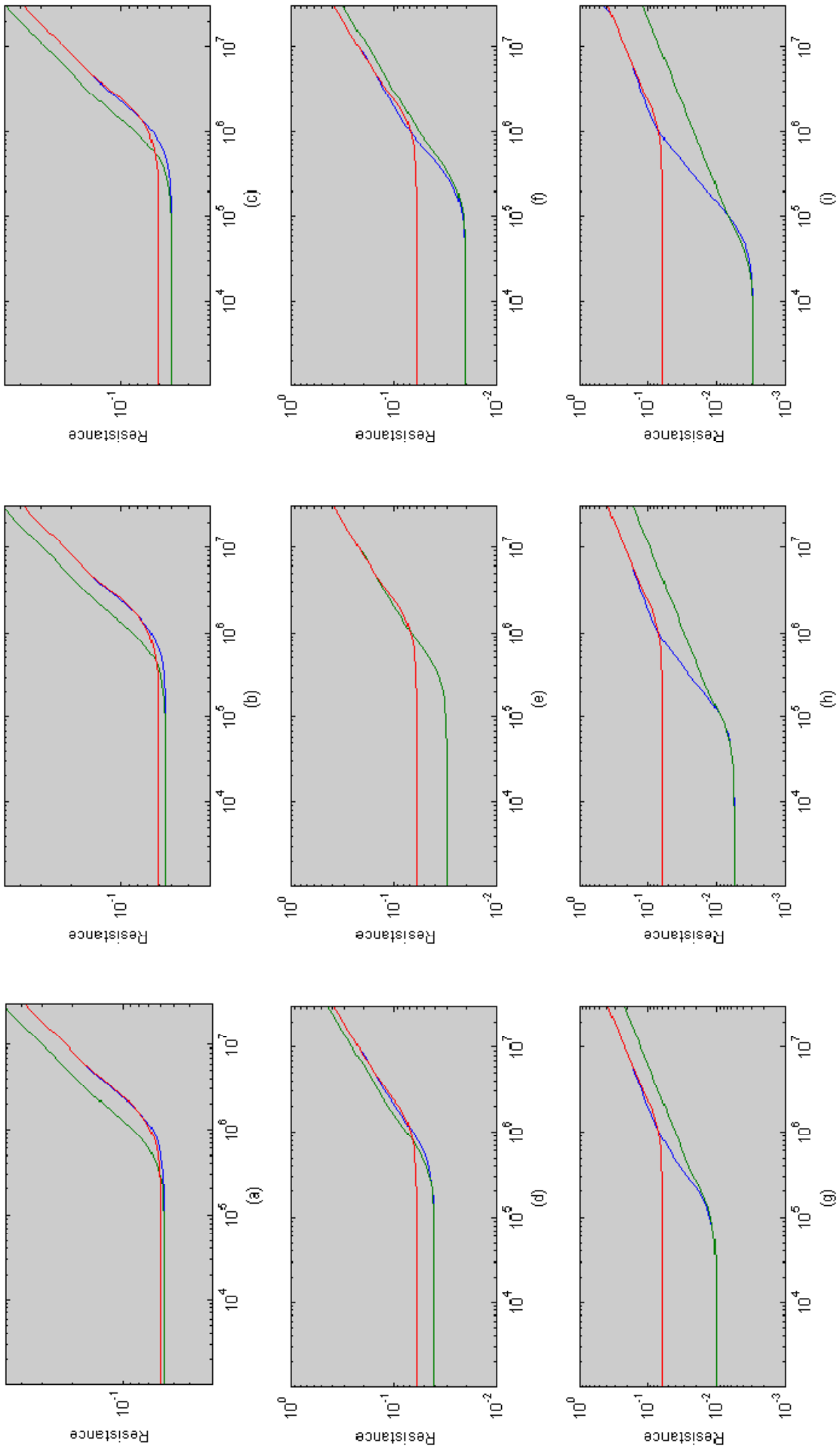


Figure 3.5. Parametric variation in σ_2, with single layer equivalents

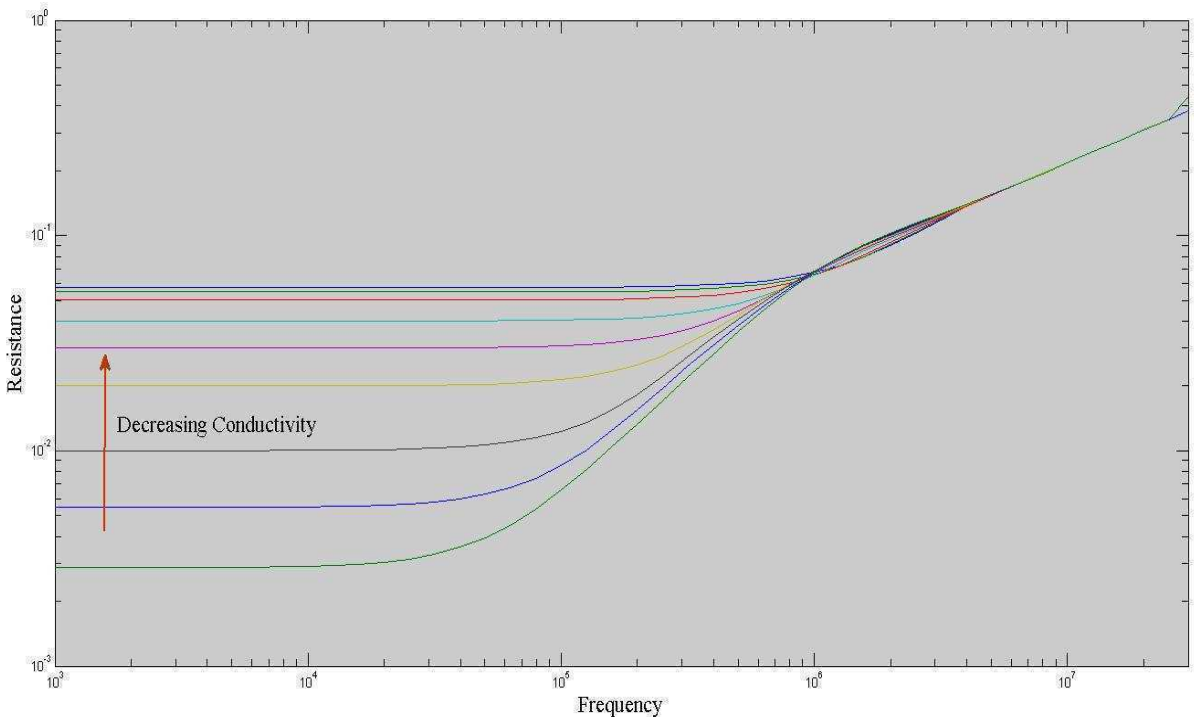


Figure 3.6. Frequency response of all structures for the case of σ_2 variations

3.4. Variations in μ_1

In this case the parameters are set out as in Table 3.1 with variation in μ_1.

$$\mu_1 \in \{\mu_2/10;\ \mu_2/5;\ \mu_2/2;\ \mu_2,\ 2\mu_2,\ 5\mu_2;\ 10\mu_2;\ 20\mu_2;\ 50\mu_2;\ 100\mu_2;\ 200\mu_2;\ 500\mu_2\}$$

Figure 3.7 shows each case in the form of Figure 3.1. Again, it can be seen how the two approximations match the real structure in the expected ranges. It should be noted that the DC resistance of each case is the same in every case. This is clear from the fact that variations in conductivity are not made in this set. The major difference here is that the two knee points reduce in frequency as μ_1 increases. An observation that can be made here is that the high-frequency knee point decreases faster than the low frequency knee point. Figure 3.8 shows the resistance of each structure indicated on the same set of axes. Other than a slight change in shape of the curve, it seems that changes in μ_1 cause a shift of the frequency response. It also has an effect on reducing both knee frequencies.

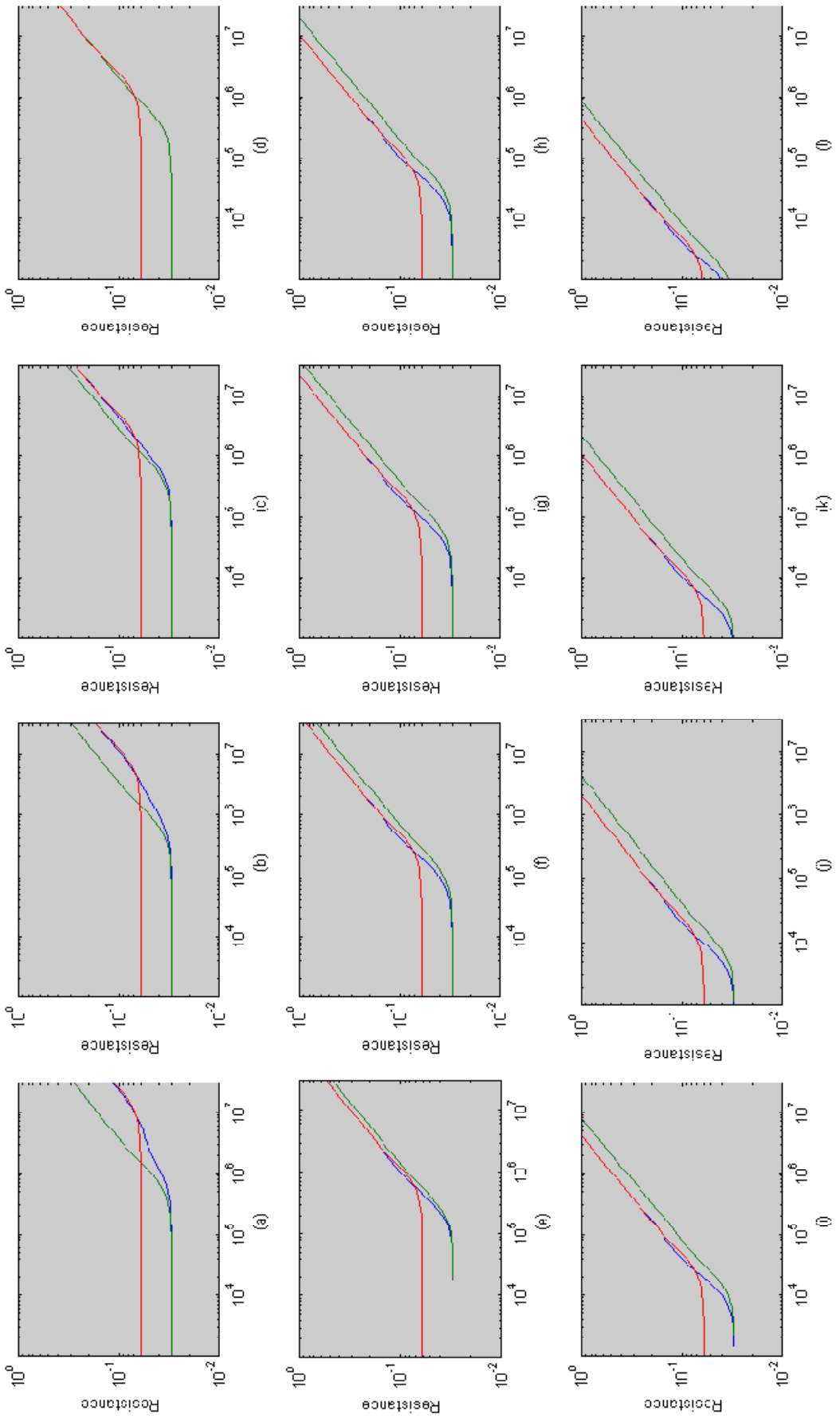


Figure 3.7. Parametric variations in μ_1, with singe layer equivalents

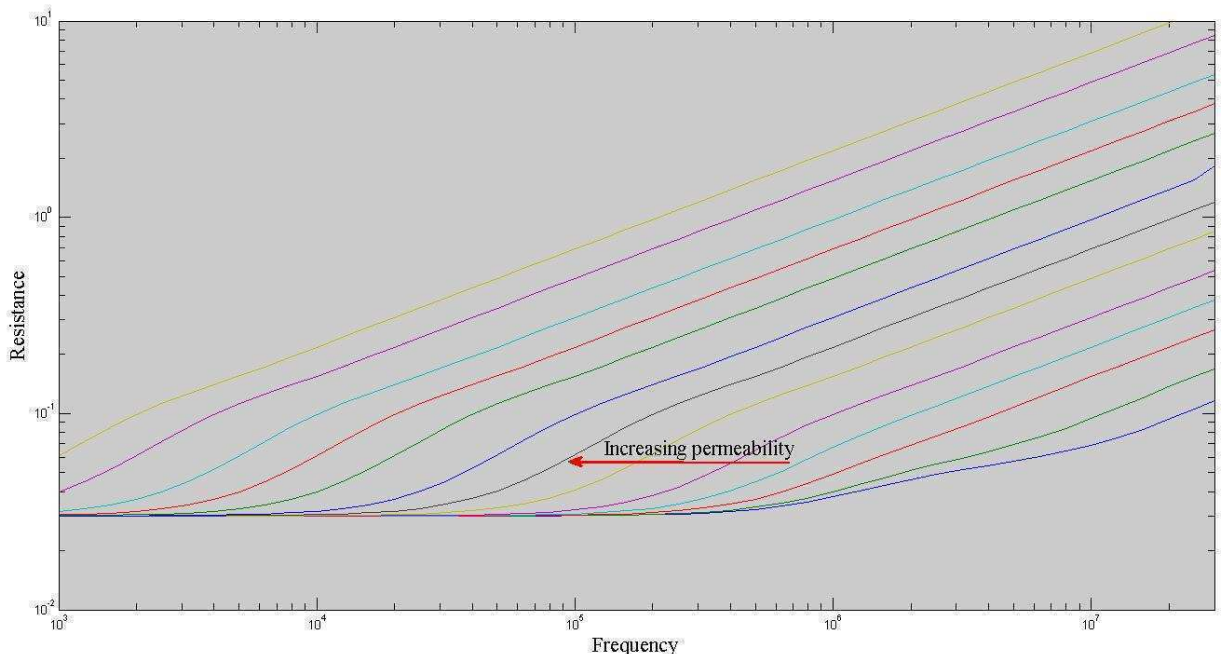


Figure 3.8. Frequency response of all structures for variations in μ_1

3.5. Variations in μ_2

In this case the parameters are set out as in Table 3.1 with variation in μ_2.

$$\mu_2 \in \{\mu_1/10;\ \mu_1/5;\ \mu_1/2;\ \mu_1;\ 2\mu_1;\ 5\mu_1;\ 10\mu_1;\ 20\mu_1;\ 50\mu_1;\ 100\mu_1;\ 200\ \mu_1;\ 500\ \mu_1\}$$

Figure 3.9 shows each case in the form of Figure 3.1. Once again, the multi-layered conductor has resistance which approximates to the single-layer equivalent frequency responses. In this case, the high frequency knee-point does not change because there are no variations in μ_1. The low frequency knee-point does however decrease. It also shows that the shape of the frequency response tends to change as μ_2 increases. The response goes from concave-left to concave-right as μ_2 increases.

This is clearly seen in Figure 3.10 which shows the resistance of each structure indicated on the same set of axes. Since none of the conductivities have been changed, all frequency responses start with the same DC resistance value. Since μ_1 and σ_1 have not been changed, all frequency responses converge upon the same resistance values at the same high frequencies. This is a clear indication that μ_2 (relative to μ_1) to a large extent controls the shape of the frequency response between the DC and high frequency resistance. A low permeability ratio $\mu_2{:}\mu_1$ (less than 1) seems to result in a steeper increase in resistance with respect to frequency, whereas a high permeability ratio (more than 1) results in essentially a "second" DC resistance value that tracks the high frequency single layer approximation. This is fairly clear from Figure 3.9(*i*)-(*l*) where the multi-layered structure converges upon the second approximation before the high-frequency knee-point. The change in shape also implies that at some μ_2 value, the response between the two knee-points will be a straight line.

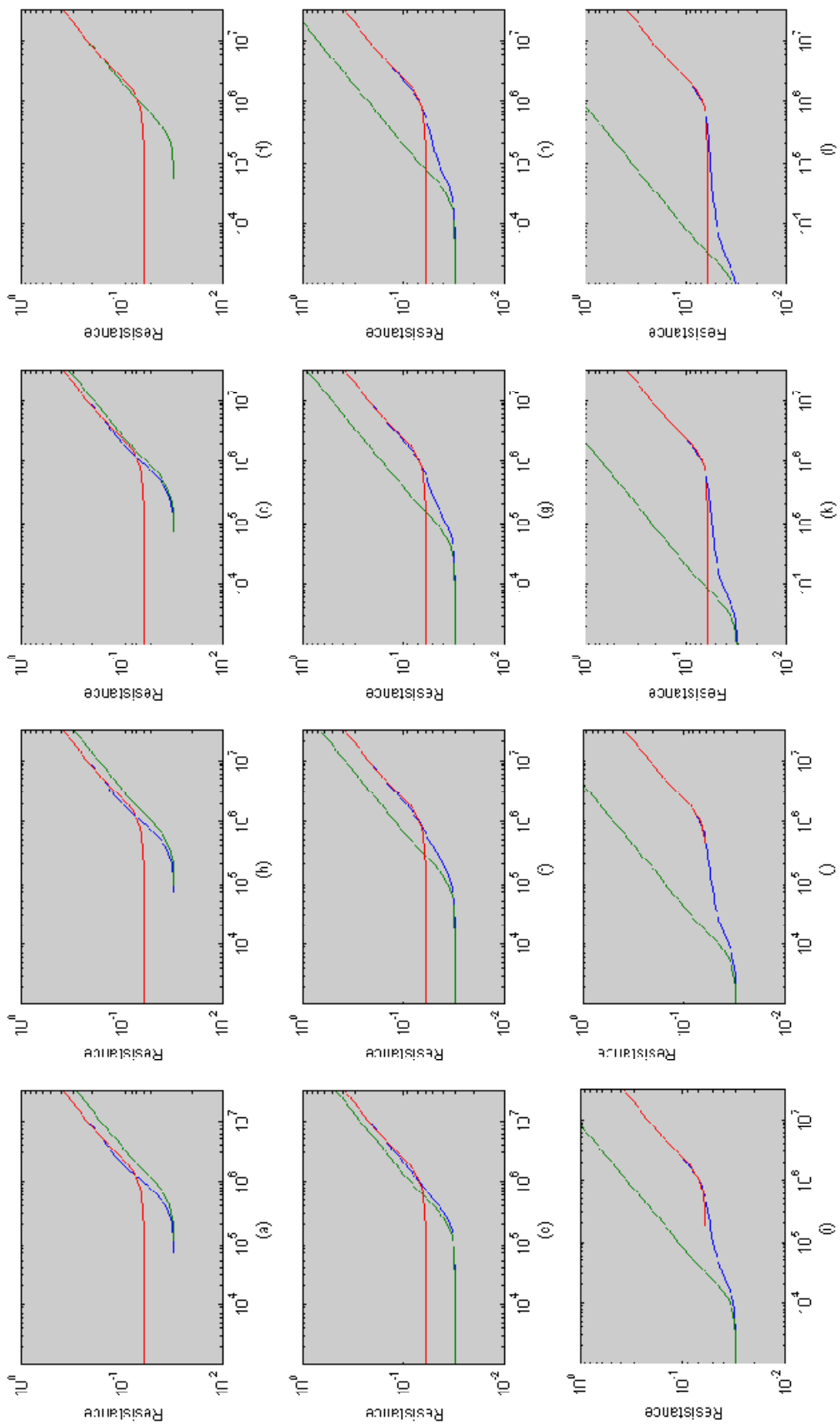


Figure 3.9. Parametric variation in μ2, with single layer equivalents

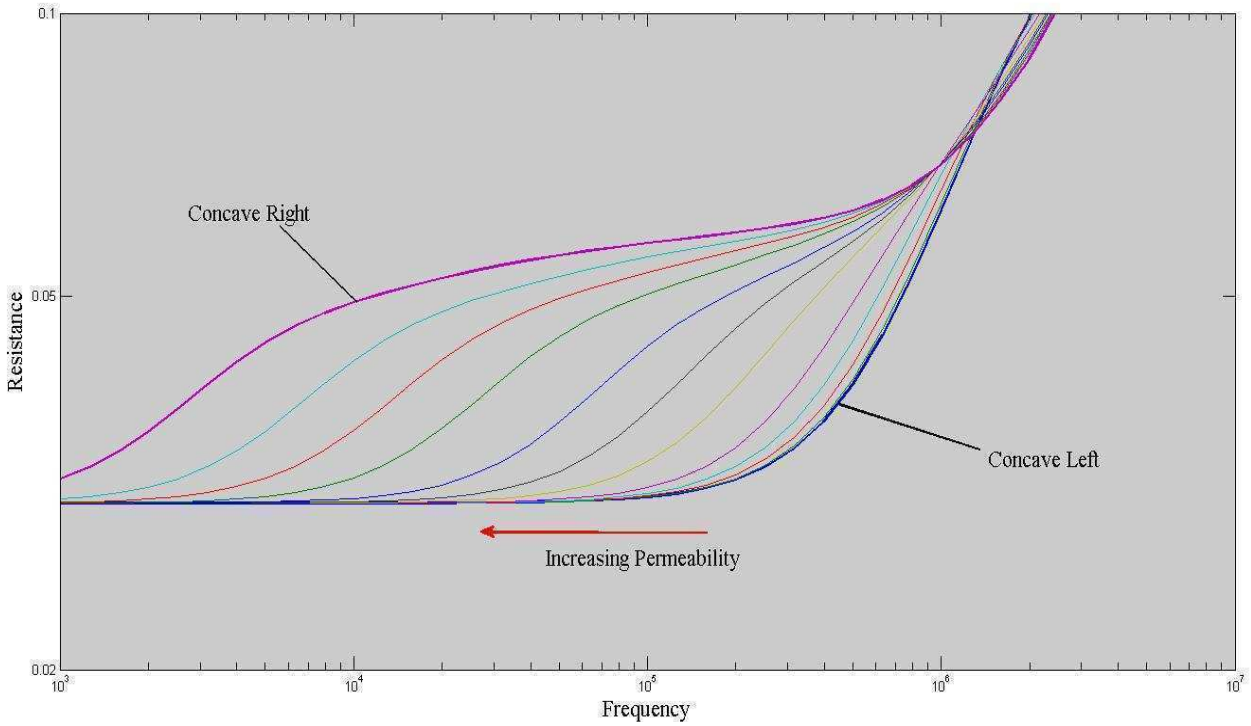


Figure 3.10. Frequency response of all structures for variations in μ_2

3.6. Analysis of parametric study conclusions

Given the apparent effects that these parameters have upon the resistance, a question that needs answering is whether these effects are independent as they seem to be in the parametric study above. In other words, can the effects of permeability and conductivity be superposed? To this end, Figure 3.11 shows two families of curves. These result from a parametric variation of σ_2 in the same values as previously, with the first family of curves being exactly that from Figure 3.6. The second family of curves has a key difference in that $\mu_2 = 100\mu_1$, whereas the two permeabilities were equal in Figure 3.6. It can quite clearly be seen that there is a significant change in shape between each corresponding responses across families, even though each structure converges upon the same DC-resistance values and high frequency resistance values. Curves in the same colour correspond to curves which have the same conductivity values, but different permeability values. Different colours correspond to different conductivity values as given in the parametric variation of σ_2.

This significant change can be explained. Given that the conductivities have not been changed at all, it means that the DC resistance as well as the resistance at the high-frequency knee-point must be the same, regardless of the values of the permeability. This necessarily implies that the range of resistances is restricted. It does not, however, mean that each resistance value has to occur at the same frequency in all cases. The skin depth, and its dependency on both conductivity and permeability, offers an explanation as to the shape of the curve. Rather than interpreting the skin depth as a thickness, it is more valuable to interpret it as a rate in this case. In other words, "how fast" the current must migrate across the conductor. A higher permeability in layer 2 means that its skin depth at every frequency is smaller than that of the corresponding lower permeability conductor of Figure 3.11. When

this skin depth is of the order of the layer thickness, the resistance starts increasing significantly with respect to frequency, and should keep increasing. However, it can quite clearly be seen that this is not the case; the resistance starts levelling off, in fact. The reason for this is that the entire structure's resistance cannot rise above the inner layer's effective DC-resistance before the high-knee point.

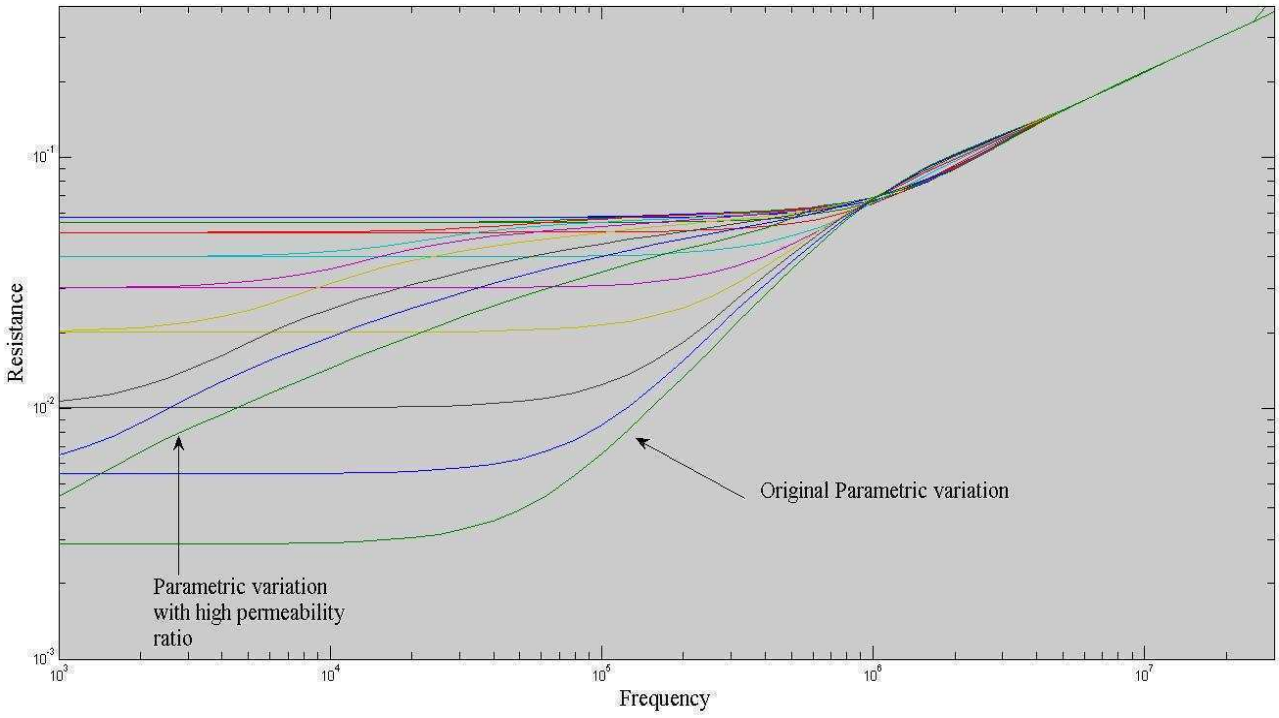


Figure 3.11. Demonstration of change in shape across families

This would suggest that while the relative difference in conductivity between layers defines the range between the DC-resistance and the high frequency resistance, the relative difference in permeability between the layers defines the shape of the resistance curve below the high frequency knee-point.

This would suggest that in order to produce a more effective dissipative differential mode filter, the inner conductor must have a lower conductivity [1] but higher permeability than the outer layer in order to have a smaller skin depth [2]. This would have the effect of increasing the range of DC- to high-frequency-resistance, but also lowering the high-frequency knee-point and bringing it closer to the low frequency knee-point. This will result in a steeper increase in resistance from the low-frequency knee-point. This can be seen in Figure 3.12 where the same set of Figure 3.6 is used, but now with a family of curves where $\mu_2 = \mu_1/100$. The skin depth of the inner layer here is now smaller than that of the outer layer. Again, pairs of curves approximate to the expected high-frequency- and DC-resistance.

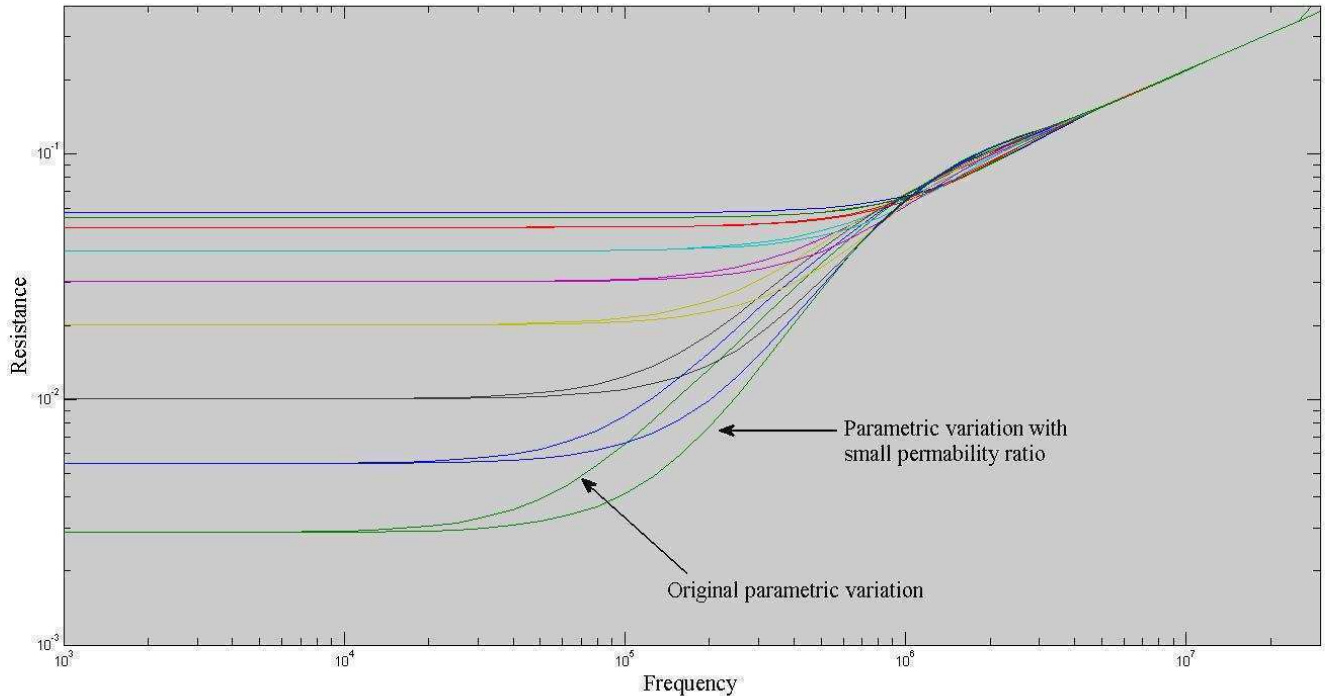


Figure 3.12. Demonstration of the effect of a low permeability ratio

Given the results of Figure 3.11 and Figure 3.12, it seems evident that the effects of the conductivities and permeabilities are independent to some extent. It shows that the conductivities define the resistance range between knee-points, while the permeabilities define the shape between the knee-points.

A conclusion reached in Section 3.2 is that the conductivity can only be lowered to a certain extent before effective filtering stops. Figure 3.13 shows that this is not entirely true. The parameters used in this curve are given in Table 3.2. Notice that the even though layer 1 has a much lower conductivity than layer2, because of its high permeability, they have the same skin depth. The result of this is that there is a three decade increase in resistance for a two decade difference in frequency. This is a dissipative filter with a very high gradient in resistance. This gives even more confidence in the conclusion above that a more dissipative filter can be achieved with a low conductivity but high permeability inner layer. The best that can be said about the conclusion in Section 3.2 is that it is true, but the value of the minimum conductivity also depends heavily upon the permeabilities of the layers as well.

Table 3.2. Layer properties

Layer 1		Layer 2	
Property	Value	Property	Value
σ_1	10^3	σ_2	10^6
μ_1	$10^3\mu 0$	μ_2	μ_0
b_1	100μm	b_2	100μm

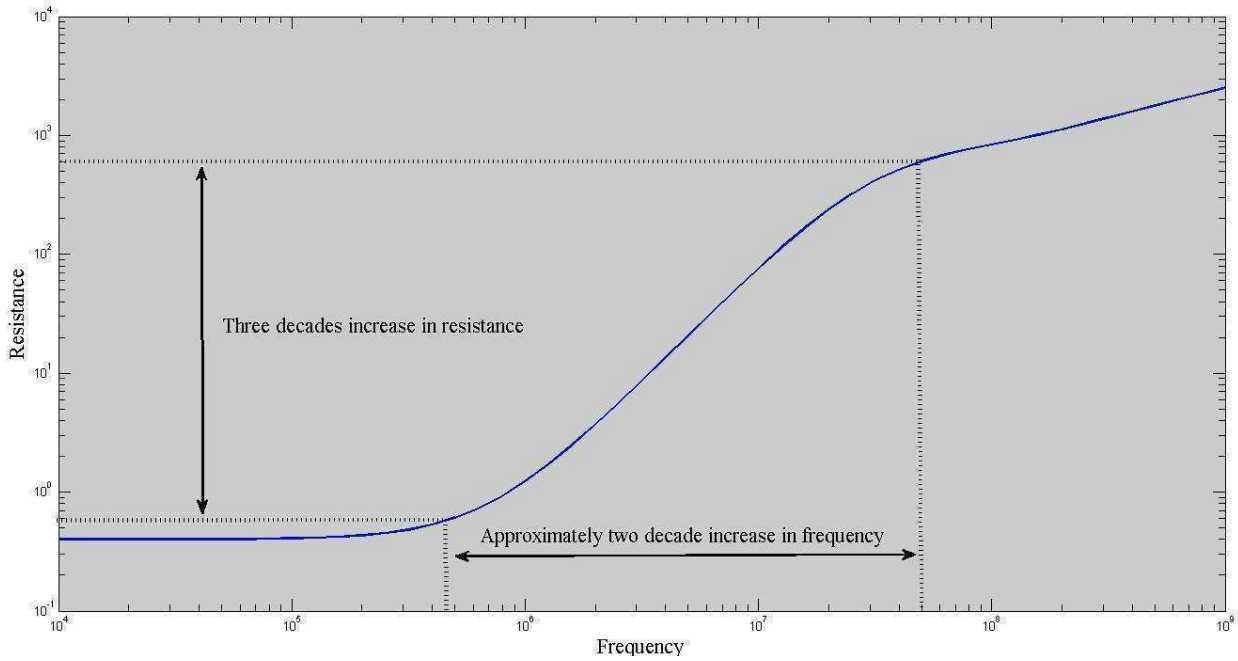


Figure 3.13. Large increase in resistance with respect to frequency

3.7. Conclusion

It should be re-iterated here that single-layer approximations accompanied the parametric study throughout. These approximations worked as anticipated with convergence at low frequencies and at high frequencies, with a large degree of agreement at the knee-frequencies. This gives an indication that this concept presents a good first approximation to two-layer conductor design. There are some discrepancies, however, which will be discussed in the next chapter.

Between the two knee frequencies, it was shown that the range of resistance is defined by the relative conductivities of the two layers, while the shape of the curve between the two is given by the relative permeabilities. As such, in designing dissipative filters, it is desired for the inner layer to have a low conductivity but higher permeability than the outer layer. The reason for this comes from looking at Figure 3.12, where a higher *outer* layer conductivity results in a large difference in resistance between knee-frequencies, and a higher *inner* layer permeability results in a smaller difference in knee-frequencies. This can be seen through inspection of the single-layer approximation applied here, which is discussed in the next chapter.

It is also vitally important to mention here that the conclusions reached here apply to "normalised conductors" with layer thicknesses that are the same. However, any rescaled conductor will have the same total permeability and total conductivity, and therefore the same response (as discussed in Chapter Two). This is enough to justify that for every conclusion reached in this chapter, it is the *total conductivity* and *total permeability* of each layer and how they relate to each other that contributes to the characterisation of the response.

3.8. References

[1] Van Wyk et al, "Power Electronic Interconnects: Skin- and Proximity Effect-based Frequency Selective Multi-path Propagation," *IEEE Transactions on Power Electronics*, vol. 20, no. 3, May 2005.

[2] Munteanu C, Racasan A, Antonescu O Hebedean C, "Technologies to Increase HF Losses in Planer Structures and their limitiations," in *13th International Conference on Optimization of Electrical and Electronic Equipment*, 2012, pp. 48-53.

Chapter Four – Single-layer approximation

Table of Contents

4.1. Introduction 49

4.2. Divergence of the single layer approximation 49

4.3. Observations on the single layer approximation 51

4.4. Design of two layer structures 53

4.4.1. Design with arbitrary materials 53

4.4.1.1. Example of arbitrary material design 54

4.4.2. Design with existing materials 56

4.4.2.1. Specifying both knee-resistances 57

4.4.2.2. Specifying both knee-frequencies 58

4.4.2.3. Specifying f_{high} and R_{DC} 59

4.4.2.4. Specifying R_H and f_{low} 60

4.4.2.5. Specifying R_{DC} and f_{low} 60

4.5. Conclusion 61

4.6. References 62

4.1. Introduction

The single-layer approximation has already been suggested as a tool in Chapter 2. In the parametric study of Chapter 3, the results showed that the single-layer approximation gives good agreement especially in the prediction of the low-frequency response, and the high frequency response. This chapter looks at the single-layer approximation in detail in order to draw further insight. This will help present the true usefulness of these approximations, especially as a design tool with regard to multi-layered conductors. The two equations for the equivalent conductivity and permeability are reproduced here as (1) and (2) for ease of reference.

$$\sigma_{eq} = \frac{\sigma_1 b_1 + \sigma_2 b_2}{b_1 + b_2} \qquad (1)$$

$$\mu_{eq} = \frac{\mu_1 b_1 + \mu_2 b_2}{b_1 + b_2} \qquad (2)$$

Each single layer approximation gives an effective single layered conductor with its own DC resistance, and knee-point. The DC-resistance of the low frequency approximation represents the DC-resistance of the real two-layered structure. The DC-resistance of the high frequency approximation approximates the resistance of the real structure at the high-frequency knee-point. As such, it will be referred to from here on as the *high-frequency knee-resistance.*

4.2. Divergence of the single layer approximation

It can be seen from Figure 4.1 that the multi-layered conductor converges upon the one approximation at low frequencies, and to the other at high frequencies, but this is not the case for the mid range. As this is an approximation, this is naturally to be expected. For the structure in Figure 4.1, it is quite clear that the resistance of the multi-layer conductor rises faster than the first approximation at the knee point. An observation that can be made, and is true throughout the parametric study as well, is that whenever the two-layered conductor rises faster than the low-frequency approximation, the frequency response of the first approximation never intersects that of the second approximation. Further, the resistance of the composite *must* converge upon the high-frequency knee-resistance near the second knee-point. This explains the faster rise of the resistance of the real structure than the approximation.

To illustrate this point, Figure 4.2 presents a scenario where the two approximations do intersect. It can be seen here that the actual response of the composite rises slower at the low knee-point than that of the first approximation. The resistance of the composite must necessarily, at frequencies below the second knee point, be less than the high frequency knee-resistance since the current is flowing in multiple layers below that frequency point. The second knee-point represents the frequency at which the skin-effect starts to take effect in inner layer. This is evidence as to why the real conductor rises faster than the initial approximation in the first case. It must reach the high-frequency knee-resistance at a frequency near that at which the second approximation does and because the two

approximations do not intersect, the real structure will reach this resistance before the first approximation.

The intersection of the two approximations is dependent upon the knee-frequencies, and the DC-resistances. The greater the difference between DC resistances, the greater the difference between the knee-frequencies needs to be in order for there to be an intersection.

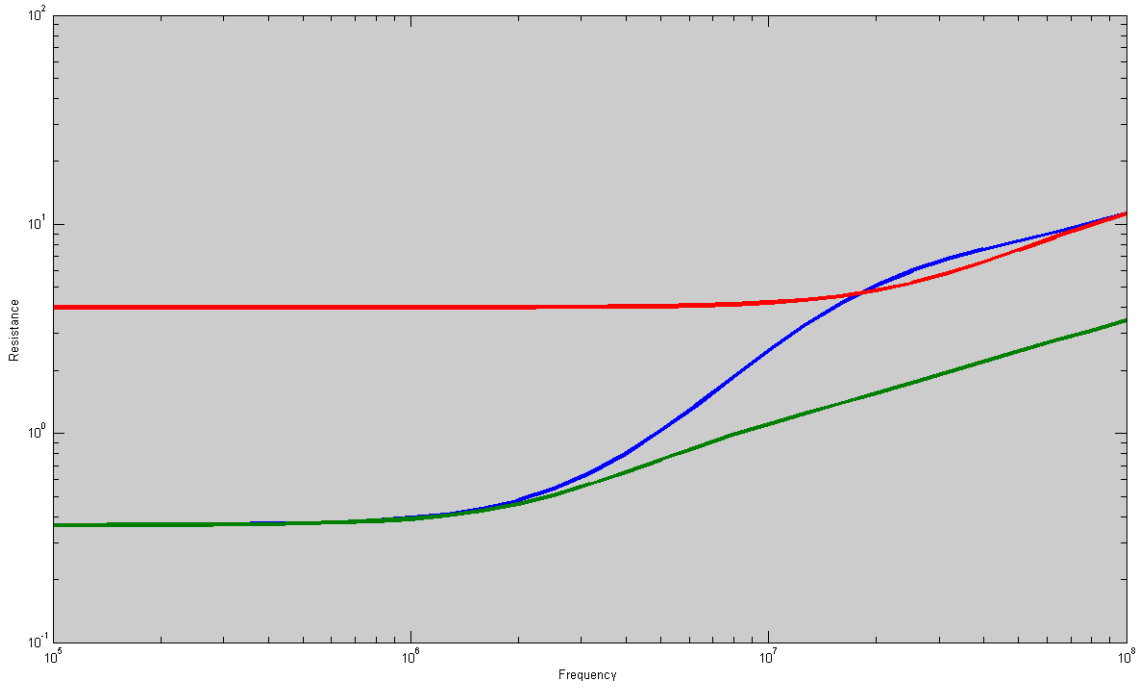


Figure 4.1. Frequency response with single layer approximations

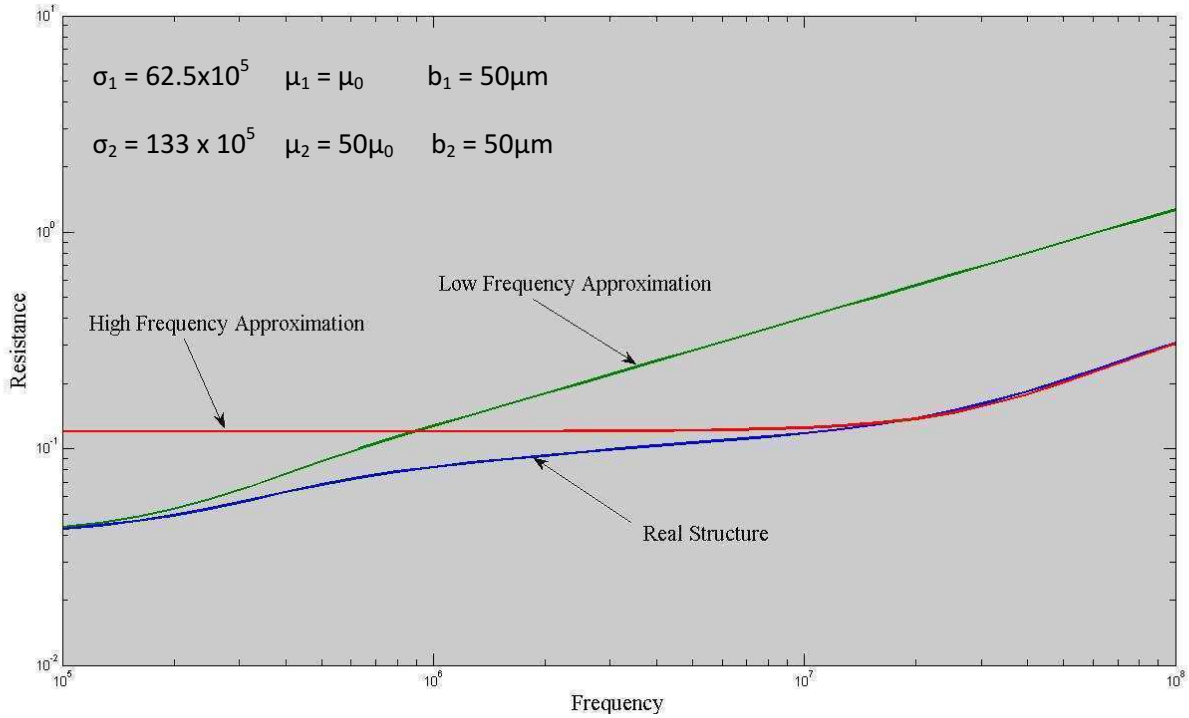


Figure 4.2. Case where approximations intersect each other

4.3. Observations on the single layer approximation

The two knee frequencies (3) and (4) can be obtained through rearranging the skin depth equation and substituting the relevant values. Here, f_{high} and f_{low} are defined as the high-frequency and low-frequency knee-points respectively. In each case, the skin-depth is given by the thickness of each approximation. Substitution of (1) and (2) into (4) results in (5).

$$f_{high} = \frac{1}{\pi {b_1}^2 \mu_1 \sigma_1} \tag{3}$$

$$f_{low} = \frac{1}{\pi (b_1 + b_2)^2 \mu_{eq} \sigma_{eq}} \tag{4}$$

$$f_{low} = \frac{1}{\pi (\mu_1 b_1 + \mu_2 b_2)(\sigma_1 b_1 + \sigma_2 b_2)} \tag{5}$$

The expression for f_{low} can be manipulated further by taking out common factors (6). This leads to an expression of the ratios of the knee-frequencies (7).

$$\frac{1}{f_{low}} = \pi {b_1}^2 \mu_1 \sigma_1 \left(1 + \frac{\mu_2}{\mu_1}\frac{b_2}{b_1}\right)\left(1 + \frac{\sigma_2}{\sigma_1}\frac{b_2}{b_1}\right) \tag{6}$$

$$\frac{f_{high}}{f_{low}} = \left(1 + \frac{\mu_2}{\mu_1}\frac{b_2}{b_1}\right)\left(1 + \frac{\sigma_2}{\sigma_1}\frac{b_2}{b_1}\right) \tag{7}$$

The implication here is that ratio of the knee-frequencies depends upon the ratio of the total permeabilities, and total conductivities of each layer, and not upon the absolute value of each of these parameters. It is however obvious that the actual value of the frequencies themselves do depend upon the absolute value of the material properties. Considering both these facts in conjunction, an interesting observation can be made. If the conductivity and permeability ratios are kept the same, but the absolute values of the parameters are changed, a linear shift should be observed in the frequency responses of the structure since a frequency response is typically presented on a log scale. This would further suggest that the shape of the frequency response does not depend upon the absolute values of each of the parameters, but rather on their ratios. Furthermore, (7) shows that the single layer approximation is consistent with the concept of the scalability of conductors. If the layer thicknesses are both increased by the same factor, the resulting conductor will have the same shape of response but will be shifted down in frequency and in resistance. In this case, the knee point ratios would be the same, just as (7) presents. It is also consistent with conductor rescaling since the rescaling preserves total permeability and total conductivity.

One of the most important observations that can be made is that the equation describing the set of single layer approximations does not take layer-order into account for each approximation. Order is however taken into account between approximations. This is best demonstrated for a two layer structure, particularly relevant given the focus of this dissertation. For a two layer structure with layers l_1 and l_2, there are two possible responses, namely (a) $\boldsymbol{M_{DM}(l_1, l_2)}$ and (b) $\boldsymbol{M_{DM}(l_2, l_1)}$.

Because it is a two layer structure, there will be two single-layer approximations for each response. At a sufficiently high frequency the current is only in one layer and the approximations are given as (8) and (9) for (a) and (b) respectively.

$$\sigma_{eq} = \sigma_1, \qquad \mu_{eq} = \mu_1 \tag{8}$$

$$\sigma_{eq} = \sigma_2, \qquad \mu_{eq} = \mu_2 \tag{9}$$

At DC, the current is distributed between the layers as though they were resistors in parallel. In this case, the approximations are given as (10) and (11) for (a) and (b) respectively. It can be seen by rearrangement that these two equations are in fact the same. This is true whether the layers have the same thickness or not. As such, it is clear that even though these two structures will clearly have different responses because their order is different, they have the same low frequency approximation. This is demonstrated in Figure 4.3 where the response for both structures (a) and (b) are plotted on the same set of axes with the low-frequency approximation. It can be seen that the approximation rises between the two real responses. This is to be expected since the single layer approximation is an average of the two layers.

$$\sigma_{eq} = \frac{\sigma_1 b_1 + \sigma_2 b_2}{b_1 + b_2}, \qquad \mu_{eq} = \frac{\mu_1 b_1 + \mu_2 b_2}{b_1 + b_2} \tag{10}$$

$$\sigma_{eq} = \frac{\sigma_2 b_2 + \sigma_1 b_1}{b_2 + b_1}, \qquad \mu_{eq} = \frac{\mu_2 b_2 + \mu_1 b_1}{b_2 + b_1} \tag{11}$$

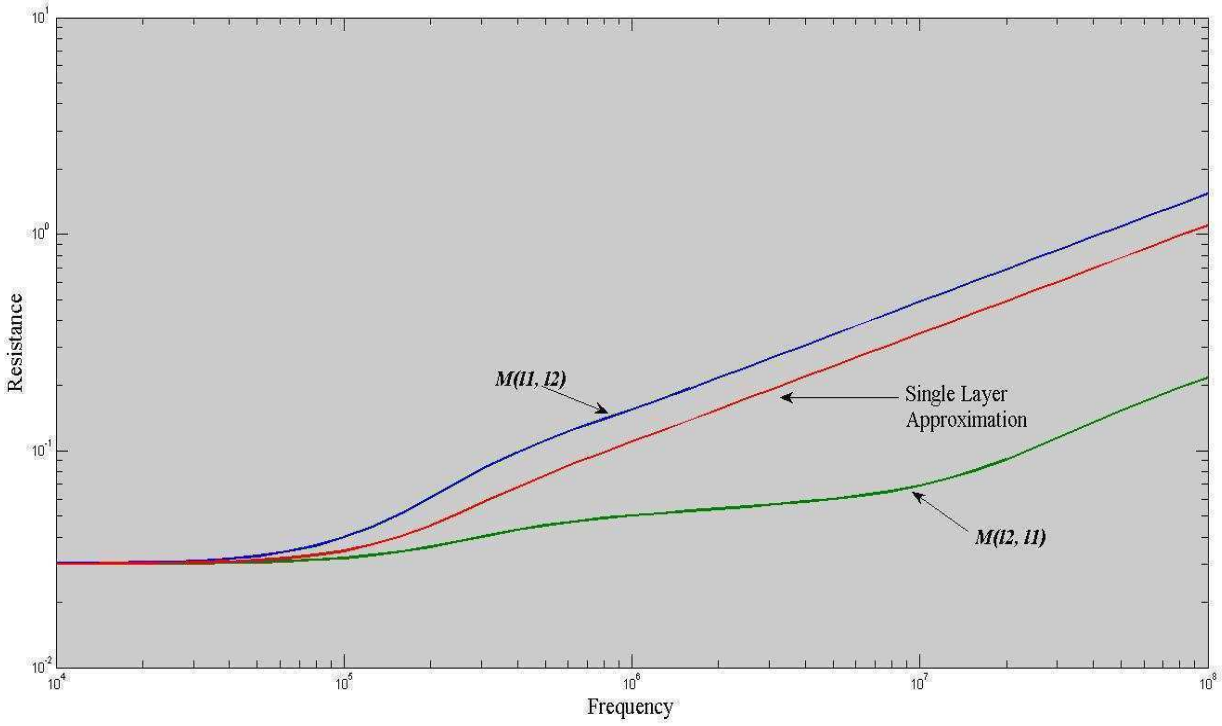


Figure 4.3. Demonstration of non order-preserving single layer approximation

4.4. Design of two layer structures

This section presents two different ways in which two layer structures can be designed with particular regard to the single layer approximation. The first is from the perspective that there is no restriction on material properties. In other words, this means that the conductivity and permeabilities could take on arbitrary values under the assumption that the material can be manufactured. The second option is to take two known materials and size the layers according to specifications. Both are explored in this section and are based upon the use of equations developed in Section 4.3.

4.4.1. Design with arbitrary materials

The single layer approximation, as discussed before, gives approximations of the knee points of the structure. For a given knee point, there is a frequency and a resistance related to that frequency. For a two-layered structure, there are two knee-frequencies, and two DC-resistances. Using the single layer approximation for design therefore gives a maximum of *four* specifiable variables (two knee-frequencies and two knee-resistances). Each layer however, has 3 parameters if the thickness of the layer is included. This means that only four of the six parameters can be solved. As such, this design process chooses to treat the design variables as the total conductivity and total permeability quantities

$$\mu_1 b_1 \qquad \sigma_1 b_1 \qquad \mu_2 b_2 \qquad \sigma_2 b_2$$

It was concluded in Chapter Three, with reference to Chapter Two, that it is the total permeability and total conductivity that characterise the response. As such, not only is solving for layer thickness unnecessary, is it also the incorrect approach; the choice of layer thickness is arbitrary to an extent because of conductor rescaling. This is fair under the assumption that the materials can be manufactured. It has been shown that is possible to change the conductivity of a material through Cold Spray Technology [1]. This means that while the technology does not yet exist to synthesise materials to specification, it may be possible in the future, and that this design method is worth pursuing. It is fair to assume that there is a maximum conductivity, σ_M, that can be achieved through synthesis. This will place some constraints on design with reference to the *total* quantities.

The DC resistance per meter of a two layer structure is given as (12)

$$R_{DC} = \frac{1}{width\ (\sigma_1 b_1 + \ \sigma_2 b_2)} \qquad (12)$$

While the approximate resistance at the high frequency knee point is given by (13)

$$R_H = \frac{1}{width\ \sigma_1 b_1} \qquad (13)$$

As such, (3) and (5) can be rewritten as (14) and (15) respectively.

$$f_{high} = \frac{width\ R_H}{\pi \mu_1 b_1} \qquad (14)$$

$$f_{low} = \frac{width\ R_{DC}}{\pi(\mu_1 b_1 + \mu_2 b_2)} \qquad (15)$$

Since the knee-point frequencies and knee-point resistance have been specified, the four design variables can be solved. These solutions are given as (16) to (19).

$$\sigma_1 b_1 = \frac{1}{width\ R_H} \qquad (16)$$

$$\sigma_2 b_2 = \frac{1}{width\ R_{DC}} - \frac{1}{width\ R_H} \qquad (17)$$

$$\mu_1 b_1 = \frac{width\ R_H}{\pi f_{high}} \qquad (18)$$

$$\mu_2 b_2 = \frac{width\ R_{DC}}{\pi f_{low}} - \frac{width\ R_H}{\pi f_{high}} \qquad (19)$$

One restriction that will be applied to these equations is that all quantities must be positive. As such, it is clear that through rearrangement of (17) and (19) respectively that the inequalities (20) and (21) must hold. These ensure that σ_2 and μ_2 are greater than zero. A further restriction that is applied here is that the permeability of each layer must be at least μ_0. The effect of this is that it specifies maximum thicknesses b_1 and b_2 for the two layers. From inspection of (18) and (19), it can be seen that any increase in permeability results in a proportional decrease in the layer thickness. Further to this, as said earlier, there is a maximum conductivity, σ_M, available for use. As such, there is also a specified minimum thickness for b_1 and b_2. Substituting σ_M and μ_o appropriately into (16) to (19), results in the restrictions (22) and (23). Any specifications resulting in the minimum thickness being larger than the maximum thickness is not a physically realisable structure.

$$R_H > R_{DC} \qquad (20)$$

$$\frac{f_{high}}{f_{low}} > \frac{R_H}{R_{DC}} \qquad (21)$$

$$b_{1_{min}} = \frac{1}{width\ R_H \sigma_M}; \qquad b_{1_{max}} = \frac{width\ R_H}{\mu_0 \pi f_{high}} \qquad (22)$$

$$b_{2_{min}} = \frac{1}{\sigma_M width\ R_{DC}} - \frac{1}{\sigma_M width\ R_H}; \qquad b_{2_{max}} = \frac{width\ R_{DC}}{\mu_0 \pi f_{low}} - \frac{width\ R_H}{\mu_0 \pi f_{high}} \qquad (23)$$

4.4.1.1. Example of arbitrary material design

Two examples of the above design process are given here. The specifications and resulting parameter values for these designs are given in Table 4.1. Simulations are done for a conductor width of 25mm. The simulated results for design 1 and 2 are given in Figure 4.4 and Figure 4.5 respectively. Both are shown with their respective single layer approximations

as well. Resistance are given in $\Omega.m^{-1}$. It can be seen in the two figures that the designed structure has knee points at approximately the right frequencies, with the correct approximate knee-resistances; as specified. This suggests that the single-layer approximation is a good tool for use in designing these structures. It is also important to note here that the structure is not expected to conform exactly to the specifications, because it has been designed using an approximation; albeit what so far has been shown to be a good one.

Table 4.1. Design Specifications

Design 1			
f_{high}	10MHz	$\sigma_1 b_1$	200
f_{low}	100kHz	$\sigma_2 b_2$	3800
R_{DC}	10mΩ	$\mu_1 b_1$	$127\text{x}10^{-7}\ \mu_0$
R_H	200mΩ	$\mu_2 b_2$	$506\text{x}10^{-6}\ \mu_0$

Design 2			
f_{high}	10MHz	$\sigma_1 b_1$	800
f_{low}	40kHz	$\sigma_2 b_2$	3200
R_{DC}	10mΩ	$\mu_1 b_1$	$31.7\text{x}10^{-6}\ \mu_0$
R_H	50mΩ	$\mu_2 b_2$	$6.3\text{x}10^{-3}\ \mu_0$

In this case, b_1 and b_2 are chosen to be 25µm and 75µm respectively. This results in actual values for these properties as given in Table 4.2. All of the resulting conductivities are less than that of copper, and all relative permeabilities are greater than 1. Both designs are therefore realisable.

Table 4.2. Real Values for the designed structure

Design 1			
σ_1	$8\text{x}10^6$	μ_1	$5.06\mu_0$
σ_2	$5\text{x}10^7$	μ_2	$6.75\mu_0$

Design 2			
σ_1	$3.2\text{x}10^6$	μ_1	$1.27\mu_0$
σ_2	$4.2\text{x}10^6$	μ_2	$20.7\mu_0$

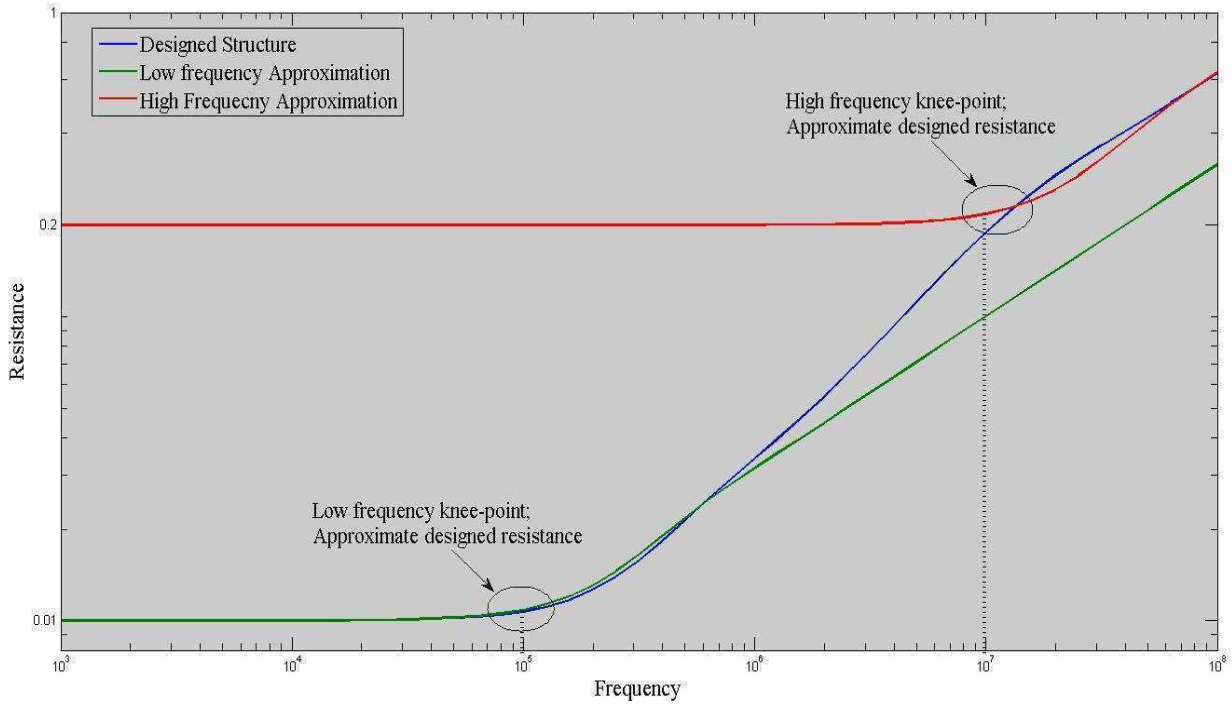


Figure 4.4. Frequency Response for Design 1

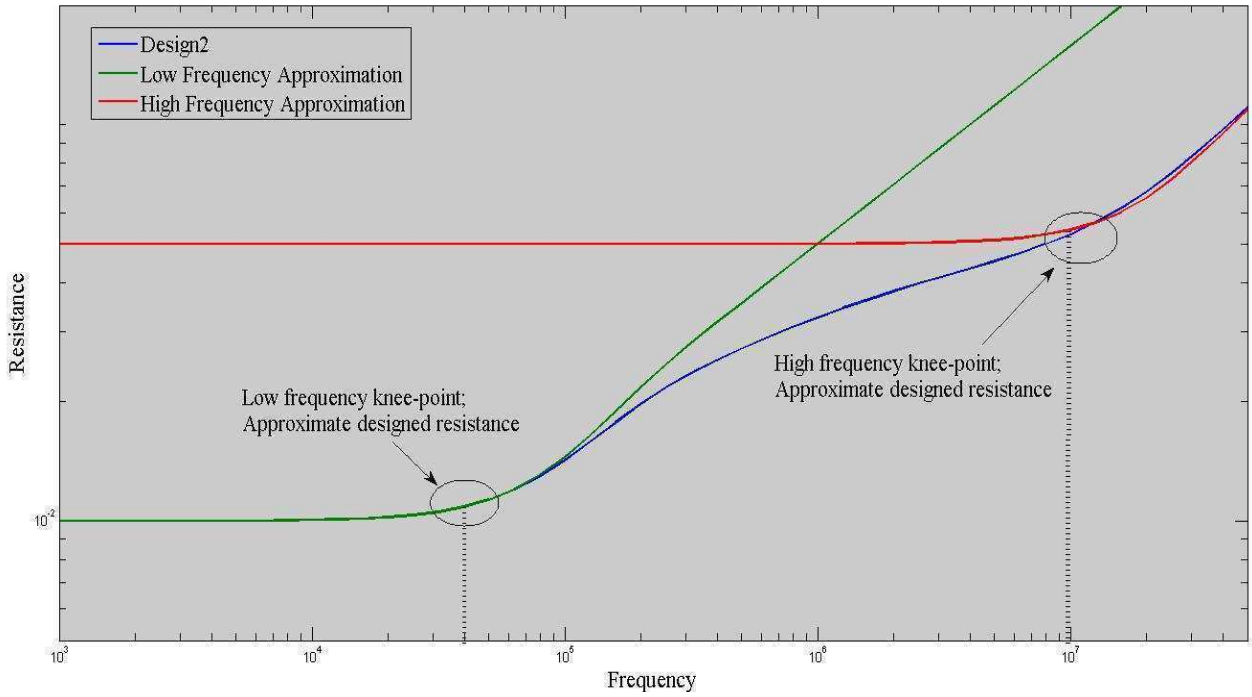


Figure 4.5. Frequency Response for Design 2

4.4.2. Design with existing materials

The key difference between this and the previous design process is that here the material properties have been specified. As such, there is only control over the respective layer thicknesses; two of the six parameters. It is clear from this that only two of the four options described in the previous design can be specified. The other two options will end up where they need to be in order to satisfy the two chosen specifications. An important point here is that it is the choice of the designer as to which pair is the most appropriate. Demonstrated here is how one would design the two-layered conductor given the choice of specifications. Further to this, it is important to understand that this is an approximation used for the sake of design. By no means does this design technique present the best solution for the specifications, but it will provide a convenient and good first approximation, and confidence can be made that the specifications are fairly well satisfied. From this point, small variations can be made to optimise around the specifications.

It is not possible to specify both R_H and f_{high} at the same time. This is because once b_1 has been solved from (13), every variable in (14) is known and as such, the knee-frequency is specified. Each of the other five pairs is possible to design. Each design is accompanied by an example; the material properties for each example are the same and are given in Table 4.3. The purpose of this is to show that for a given pair of materials, it is possible to use them in different ways for designing multi-layered conductors. Further to this, the specifications are chosen somewhat arbitrarily for the express purpose of demonstrating the value of the single-layer approximation as a design tool.

Table 4.3. Material properties for design of two layered structures

Layer 1		Layer 2	
Property	Value	Property	Value
σ_1	10^5	σ_2	10^6
μ_1	$20\mu_0$	μ_2	μ_0

4.4.2.1. Specifying both knee-resistances

This is the simplest of all cases. Equations (12) and (13) are re-arranged in order to obtain (24) and (25)

$$b_1 = \frac{1}{\sigma_1 width}\frac{1}{R_H} \qquad (24)$$

$$b_2 = \frac{1}{\sigma_2 width}\left(\frac{1}{R_{DC}} - \frac{1}{R_H}\right) \qquad (25)$$

In this case, the two chosen resistance values are specified as R_H = 500mΩ.m^{-1}, and R_{DC} = 20mΩ.m^{-1}. This results in values for the layer thicknesses as b_1 = 800μm, and b_2 = 1.92mm. The simulated results are given in Figure 4.6. It should be noted that using the approximation gives a specification of the approximate resistance at the two knee points. In Figure 4.6, the high frequency knee-point has been highlighted to demonstrate that the resistance specified coincides with the knee-point. The same is true for the low frequency knee-point. The low-frequency knee-resistance is the same as the DC-resistance, and so was always going to be correct. However, attention is drawn here to the fact that the low-frequency knee point for the structure, as well as the single-layer approximation coincide. This gives more confidence in the use of the approximation as a design tool.

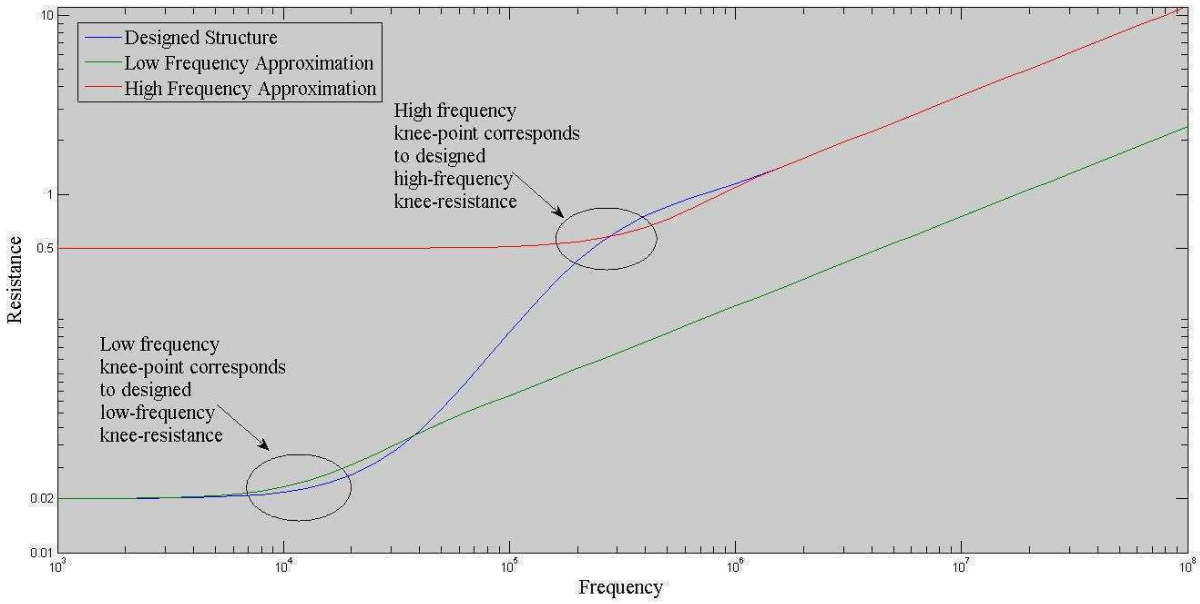


Figure 4.6. Response of structure when two knee-resistances are specified

4.4.2.2. Specifying both knee-frequencies

In this case, the layer thicknesses (26) and (27) are given by the skin depth equations applied to each of the two equivalent single layer approximations.

$$b_1 = \sqrt{\frac{1}{\pi f_{high}\mu_1\sigma_1}} \qquad (26)$$

$$b_1 + b_2 = \sqrt{\frac{1}{\pi f_{low}\mu_{eq}\sigma_{eq}}} \qquad (27)$$

It is clear, though, that because of the dependency of (27) upon the equivalent permeability and conductivity, b_2 is not yet the subject of the formula. It can be rewritten as (28) and results in the simplification (29).

$$b_1 + b_2 = \sqrt{\frac{(b_1 + b_2)^2}{\pi f_{low}(\mu_1 b_1+\mu_2 b_2)(\sigma_1 b_1+\sigma_2 b_2)}} \qquad (28)$$

$$\pi f_{low}(\mu_1 b_1+\mu_2 b_2)(\sigma_1 b_1+\sigma_2 b_2) = 1 \qquad (29)$$

Since everything except b_2 is known here, multiplying out will result in a quadratic equation in b_2 with solution (30).

$$b_2 = -\frac{(\mu_2\sigma_1+\mu_1\sigma_2)b_1}{2\mu_2\sigma_2} \pm \frac{\sqrt{(\mu_2\sigma_1+\mu_1\sigma_2)^2 b_1^2 - 4(\mu_2\sigma_2)\left(\mu_1\sigma_1 b_1^2 - \frac{1}{\pi f_{low}}\right)}}{2\mu_2\sigma_2} \qquad (30)$$

Substitution of (3) into this gives (31). By consideration of material properties (in that they are real), and provided that f_{high} is greater than f_{low}, this equation will always have only one positive root. This is quite clearly the correct choice for the layer thickness.

$$b_2 = -\frac{(\mu_2\sigma_1+\mu_1\sigma_2)b_1}{2\mu_2\sigma_2} \pm \frac{\sqrt{(\mu_2\sigma_1+\mu_1\sigma_2)^2 b_1^2 - 4(\mu_2\sigma_2)\left(\frac{1}{\pi f_{high}} - \frac{1}{\pi f_{low}}\right)}}{2\mu_2\sigma_2} \qquad (31)$$

It is interesting to note here that the width of the conductors do not appear in these equations. This is because the knee frequencies are only dependent on the thickness of the conductor. Changing the width of the conductor will change the two knee-resistances. However, this will just shift the response up or down, but will not separate the two resistances. The shape will be the same, resulting in essentially the same filter in terms of attenuation. In the example for this design, the knee frequencies are specified as 100kHz and 1MHz, the resulting layer thicknesses are then b_1 = 355µm, and b_2 = 305µm. The simulation results are given in Figure 4.7. It can be seen here that both knee-frequencies are fairly well approximated.

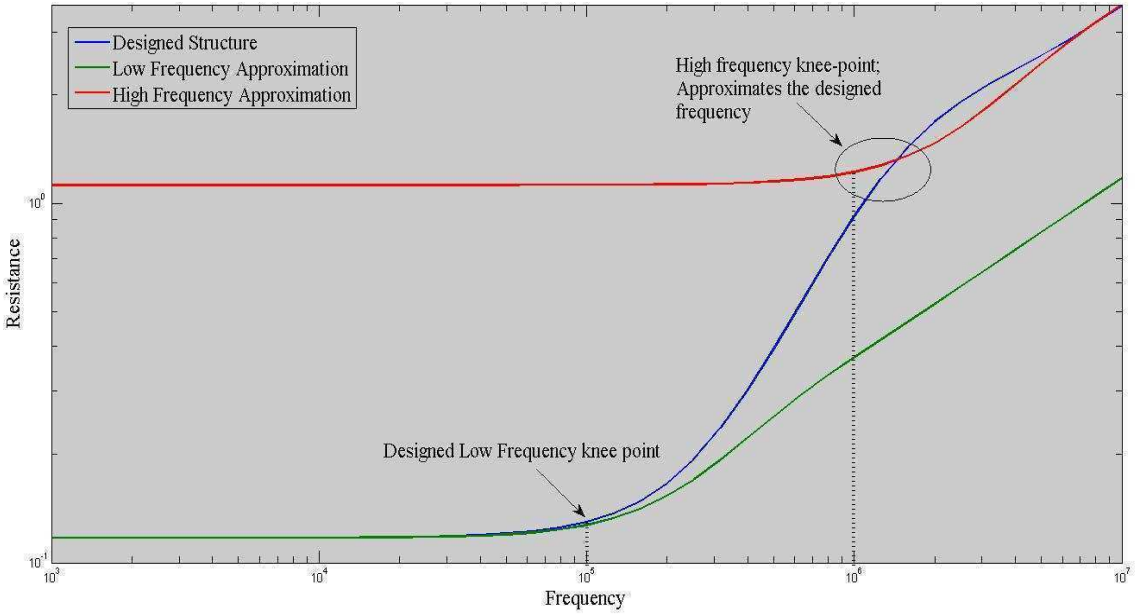


Figure 4.7. Response of structure when two knee-points are specified

4.4.2.3. Specifying f_{high} and R_{DC}

Specifying f_{high} results in a solution for b_1 as given in (24). Now this is known, rearranging (14) results in (32). From here, b_2 is given by (25).

$$R_H = \frac{\pi f_{high} \mu_1 b_1}{width} \qquad (32)$$

The example for this case specifies f_{high} = 1MHz, and R_{DC} = 50mΩ.m^{-1}. This results in layer thicknesses b_1 = 355µm, and b_2 = 765µm. Figure 4.8 shows the simulated result for this design. It can be seen that f_{high} is fairly well approximated, as well as R_{DC} at the low frequency knee-point.

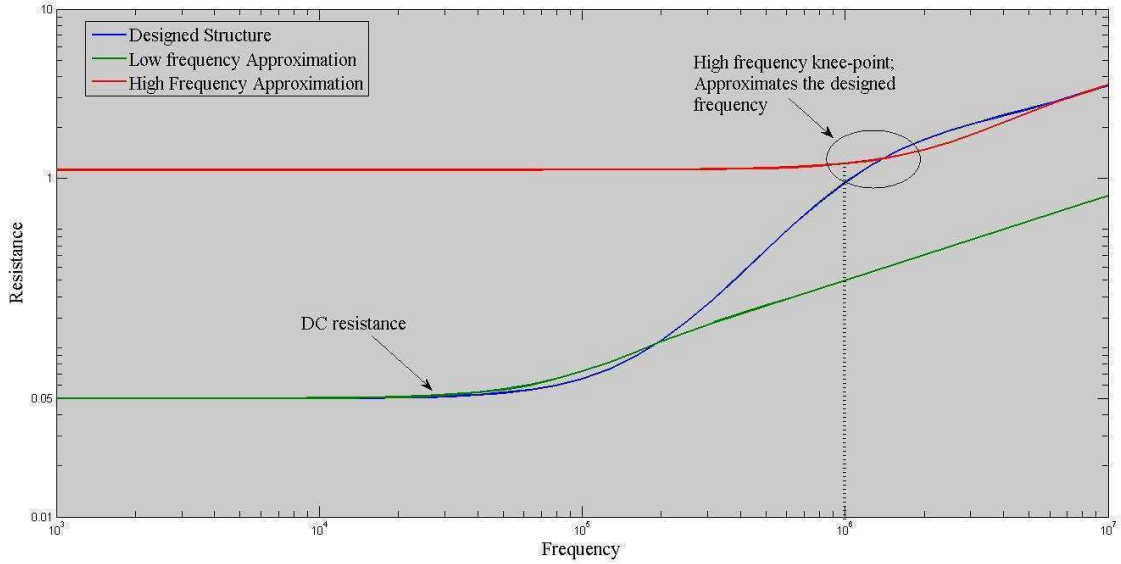


Figure 4.8. Response when R_{DC} and f_{high} are specified

4.4.2.4. Specifying R_H and f_{low}

Rearrangement of (13) gives (33). From this, f_{high} is given by (3). The second thickness b_2 follows through use of (31).

$$b_1 = \frac{1}{width\ \sigma_1 R_H} \qquad (33)$$

The example for this case specifies R_H = 300mΩ.m^{-1}, and f_{low} = 10kHz. These specifications result in b_1 = 1.33mm and b_2 = 790µm. It can clearly be seen in Figure 4.9 that the specifications are fairly well met in this case, with very little discrepancy.

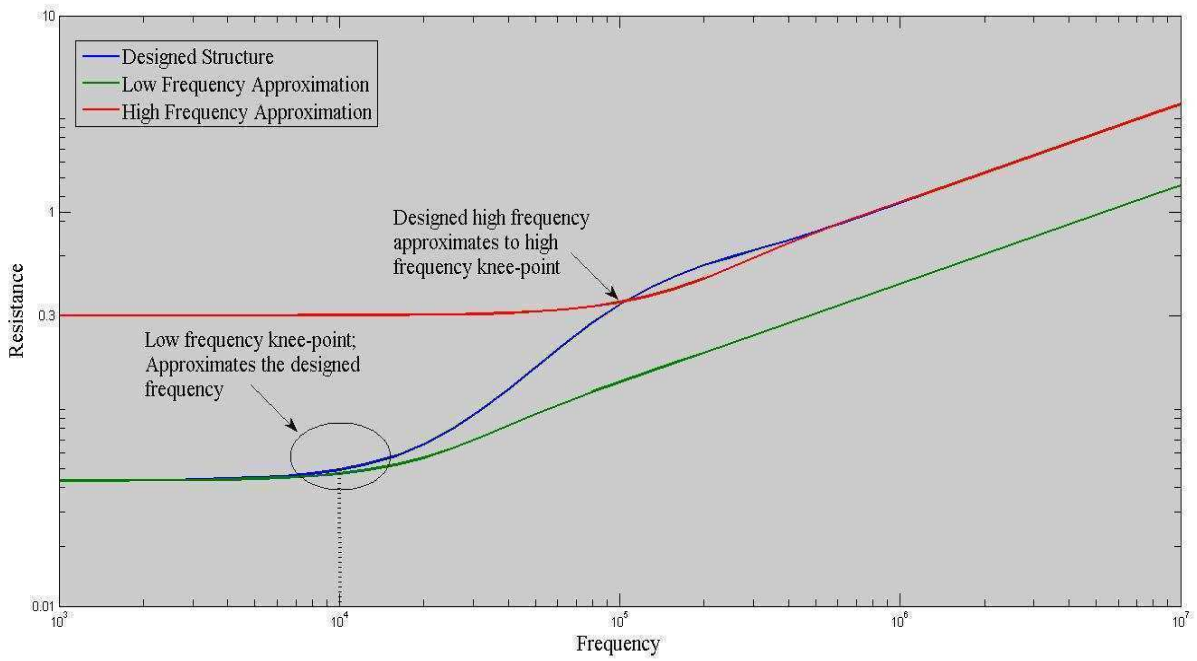


Figure 4.9. Response when R_H and f_{low} are specified

4.4.2.5. Specifying R_{DC} and f_{low}

Rearrangement of (12) gives (34). Substitution of (34) into (15) and rearranging gives (35). This, once solved, can be substituted back into (34) in order to solve for b_1.

$$b_1 = \frac{1}{\sigma_1 width R_{DC}} - \frac{\sigma_2}{\sigma_1} b_2 \qquad (34)$$

$$b_2 = \frac{\sigma_1}{\sigma_1\mu_2 - \sigma_2\mu_1}\left[\frac{width R_{DC}}{\pi f_{low}} - \frac{\mu_1}{\sigma_1}\frac{1}{width R_{DC}}\right] \qquad (35)$$

The example for this case specifies R_{DC} = 100mΩ, and f_{low} = 10kHz. These specifications result in b_1 = 3.2mm, and b_2 = 84µm. It can be seen in Figure 4.10 that the specifications are fairly well met, with little discrepancy.

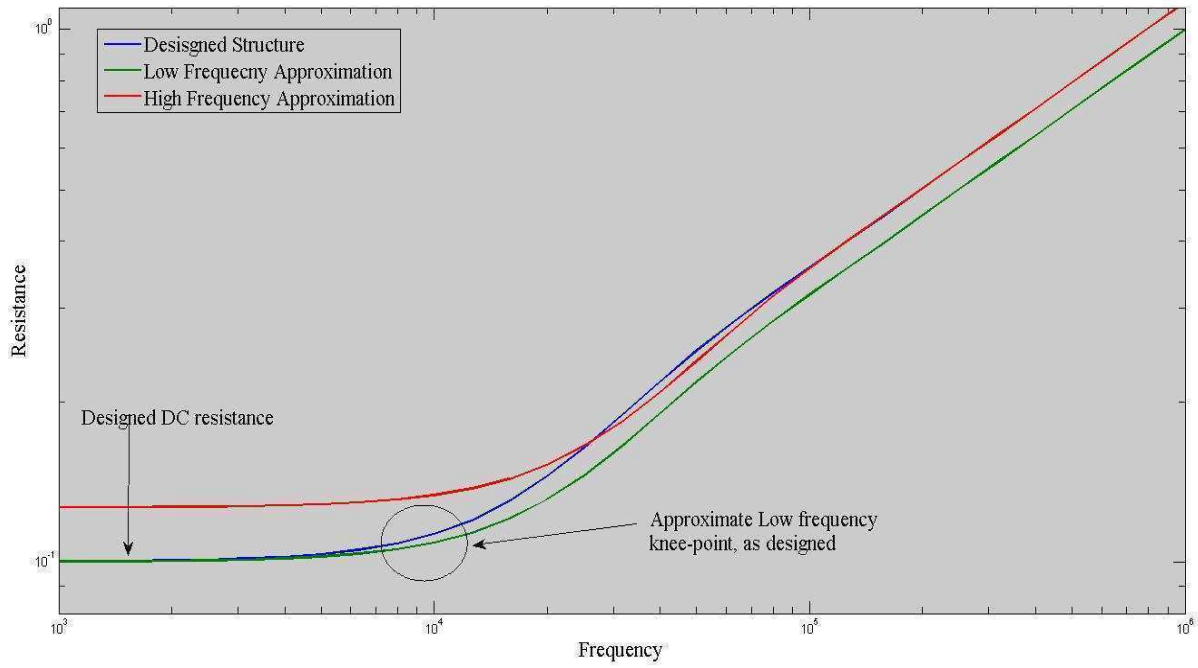


Figure 4.10. Response when R_{DC} and f_{low} are specified

4.5. Conclusion

The use of single-layer approximation has been discussed. It was shown in Chapter 3 to fairly accurately represent the real structure it approximates. Here it was shown that there are discrepancies particularly in the sense that it does not take order into account. With the approximation as it stands, and using the knee-points that it specifies as is, it is clear that the approximation is a good design tool at least for two-layered conductors. This is especially true given the design examples presented here.

A proposed generalisation to more than two layers was given in [2] and [3]. Verifying to what extent this technique is generalisable is not within the scope of this dissertation. The focus here is to characterise two-layer structures and present a design tool. The work of [2] and [3] has been verified for the two layered case, and while it was mentioned in that work that this technique presents a design tool for filtering applications, the process of doing so was not addressed. This chapter expanded on that work by presenting design equations and restrictions on possible filters that can be designed.

It was shown here that for arbitrary materials, there is a minimum, as well as a maximum, thickness for the layers of the structure. This means that there are some filters that are not realisable because the total permeability and total conductivity might not both be achievable within these restrictions.

4.6. References

[1] I Hofsajer and I Botef, "Cold Spray Technology for High Performance Frequency Selective Conductive Structures," *In Press*.

[2] NJ Botes, "Aspects of Computational Electromagnetics for the Treatment of Multi-layer Composite Conductive Structures," University of the Witwatersrand, Lab Project 2011.

[3] FJ Lange, "Aspects of Computational Electromagnetics for the treatment of Multi-layer Composite Conductive structures - Impedance Profile Prediction," University of the Witwatersrand, Lab Project 2011.

Chapter Five – Experimental Results

Table of Contents

5.1. Introduction 64
5.2. Experiment Design 64
5.3. Justification of Experiment 67
5.4. Experimental Results 68
5.4.1. Determination of material properties 68
5.4.2. Results 69
5.4.2.1. Single Layer Aluminium 69
5.4.2.2. Aluminium and Brass 70
5.4.2.3. Aluminium and Nickel 71
5.4.3. Consolidation of results 72
5.5. Conclusion 73
5.6. References 73

5.1. Introduction

In this chapter, experimental results are presented in order to verify the results obtained in the parametric study. The parametric study suggests that in order to produce a more dissipative filter, the conductivity of the inner layer must be lower than that of the outer layer. Further to this, it also suggests that better results are obtainable when the inner layer also has a higher permeability than the outer layer.

In order to verify that this is the case, it is desirable to make a measurement to show that a non-magnetic material with a low conductivity gives the suggested result and then carry out a measurement where a magnetic material with a similarly low conductivity gives a better result. Figure 5.1 shows graphically the two conceptual structures that will be measured. In order to conduct this experiment, three different materials are needed.

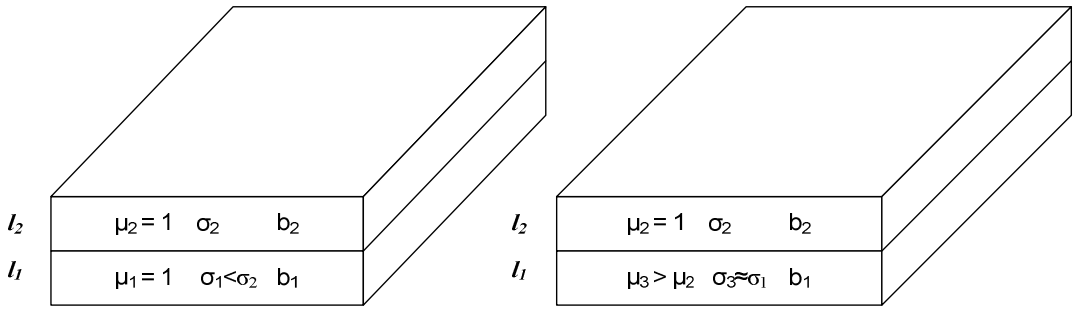


Figure 5.1. Graphical representation of the two measurements

5.2. Experiment Design

Brass is a non-magnetic material with a conductivity of approximately 16×10^6S, while nickel is a magnetic material with a conductivity of approximately 14×10^6S and a relative permeability of between 20 and 600 depending on the batch. These two materials have similar conductivities, but different permeabilities; making them ideal for use as the inner layer for the two measurements mentioned above. The outer layer for these measurements is chosen to be aluminium, with a conductivity of approximately 37×10^6S, again this depends on the batch of aluminium. The rationale behind this choice is so that the resistance of the structure will be within the accurately measurable range of the measurement equipment [1].

This dissertation concerns itself with differential mode excitation and as such, differential measurements will be taken. This is shown in Figure 5.2. The gap between the conductors is effectively a parallel plate capacitor, and at the same time is a loop volume for external inductance. Care must be taken when designing the structure that the dimensions are not such that the resonant frequency is within the range of measurements. The external inductance of the structure is given in (1), calculated from the magnetic energy in the air between the conductors. The capacitance is given in (2) and the resonant frequency is given in (3). Note its dependence only on the length, and not on the width or height. The difficulty here is that in order to have a high enough resistance for the measurement device, the conductor must be long, however, the longer the conductor, the lower the resonant frequency. One note, however, is because the conductor forms a returning loop; the length contributing to the

resistance is twice the length contributing to the resonant frequency. For a length of 2m, the resonant frequency is approximately 24MHz.

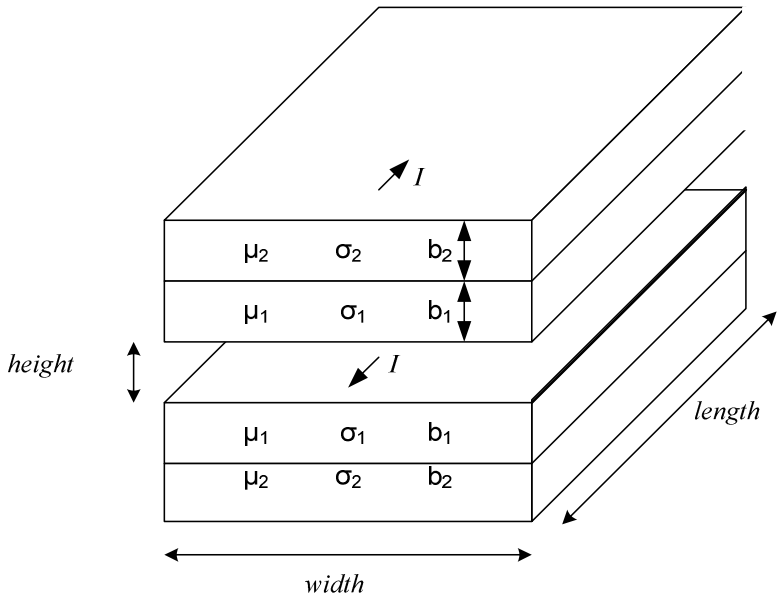


Figure 5.2. Experimental Schematic

$$L_{ext} = \frac{\mu_0 length\ height}{width} \qquad (1)$$

$$C = \frac{\varepsilon_0\ width\ length}{height} \qquad (2)$$

$$f_{res} = \frac{1}{2\pi\sqrt{L_{ext}C}} = \frac{\sqrt{\mu_0\varepsilon_0}}{length} \qquad (3)$$

Due to availability of materials, both layer thicknesses are taken to be 100μm. The separation height will be created with insulating paper approximately 100μm. This gives a total structure thickness of approximately 0.5mm. The width of the conductors is 30mm in order to satisfy the minimum 25:1 width to thickness ratio given as a restriction previously. This means that the structure falls within the restrictions necessary in order to model it with the one-dimensional approximation.

It is also important to ensure that the layers of the conductors are kept tightly together, and parallel to each other. As such, the structure will be mounted in a two metre Perspex jig with two rows of bolt-holes along the length of the Perspex as used by Brink in [2]. The rows have a separation distance of 50mm, and within each row, the holes are separated by 100mm. A picture of the experimental set up is shown in Figure 5.3. The way in which the setup was mounted to the impedance analyser is shown in Figure 5.4.

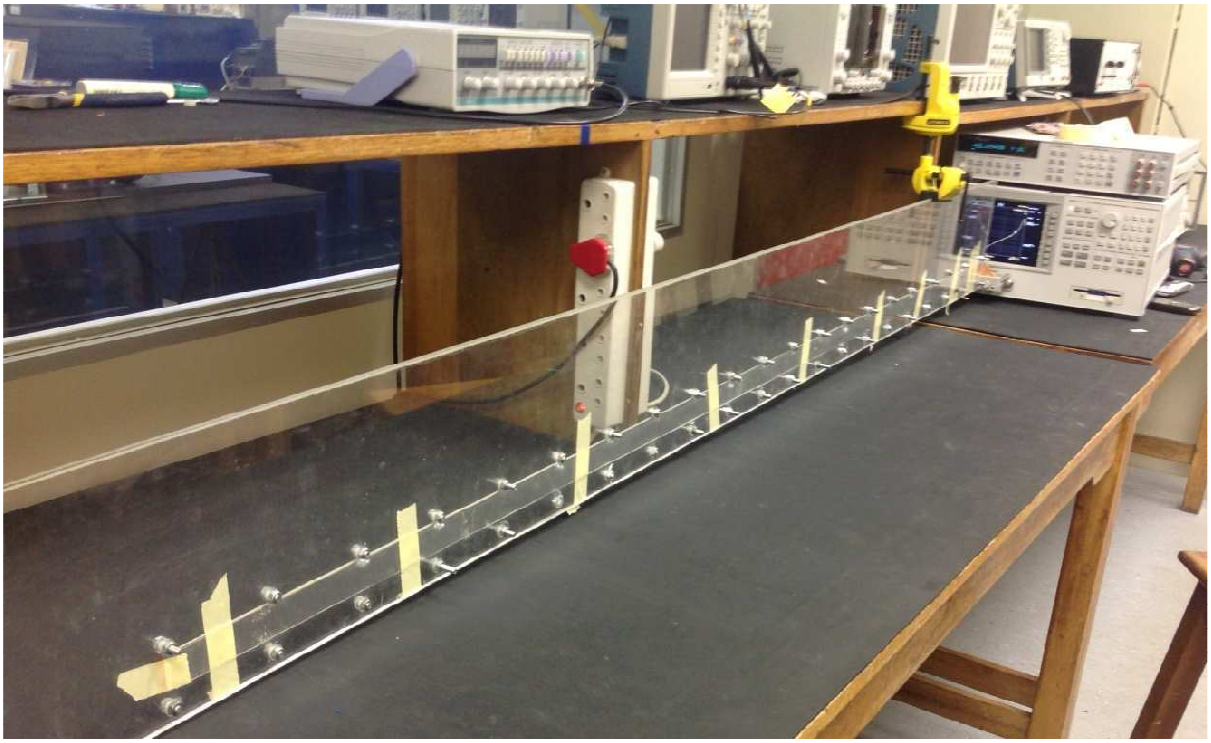


Figure 5.3. Experimental Setup

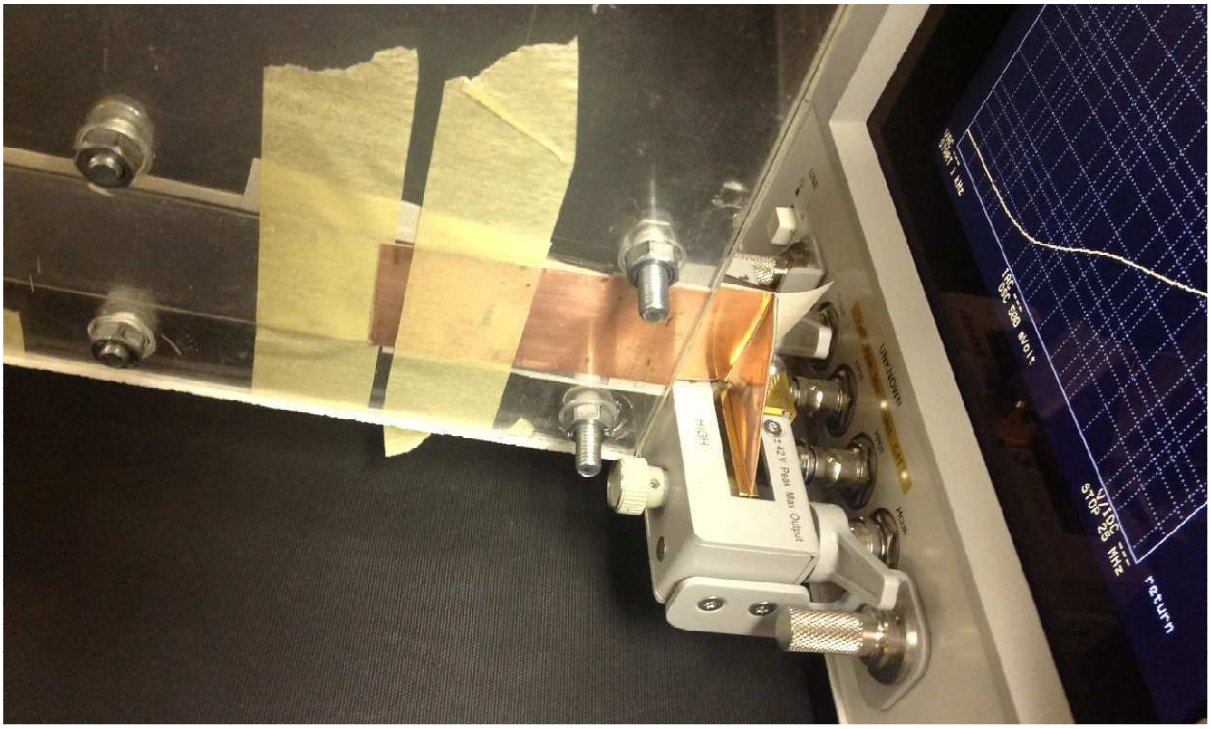


Figure 5.4. Mounting of setup

The expected range of resistances for a 2m structure is from 30mΩ at 1kHz to 2.85Ω at 10MHz. Consulting [1], the error will be no more than 10% at low frequencies, and no more than 3% at 10MHz, provided that resonant effects have not been introduced. Because the resonant frequency is at approximately 24MHz, it is expected that these effects will start to be seen at least as low as 10MHz.

5.3. Justification of Experiment

Figure 5.5 shows the expected results for the two structures with their expected parameters as laid out above. On the same set of axes is given the resistance curve for a pure aluminium structure. The nickel structure has been assumed to have a relative permeability of 50. The choice of 50 in this case is so that it is within the range of permeabilities mentioned previously. It also helps to accentuate in this case the fact that the permeability of the second layer is of major importance. In order to see that the two composite structures give better dissipative filtering, the three curves are normalised in Figure 5.6. The structure with Brass has its low knee-point after the pure aluminium structure's low knee-point – meaning it starts increasing later – but reaches (in this case) a resistance of 4Ω before the pure aluminium structure. It can also quite clearly be seen that the structure with nickel has a steeper gradient during the transition between the two knee points. A steeper gradient implies more attenuation.

This figure clearly demonstrates that a more dissipative filter can be realised by using a material with lower conductivity and higher permeability as the inner layer. In this case nickel is the material of choice. As such, it is clear that conducting these measurements experimentally will verify the conclusions with regard to dissipative filtering. This will also give confidence to the results obtained in the parametric study.

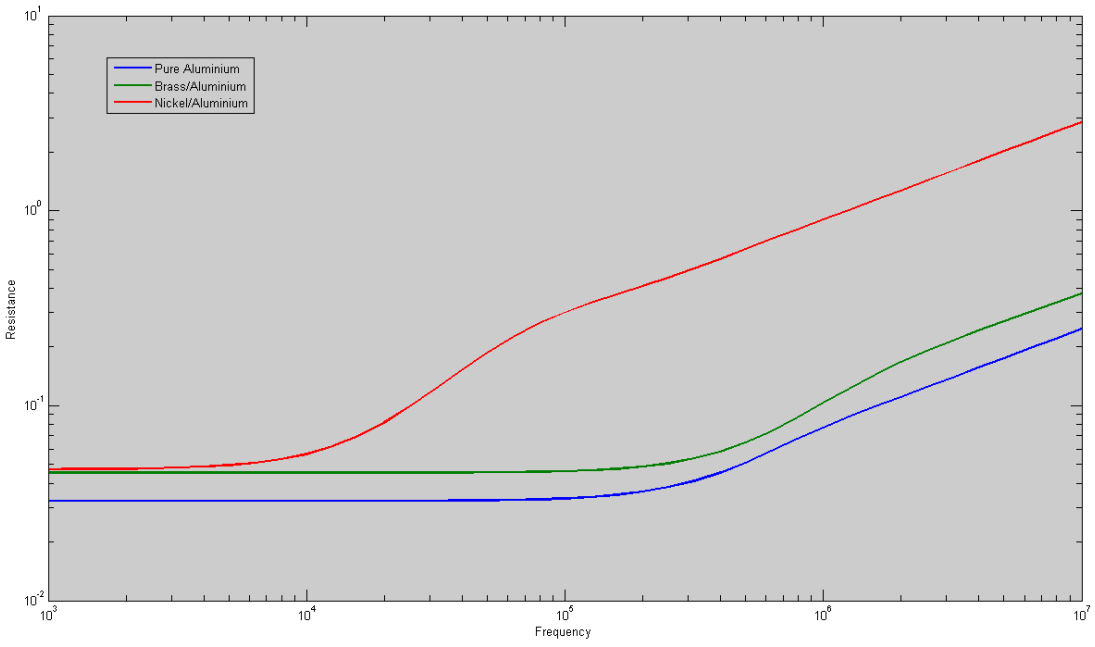


Figure 5.5. Expected Results fro a 3m long conductor (effective 6m of resistance)

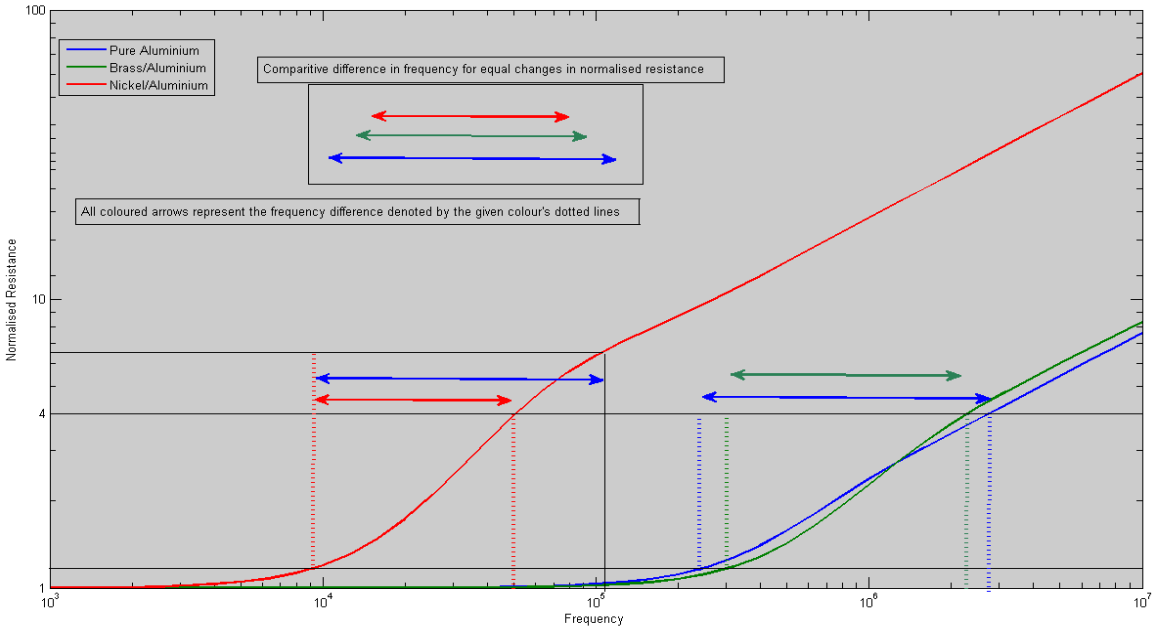


Figure 5.6. Normalised Resistance curves

5.4. Experimental Results

5.4.1. Determination of material properties

Seeing as material properties vary from batch to batch, it is necessary to measure properties of the materials first, before the experiment can take place. Measuring the conductivity can be done with a four terminal DC test. The permeability is more difficult, although it will be assumed that brass and aluminium are non-magnetic. Measuring the permeability of nickel can be done by measuring its frequency dependent resistance and approximating the knee-point. Since the conductivity will be known from a DC test, the permeability can be approximated according to the skin-depth equation. It is important to observe that this is an approximation.

A single 100µm (measured with a micrometer) layer of aluminium was mounted in the jig and a DC test was conducted. A 1.0A DC current was applied to the structure and a terminal voltage of 38.80mV was measured. This gives a DC resistance of 38.8mΩ for the particular sample of aluminium. The conductivity is calculated using (4) with a conductor length of 4m and width 30mm. From this, the conductivity of aluminium is measured to be $34.4 \times 10^6 S.m^{-1}$ as opposed to a textbook value of $38 \times 10^6 S.m^{-1}$.

$$\sigma = \frac{l}{R_{DC}.width.thickness} \qquad (4)$$

In a similar way, the conductivities for 100µm layers of Nickel and Brass were calculated to be $10.9 \times 10^6 S.m^{-1}$ and $13.1 \times 10^6 S.m^{-1}$ respectively. The relative permeability of the particular sample of Nickel was calculated to be approximately 12. This was done by approximating the knee point of the Nickel measurement. It is uncertain as to why the nickel has a relative permeability outside of the suggested range mentioned above.

5.4.2. Results

5.4.2.1. Single Layer Aluminium

A single 100µm layer of aluminium was measured in the frequency range from 1kHz to 5MHz. Measurements are taken in R-X form, with the reactance of the structure ignored. Even though the other two measurements are made with conductors of total thickness 200µm, it is not necessary to do the same with this measurement. Since it is just a single layer measurement, changing the thickness of the layer will only lower the knee-frequency and DC resistance. The shape of the curve will remain the same. The expected and measured results for this measurement are shown in Figure 5.7.

It can be seen that there is a discrepancy at high frequencies. It was noticed that if the relative permeability of the aluminium was taken to be 1.2, the high frequency resistances match up; the results for which are shown in Figure 5.8. However, it should be noticed that there is still a gap between the curves near the knee-points. It should also be observed that the measured resistance of the aluminium is increasing up until the knee-point, whereas the typical expected resistance value (for any single layered conductor) should remain largely constant until the knee point. It is suspected that the aluminium is not pure since a slight change to the magnetic parameters gives better agreement between the measure and expected results. Because there is no information available as to the nature of these impurities, both in terms of what they are, and degrees of homogeneity throughout the aluminium, it is not possible to fully characterise the aluminium.

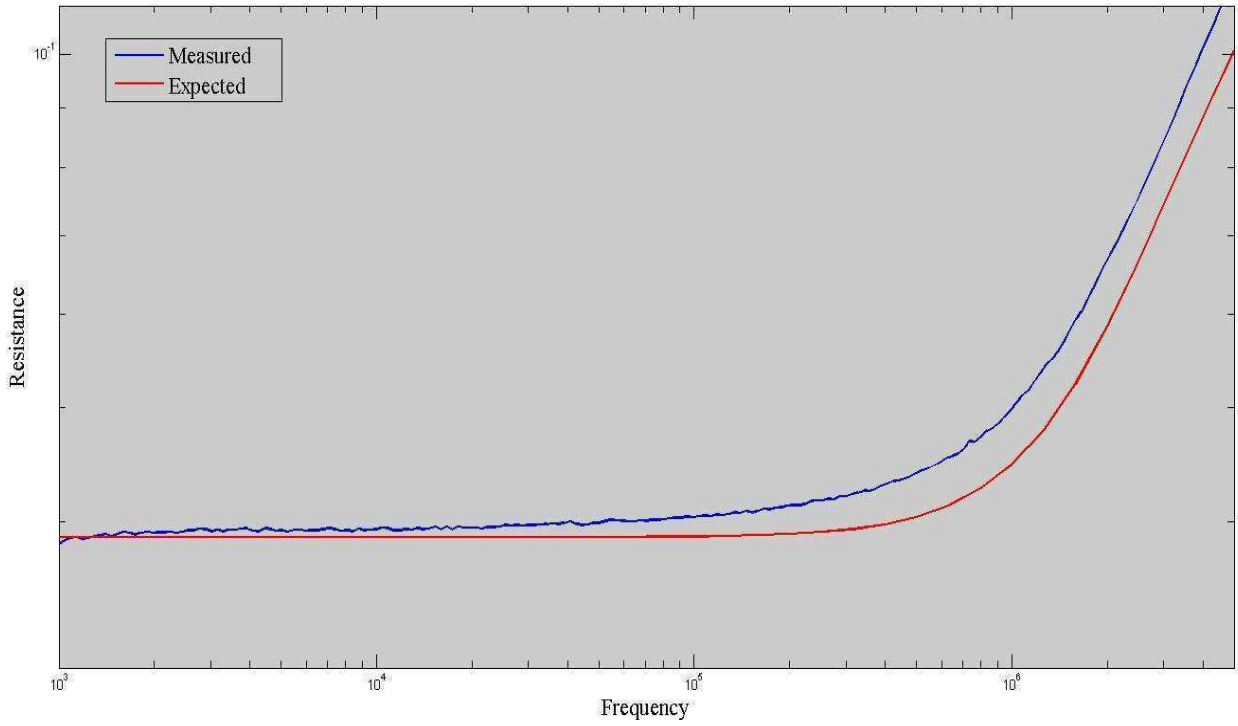


Figure 5.7. Measured vs. Expected results for aluminium only

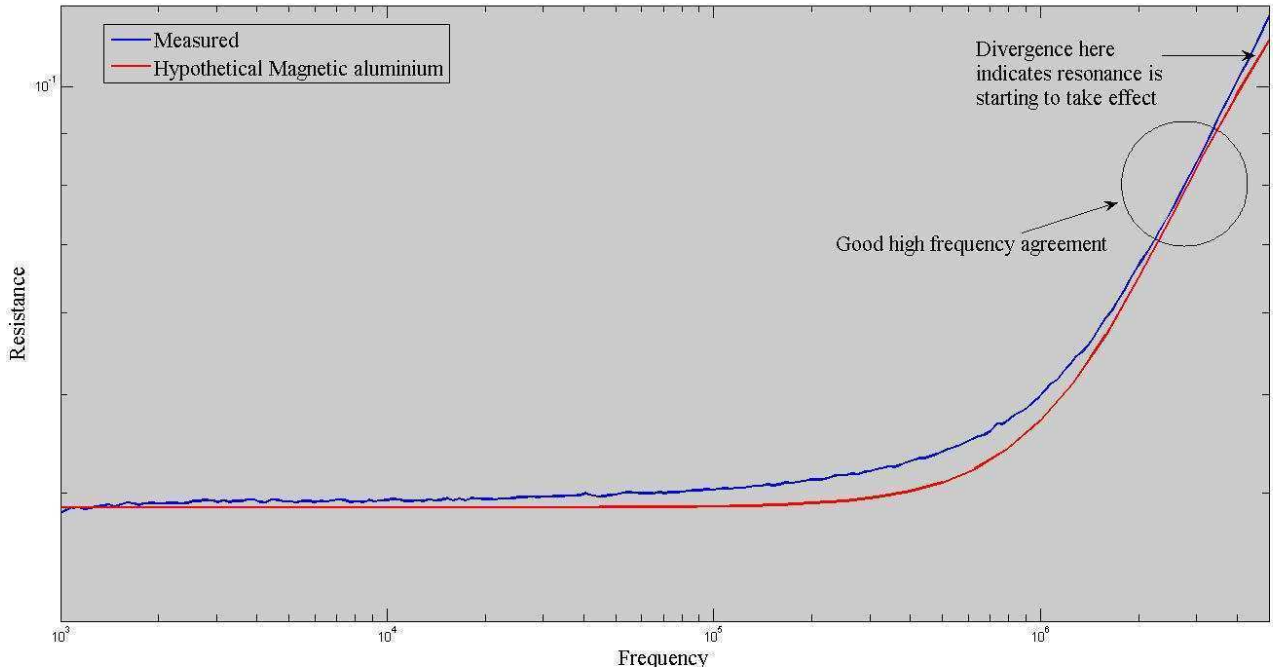


Figure 5.8. Measured vs. Expected results for hypothetical magnetic aluminium

5.4.2.2. Aluminium and Brass

In this case, a 100µm layer of aluminium is placed upon a 100µm layer of brass. The brass layer of this multi-layered conductor is the inner layer in the differential configuration. The measurements are in the range from 1kHz to 25MHz. Measurements are taken in R-X form, with the reactance of the structure ignored. The results are given in Figure 5.9. The resonant point can clearly be seen. At this point the reactance is so high (because of parallel resonance) that the measurement device has trouble measuring the resistance of the structure since the R-X model is no longer necessarily valid. In this case, the high-frequency knee point may in fact be affected by the resonance effects because the point at which the gradient increases is close to the knee-point. However, the gradient does decrease at the point indicated giving confidence that the knee point is in fact correctly placed. There is good agreement between the measured results and the expected results, with the high frequency knee-points happening at approximately the same frequencies and resistances. However, because resonance starts taking effect near the knee point, it is not possible to comment on how the high-frequency resistance matches with the expected results. But it is still reasonable to make the conclusion on the matching of the high frequency knee-points.

The deviation at the lower frequency can be attributed to the issues raised above with regard to the aluminium. At the low frequencies, current is still in the aluminium layer (as well as the brass) and as such, any effects due to impurities will still be present.

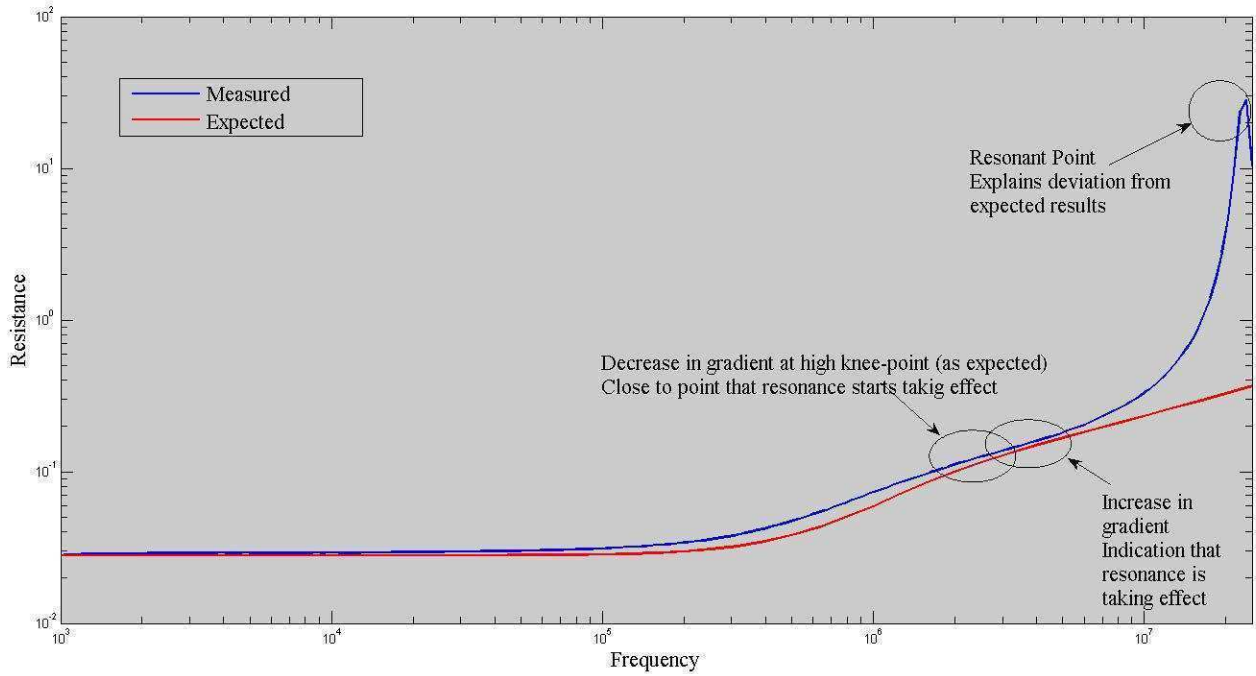


Figure 5.9. Measured vs. Expected results for Aluminium-Brass

5.4.2.3. Aluminium and Nickel

In this case, a 100µm layer of aluminium is placed upon a 100µm layer of nickel. The nickel layer of this multi-layered conductor is the inner layer in the differential configuration. The measurements are in the range from 1kHz to 25MHz. Measurements are taken in R-X form, with the reactance of the structure ignored. The results are given in Figure 5.10. Again, the resonant point can quite clearly be seen. Once again, it can easily be seen that the high-frequency knee-point is not affected by the resonance. The point at which resonance starts to take effect is demonstrated on the figure. It can quite confidently be concluded that the high frequency knee-point indicated is not affected by resonance effects due to the separation in frequency of the two points. The reason for this is that at the high frequency knee point, there is a decrease in the gradient of the resistance curve, with the gradient after the knee-point being maintained for a while before the increases due to resonance take effect.

There is good agreement here between the measured and expected results, especially in terms of the high frequency knee-points, and the resistance values. Once again, the discrepancy can be attributed to the issues raised with regard to the aluminium. The very good agreement at the high frequencies (before the resonant effects) is expected, especially because the nickel is 99.99% pure.

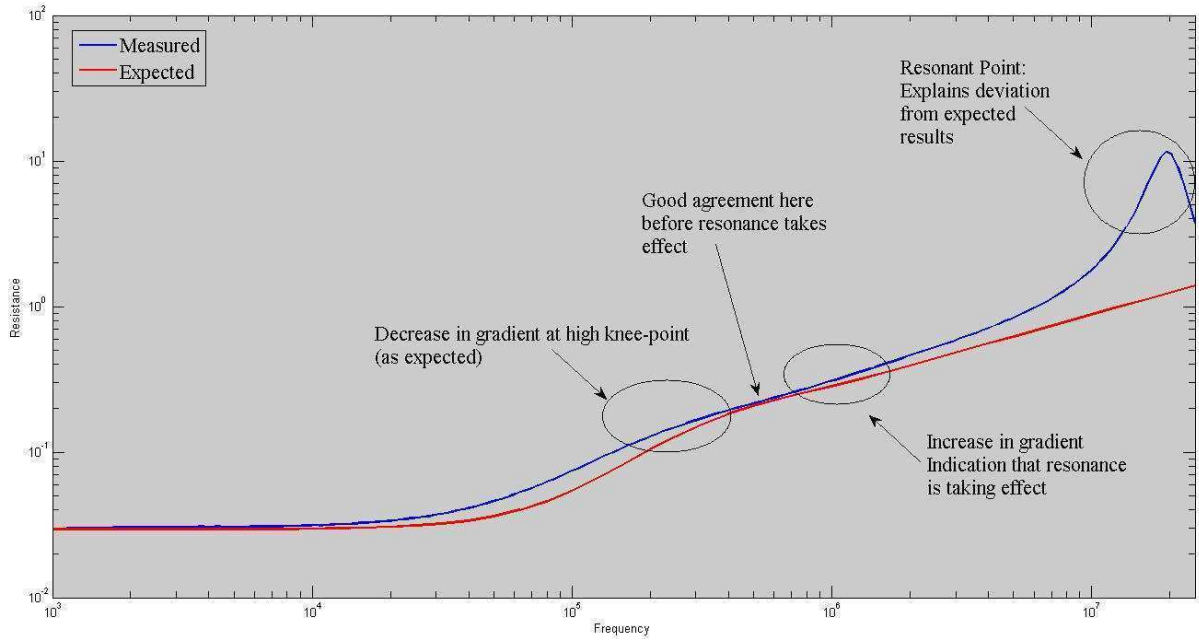


Figure 5.10. Measured vs. Expected Results for Aluminium-Nickel

5.4.3. Consolidation of results

The measured results of the two multi-layered conductors are normalised and presented on the same set of axes in Figure 5.11. The two curves demonstrate what was explained graphically in Figure 5.6 in that an inner layer with a higher permeability has a better effect in terms of dissipative filtering. Attention is not drawn to the knee-point frequencies – since these can be shifted through scaling the structure either bigger or smaller – but rather to the average gradient between these frequencies. There are two important observations to which attention needs to be drawn; both annotated in the figure.

The change in resistance between the two knee points of the Aluminium-Brass structure has been shown, and its corresponding frequency difference has been annotated. The frequency difference for the Aluminium-Nickel structure for the same change in resistance has been shown. Comparing the two graphically, it can be seen that there is a significantly smaller frequency difference for the Aluminium-Nickel structure than for the Aluminium-Brass. Secondly, the frequency difference annotated for the Aluminium-Brass has been applied to the Aluminium-Nickel and the comparative changes in resistance have been shown. It is also clear in this case that, for the same change in frequency, there is a significantly greater increase in resistance for the Aluminium-Nickel than for the Aluminium-Brass.

These two observations demonstrate essentially the same thing. Viewing the structures' dissipative filtering capabilities in either way is sufficient to quantify the relative dissipative qualities of the two. In this case, it is clear that the Aluminium-Nickel structure is better with regard to dissipative filtering.

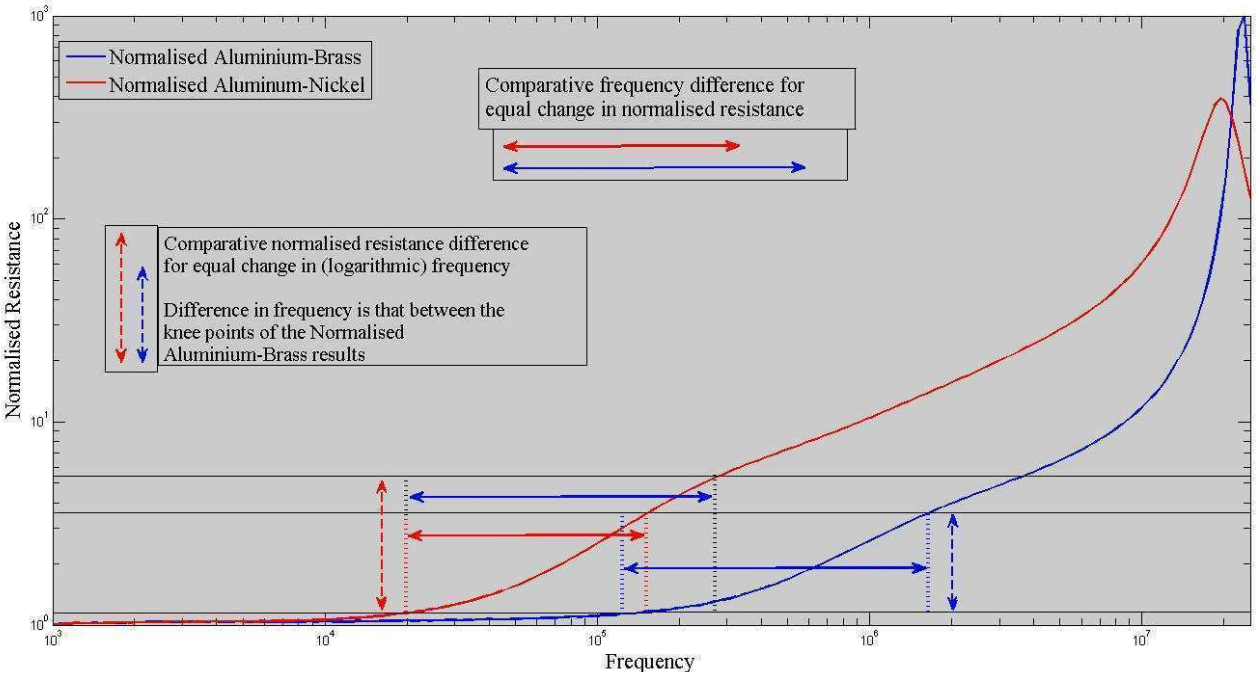


Figure 5.11. Normalised Multi-layered conductor results

5.5. Conclusion

A major conclusion from the parametric study has been verified in this experiment. It has been shown that a better dissipative filter can be obtained by having the inner layer in a two-layered conductor less conductive but more permeable than the outer layer. This is of course only true for the differential mode. In the common mode, the opposite is true. Seeing as the experiment has served to verify this conclusion, confidence can now be placed in the validity of results of the parametric study, as well as the usefulness of the single-layer approximation.

5.6. References

[1] Agilent Technologies, *Agilent 4294A Precision Impedance Analyzer Operation Manual*, Sixth Edition ed.: Agilent Technologies, 2002.

[2] E Brink, *Aspects of Electromagnetic Field Distributions in Multipath Conductive Structures*. Ph.D Thesis: University of the Witwatersrand, 2011.

Chapter Six – Conclusions and Recommendations

Table of Contents

6.1. Introduction 75
6.2. Characterisation of two-layer conductors 75
6.3. Single Layer Approximation 76
6.4. Dissipative filters 77
6.5. Consolidated conclusions 77
6.6. Recommendations for future work 78

6.1. Introduction

In Chapter One it was shown that multi-layered conductors are an important part of Power Electronic Integration, and that understanding these structures may have applications in the use of dissipative filters. As such, the objectives of this dissertation were as follows:

- To characterise two-layer conductors in terms of how the properties of the materials affect the frequency dependent resistance of the structure
- Demonstrate a possible design technique using the results obtained from the characterisation of two layer conductors
- Show that two-layer conductors show different dissipative effects than single-layer structures

Each of these objectives is discussed in turn, with reference to the particular chapters relevant to the objectives.

6.2. Characterisation of two-layer conductors

In order to characterise two-layered conductors, it was important to define the parameter space before a parametric study was conducted. In Chapter Two, it was shown that it was adequate to restrict attention to the case of differential mode excitation because of equivalence between the common and differential modes. Further to this, it was shown that a conductor can be rescaled with suitable changes in its properties in order to produce the same frequency dependent resistance. A conclusion that can be drawn from this rescalability is that the values of importance for the structure are the *total permeability* and *total conductivity* of each layer and how they relate to each other. The absolute values of the conductivity and permeability are somewhat irrelevant in the characterisation of two-layered structures. As such, it is only necessary to consider conductors where the two layers have the same thickness.

In Chapters Two and Three it was suggested that a two layer conductor can be characterised as having two knee frequencies, through the application of a single-layer approximation. It was shown in Chapter Three that the resistance of the structure at the high frequency knee-point is well approximated by the DC-resistance of the inner layer conductor, called the *high-frequency knee-resistance*. The DC-resistance of the total conductor was also determined by the parallel combination of the two layers. From this is can be concluded that the range between DC-resistance and the high-frequency knee-resistance is largely controlled by the difference between the conductivities. In order to have a large range, it is required that the inner layer have a lower conductivity than the outer layer. Intuitively, this means a larger degree of dissipation at high frequencies with respect to the dissipation at low frequencies than would be possible with a single-layered conductor.

Also, in the parametric study it was shown that the shape of the resistance curve between the two knee-points is determined by the total permeability of the layers in relation to each other. A large permeability ratio between the outer and inner layers results in a response which is concave-right between the two knee points. A low permeability ratio (smaller than 1 when

the inner layer has a greater permeability than the inner) results in a response that is concave-left. This also leads to an overall better dissipation ability. Because the shape changes significantly with relation to the permeability ratio, it is very possible that there exists a point at which the response between the two knee points is a straight line.

With a significantly concave-right response, it is possible to create a structure which essentially has two DC resistances. One is the *DC-resistance* of the structure, while the other is the *high-frequency knee-resistance*. These two DC resistances are valid in different frequency ranges. The first is valid up until the first knee point, with the second valid in a significant portion of the frequency range between the two knee-points. With a significant concave-left response there is very large gradient that results between the DC resistance and the high-frequency knee-point. These were both demonstrated in Chapter 3.

6.3. Single Layer Approximation

Once two layer conductors have been characterised, the question now arises as to whether structures can be designed using these concepts. The single-layer approximation represents a hypothesised design tool and was conceptualised in Chapter Two. The concept is to take a two-layer conductor and turn it into a hypothetical effective single homogenous material. This material has a typical single-layer knee-point, from which the low-frequency knee-point is approximated. The high frequency knee-point is approximated from the inner layer's knee-point.

Throughout the parametric study in Chapter Three, the single-layer approximations were calculated for each parametric structure. They were shown to give good agreement for the DC-resistance, and the high-frequency resistance (beyond the high-frequency knee-point) of the two-layer structure. It also gave good agreement for the high-frequency knee-point and knee-resistance. Discrepancies were pointed out in the approximation for the low frequency knee-point; this was demonstrated in Chapter Four to be because the approximation does not discriminate between the orders of the two layers. However, because this is a very simple approximation, this discrepancy is not of too much concern. Having a more accurate approximation would only serve to make working with these structures more complicated.

The important note here is that is just an approximation, albeit a fairly good one. Whether the actual low-frequency knee-point of the real structure is higher or lower in frequency for a given structure can be determined using the single layer approximations. If the approximations do not intersect, the real structure will have a knee-point at a lower frequency than the low-frequency approximation; if they do intersect, the real structure will have a knee-point at a higher frequency.

In Chapter 4, it was shown that the approximation is a good first approximation at designing dissipative filters. The necessary equations were developed, and can be done either with or without restriction. The design with restriction is a far more likely process to be used simply due to the availability of materials. The disadvantage to this design process is the fact that the only controllable variables are the individual layer thicknesses.

6.4. Dissipative filters

With regard to dissipative filters, it was identified in Chapter One that a single layer structure will not produce the desired effect. At sufficiently high frequencies, the resistance represents an unavoidable part of the resistance curve. As such, it was concluded that the response below the knee-point was the only place at which changes can occur. One way to address this was identified to be the use of multi-layered conductors.

The main conclusion from Chapter Three with respect to dissipative filters is that the inner layer should have a lower conductivity than the outer layer. This has the effect of increasing the resistance range between the two knee-points. This represents a good first step towards better dissipative filtering, since the structure must go through a large range below the same knee-frequency. It is possible to push the frequency, at which this resistance-increase starts, higher by having an inner layer with a higher permeability than the outer layer. This gives a low permeability ratio which, from the characterisation of two-layer structures, was shown to produce a steep gradient in frequency dependent resistance.

As such, in order to produce a more dissipative filter than a single-layer conductor, at least a two-layer structure is required, with the inner layer having a lower conductivity and higher permeability than the outer layer. This conclusion is very well supported by the experimental verification of Chapter 5, where it was clearly shown that there is a larger average gradient, and resistance change for a structure made from aluminium and nickel than a structure made from aluminium and brass. Since the conductivities of brass and nickel are similar, this particular experiment served to verify that a higher permeability is desired for the inner layer.

6.5. Consolidated conclusions

It is suggested that the work outlined here will be useful in terms of power electronic integration design. This is because it provides a convenient way of modelling and analysing these structures. Further to this, two-layer structures have been fully characterised as to the effects of their properties upon the resistance of the structure; the conclusions having been laid out in Section 6.2 above. A design technique and approximation has been presented which allows for a rough idea on what the resistance curve will look like based upon the knee-points, and the characterisation of two-layer structures.

The concept of dissipative filtering has been presented as a possible application for two layer structures. This is by no means the only application possible. In fact, it is quite clear that, with regard to dissipative noise filtering, it is likely undesirable to have a response which is concave-right – which is certainly a possible occurrence with these structures and was show in Chapter Three. What has been shown here is how to create a dissipative filter restricted to two-layers. Not only that, but a two-layer structure will have a different response to common- and differential-mode excitation. As such, this does not necessarily represent a good EMI filter. It is probable that a structure of at least three layers is necessary in order to create such a filter; it was shown in Chapter 2 that an odd-layered structure is necessary to have the same response in both common- and differential-mode excitiation.

It is also possible that an application exists for a structure which is concave-right, with effectively two different DC resistances but applied to different frequency ranges. This has been shown to be possible through the characterisation of two-layer structures; the relevant characterisation being that the inner layer must at least have a lower permeability than the outer layer. Also, given the different response of the structure under the two modes of excitation, it is also relevant to applications where differential mode is desired to pass, while attenuation of common mode is desired. The converse case is also possible.

6.6. Recommendations for future work

Exploration of the extent to which generalisation of the single layer approximation to more than two layers is possible is also suggested. Coupled with this, a characterisation of three-layer structures is the next logical step. With regard to this, it should be investigated as to what extent the two-layer characterisation is applicable to three-layers, if at all. It is expected that at sufficiently high frequencies the two layer characterisation is fully applicable (since the current wouldn't be in the outer layer). At low enough frequencies, however, all three layers would be contributors to the response of the structure

Having characterised three-layer structures, it is worth pursuing to what extent they are applicable to EMI filters. As was mentioned in Chapter Two, a symmetrical structure will give the same response for common and differential mode. A non-symmetrical structure will not, but to what extent they will be different is worth quantifying and pursuing.

The theoretical background to this work was based upon a thickness to width ratio of 1:25, and the assumption that the conductor is long compared to the other dimensions of the structure. This is in an effort to minimise end- and edge-effects. In many real applications this is not likely to be the case. This does not, however, negate the value of this work. It is good to understand the characteristics of multi-layered conductors at least from a simple perspective before moving to a more comprehensive and complicated understanding. Now that two-layer conductors have been characterised, it is worth exploring the extent to which the assumptions above are necessary, as well quantifying to what extent the relaxation of these requirements introduces errors into the theory.

This work focussed on the characterisation of two-layer conductors with a view to planar integration. The theory behind the work was also equally well developed for cylindrical concentric conductors, but these conductors were also not characterised. Research towards the characterisation of two-layer conductors in this regard is also suggested, albeit that it may not have direct application to power electronic integration.

Appendix A: Background theory

Table of Contents

Acknowledgement 80
A.1. Introduction 80
A.2. Single Layer Solution 80
A.3. Multi-Layer Generalisation 85
A.4. Resistance calculations 86
A.5. References 86

Acknowledgement

The derivation set out below is largely based upon the work by Emile Brink [1]. While the words are not the same, the flow of logic in terms of the derivation is the same due its simplicity. This particular derivation is by no means complete nor as in depth as that found in [1], but serves as a basic outline in order to bring the reader up to speed with the knowledge base and theory upon which this dissertation is based. On a particular note, this derivation here only concerns planar conductors, and not cylindrical concentric conductors which are treated in [1] as well. Should a fuller, in depth derivation be required, the reader is directed to chapters 2 and 4 in [1].

A.1. Introduction

The theory supporting this body of work is fundamentally based upon Maxwell's equations, and the solution of the boundary conditions pertaining to each individual conductive structure. This chapter is dedicated to the development of the equations that are implemented in obtaining results for multi-layered conducting structures, from Maxwell's equations. This is done from a magnetic and electric field perspective. The final set of equations will be shown to be dependent upon the total current flowing in the conductors, as well as upon the material properties of each conductive layer.

First the solution for just a single, generic conductive layer will be derived from Maxwell's equations. Restrictions of the domain of application of these results will also be discussed particularly with respect to the one-dimensional approximation, which is used in order to simplify the derivation of the final set of equations. Following that is a generalisation to *n*-layers of conductive material through treatment of boundary conditions through the use of Faraday's and Ampere's laws.

Having suitably obtained the equations governing the fields in a given structure, Chapter 3 will then present parametric studies of two-layer structures. This is in an effort identify the extent to which the frequency response can be controlled and modified with consideration of material properties and dimensions, as well as identify, to some extent how the relative values of separate-layer properties have an effect of said frequency response.

Attention is restricted, only, to conductor configurations where the incident magnetic field is parallel to the conductor surface, and not perpendicular. This allows for a simplification testing configurations. This is not to say that eddy currents have not been taken into account at all, just that the eddy currents that are used for eddy-current testing are not those present in the solutions derived here.

A.2. Single Layer Solution

The single layer conductor is approximated as a semi-infinite flat conductor. In this sense, it is of finite thickness, and is infinitely wide, and infinitely long. This can be seen in Figure 2.1. Under many conditions, this is a good approximation to make, and is also necessary in order to avoid needing to take edge-effects into account. This also allows for a one-

dimensional solution which is very much desirable. These approximations are valid under the condition that the thickness to width ratio of the conductor should be at least 25:1 in order to minimise the extent to which edge-effects have an impact upon the impedance of the structure. The length of the conductor should also be significantly longer than its thickness in order to rule out edge-effects in that plane. In this case, attention is drawn to the fact that, in configurations under study, the current flows only along the length of the conductor, and not in any other direction.

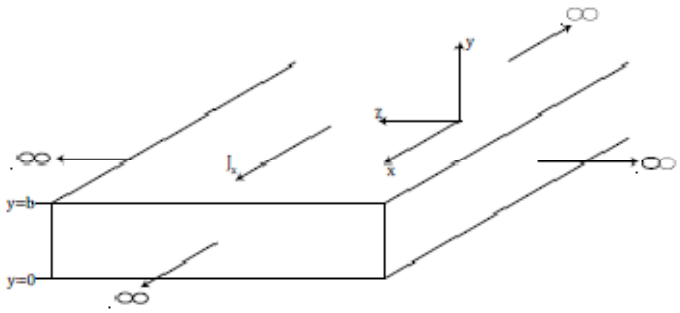


Figure 2.1. Single layer semi-infinite flat conductor

Maxwell's equations are as follows

$$\nabla \times \bar{E} = -\frac{\partial \bar{B}}{\partial t} = -\mu \frac{\partial \bar{H}}{\partial t} \qquad (1)$$

$$\nabla \cdot \bar{E} = \frac{\rho}{\epsilon} \qquad (2)$$

$$\nabla \times \bar{H} = \bar{J} + \epsilon \frac{\partial \bar{E}}{\partial t} \qquad (3)$$

$$\nabla \cdot \bar{B} = 0 \qquad (4)$$

Where

$$\bar{B} = \mu \bar{H} \qquad (5)$$

And

$$\bar{J} = \sigma \bar{E} \qquad (6)$$

Given that the current density is only in the *x*-direction, the electric field will also be in this direction. It also can only change with respect to *y*. From this, the left hand side of (1) can be rewritten as

$$\nabla \times \bar{E} = -\frac{\partial \overline{E_x}}{\partial y} \hat{k} \qquad (7)$$

Considering our restrictions laid out previously in we are only considering situations where the magnetic field is parallel to the surface of the conductor, it becomes obvious that *H* has only a *z*-component. From this, looking at (1) again, with knowledge of (7) we get that

$$-\frac{\partial \overline{E_x}}{\partial y}\hat{k} = -\frac{\partial \overline{H_z}}{\partial t}\hat{k} \qquad (8)$$

And hence, with (6)

$$\frac{\partial J_x}{\partial y} = \sigma\mu\frac{\partial H_z}{\partial t} \qquad (9)$$

where the vector notation has been dropped because we are now looking at components. Looking at (3), neglecting the displacement current term, and taking into account the components of both the magnetic field and current density, it is found that

$$\frac{\partial H_z}{\partial y} = J_x \qquad (10)$$

Differentiating both sides and substituting back into (9), the result is the second order partial differential equation

$$\frac{\partial^2 H_z}{\partial y^2} = \sigma\mu\frac{\partial H_z}{\partial t} \qquad (11)$$

This equation is a well known one-dimensional result. A further fundamental assumption that has not thus far been mentioned is the fact that all materials under consideration are assumed to be linear. Given that this body of work is aimed at characterising the frequency-dependent impedance of multi-layered structure, (11) can be transformed into the frequency domain because the materials are linear. This gives us

$$\frac{d^2 H_z}{dy^2} = j\omega\sigma\mu H_z \qquad (12)$$

The solution to a differential equation of the form

$$\frac{d^2 f}{dy^2} - D^2 f = 0 \qquad (13)$$

Is given by

$$f(y) = A_1 e^{Dy} + B_1 e^{-Dy} \qquad (14)$$

In this case, it can be shown that

$$D = (1+j)\sqrt{\frac{\omega\sigma\mu}{2}} = \frac{(1+j)}{\delta} \qquad (15)$$

Where δ is the classical skin-depth. In this case *f(y)* is identified with $H_z(y)$. The arbitrary constants A_1 and B_1 are dependent on the relevant boundary conditions for each given geometry and set of material properties. Equation (14) can be rewritten as

$$H_z(y) = F\cosh(Dy) + G\sinh(Dy) \qquad (16)$$

Solving for F and G can be done through consideration of the boundary conditions, which can be arbitrarily designated. For this, $H_z(0)$ is set to H_{s0} and $H_z(b)$ is set to H_{s1}, where b is the thickness of the conductor. The values for both H_{s0} and H_{s1} can be found through consideration of the total current within the conductor and an application of Ampere's Law.

The generic current density and electric field intensity can the be derived from the solution to the magnetic field intensity from consideration of the simple relations given in (6) and (10). These results are

$$J_x(y) = FDsinh(Dy) + GDcosh(Dy) \qquad (17)$$

$$E_x(y) = \frac{FD}{\sigma}sinh(Dy) + \frac{GD}{\sigma}cosh(Dy) \qquad (18)$$

Under the assumption that the total current in the conductor is known, which is fair given that control over the excitation to the conductor is available, Amperes law can be used around the boundary of the conductor. Since it is assumed that the width is much larger than the thickness of the conductor, the portions of the boundary given by the thickness can be neglected.

Now, these boundary conditions are a superposition of skin- and proximity-effect scenarios. In other words, the scenario where there is no external magnetic field and the scenario where there is only an external magnetic field. As such, each situation can be solved individually. This solution will be generic, and does not require that the configuration be in a common- or differential-mode with respect to the current in each of the conductors – the conductor under consideration, and any set of proximate conductors.

For the pure skin-effect scenario, the magnitudes of the boundary magnetic fields will be the same, but in opposite directions due to Ampere's Law and symmetry considerations. This is demonstrated in Figure 2.2. Ampere's Law is applied anti-clockwise around path c, because of the defined direction of the current. H_0 and H_1 are the contributions to the integral for the bottom and top edge of the boundary respectively. H_{s0} and H_{s1} are both defined in the positive z-direction because of their relationship with the derived equations above. From Figure 2.2 it is obvious that $H_{s0} = -H_0$. Also from symmetry, H_1 and H_0 are both constant along the width of the conductor and equal to each other. Therefore

$$H_{s1} = \frac{I_x}{2w} = -H_{s0} \qquad (19)$$

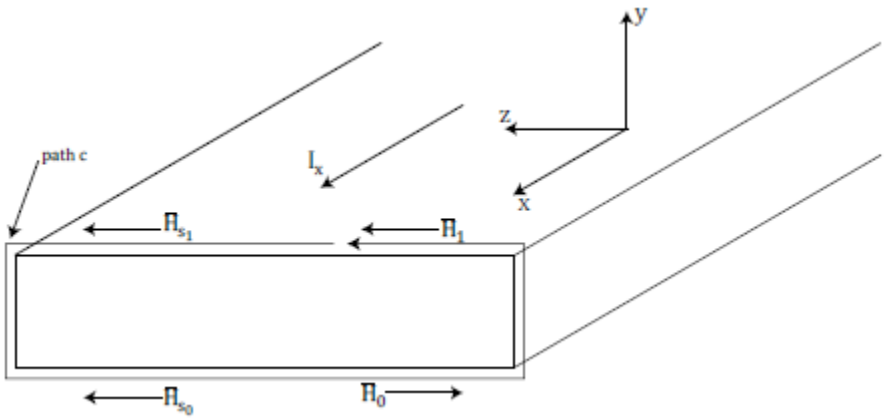


Figure 2.2. Boundary conditions under the skin effect

For the case of the pure proximity effect, both the magnitudes and directions of the magnetic fields at the boundaries will be the same. Figure 2.3 demonstrates this. The reason for this comes from consideration of the semi-infinite approximation which ensures that the magnetic field will be constant outside of a conductor for all *y* on the same side of the conductor. Bear in mind that this field is *not* as a result of the conductor under consideration, but as a result of a *different* conductor also approximated as semi-infinite flat. What this means is that this secondary conductor will produce a constant magnetic field, in terms of both magnitude and direction, in the space in which our primary conductor is situated. In this case, the boundary conditions are given by

$$H_{s1} = \frac{I_x}{2w} = H_{s0} \qquad (20)$$

but where caution must be given to distinguish this current, which is from the proximate conductor, from the current of the primary conductor.

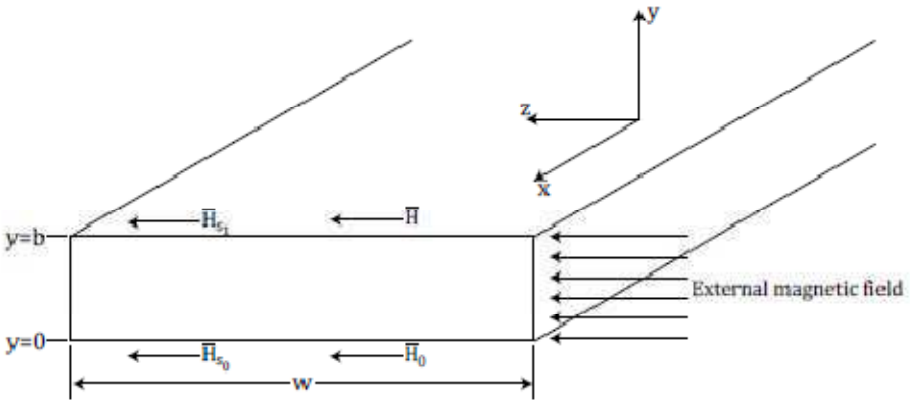


Figure 2.3. Boundary conditions under the proximity effect

As such, in the general case with no restriction on the values of the currents in each conductor, the boundary magnetic fields are given by

$$H_{s1} = \frac{1}{2w}\left(I_{px} + I_x\right) \qquad (21)$$

$$H_{s0} = \frac{1}{2w}\left(I_{px} - I_x\right) \qquad (22)$$

where I_x and I_{px} are the currents in the primary and proximate conductors respectively. From these, the constants F and G can be solved and are as follows

$$F = H_{s0} = \frac{1}{2w}\left(I_{px} - I_x\right) \qquad (23)$$

$$G = H_{s1}\frac{1+\cosh(Db)}{\sinh(Db)} = \frac{1}{2w}\left(I_{px} + I_x\right)\frac{1+\cosh(Db)}{\sinh(Db)} \qquad (24)$$

Now substitution of F and G into the field equations gives the complete solution to a generic single layer conductor under a superposition of both skin- and proximity-effects.

A.3. Multi-Layer Generalisation

The multi-layer generalisation is largely the same as that for the single layer approximation. In this case, each layer of the conductor is treated as a single layer conductor, and therefore has equations that are very similar to those of the single layer approximation. These equations are given as follows, where i denotes the layer number.

$$E_{xi}(y) = L_i cosh(D_i(y - b_{i-1})) + M_i cosh(D_i(y - b_{i-1}))$$

$$H_{xi}(y) = \frac{L_i D_i}{j\omega\mu_i} sinh(D_i(y - b_{i-1})) + \frac{M_i D_i}{j\omega\mu_i} cosh(D_i(y - b_{i-1}))$$

$$J_{xi}(y) = \sigma_i E_{xi}(y)$$

$$b_{i-1} \leq y \leq b_i$$

In this case, the coefficients L_i and M_i are constants that need to be solved in terms of the boundary conditions. As such, it can easily be seen that there are *2n* unknowns for an *n*-layer structure. For an *n*-layer structure, there are *n-1* shared boundaries between layers. At each of these boundaries we can apply the knowledge that the tangential electric and magnetic fields must be continuous across these boundaries. Therefore for each of these boundaries we enforce the following conditions

$$E_{xi}(b_i) = E_{xi+1}(b_i)$$

$$H_{xi}(b_i) = H_{xi+1}(b_i)$$

This gives us 2 equations for each of the *n-1* boundaries between layers. The final two boundary conditions are just those as given in the single layer approximation, since these two, in particular, are not dependent upon the internal structure of the conductor, nor upon the internal structure of any proximate conductor either. We therefore have obtained *2n* equations for the *2n* unknowns, allowing for a solution to be obtained.

A.4. Resistance calculations

From the above derivation, the current density has been calculated on a per-layer basis. This was necessary in order to obtain the distributions of current, and fields. In order to calculate the resistance of the structure, it is necessary to approach it from the perspective of power dissipated as heat by the structure. An important note here is that it is useful to calculate these values on a per-unit-length basis because of the assumption that the conductor is infinitely long. The total power dissipated and total resistance encountered can each be thought of as infinitesimal powers and resistances summed over the total area of the conductor. This leads to an equation of the form

$$\frac{P_i}{l} = \frac{1}{2\sigma} \iint \left| J_{i\,peak} \right|^2 da$$

P_i is, in this case, the power dissipated by layer i. Given that this derivation is based upon a one-dimensional approximation, the current density J_i is constant along the width of the conductor. This gives an integral dependent only upon y, after the width has been taken in to account.

$$\frac{P_i}{l} = \frac{w}{2\sigma_i} \int_{b_{i-1}}^{b_i} \left| J_{i\,peak}(y) \right|^2 dy$$

The total power dissipated is naturally the sum of the powers in each layer, and can be denoted as P_T. The total resistance of the structure, at a given frequency is thus given as

$$\frac{R}{l} = \frac{2P_T}{I_{peak}^2}$$

Now that the resistance has been obtained, it allows for calculation of the frequency-dependent resistances of various structures. This will help in determining the effect that the conductivity and permeability of the individual layers will have upon the shape of the frequency response.

A.5. References

[1] E Brink, *Aspects of Electromagnetic Field Distributions in Multipath Conductive Structures*. Ph.D Thesis: University of the Witwatersrand, 2011.